Damage assessment of churches exposed to slope displacements in sliding areas

Ludovica Cambiaggi, BSc., MSc.

DAMAGE ASSESSMENT OF CHURCHES EXPOSED TO SLOPE DISPLACEMENTS IN SLIDE AREAS

BY

LUDOVICA CAMBIAGGI, BSC., MSC.

Dissertation discussed in partial fulfilment of
the requirements for the Degree of

DOCTOR OF PHILOSOPHY

Civil, Chemical and Environmental Engineering
curriculum in Structural and Geotechnical Engineering, Mechanics and Materials,
Department of Civil, Chemical and Environmental Engineering, University of Genoa, Italy

September 2020

Adviser(s):

Prof. Riccardo Berardi– Department of Civil, Chemical and Environmental Engineering, Polytechnic School, University of Genoa, Italy

External Reviewers:
Prof. Nicola Moraci – Dipartimento di Ingegneria Civile, dell'Energia, dell'Ambiente e dei Materiali, Università Mediterranea di Reggio Calabria
Prof. Jamie Standing – Faculty of Engineering, Department of Civil and Environmental Engineering, Imperial College London

Examination Committee:
Prof. Luca Bruno – Dipartimento di Architettura e Design – Politecnico di Torino

Prof. Dario Peduto – Dipartimento di Ingegneria Civile – Università degli studi di Palermo

Prof. Sergio Lagomarsino – Dipartimento di Ingegneria Civile, Chimica e Ambientale – Università degli studi di Genova

Ph.D. program in Civil, Chemical and Environmental Engineering

Curriculum in Structural and Geotechnical Engineering, Mechanics and Materials

Cycle XXXII

ABSTRACT

Protecting cultural heritage from water-soil interaction related threats is a current issue and the prediction of the effects of slope displacements on buildings is very challenging. The achievement of this goal is not straightforward since it usually requires high costs due to the great amount of data to be collected for setting up reliable forecasting models. Among these threats, slow moving landslides are considered in this research, because also small slope movements can seriously affect existing structures and cause damages. In this regard, the aim is to develop a simple but effective procedure to correlate the potential damage caused to soil displacements to the slope safety conditions, represented by an "intensity parameter" such as the slope safety factor. Churches located in, or close to, landslide areas, have been chosen as exposed structures: this choice makes the theme more challenging for the structural and geometric complexities of these particular historic buildings. Furthermore, while modelling and estimating the effects induced by deep excavations or tunnelling on existing buildings are known and widely treated geotechnical problems, the assessment of the damage caused by landslide movement has not been fully developed and only limited material exists in the literature.

The procedure developed and proposed in the Thesis takes into account:

i)   identification and characterization of the exposed elements;

ii)   assessment of displacements and associated strain level components caused by slope movement via numerical analyses;

iii)   iii) proposal and assessment of an intensity parameter representative of deformations and stability conditions;

iv)   iv) assessment of damage severity levels and develop of fragility curves,

v)   v) validation of the proposed approach.

SUMMARY OF DISSERTATION.

The topics treated in this PHD Thesis are part of a research program having as objective the study of the possible interaction phenomena between slow-moving landslides, as considered *natural hazard*, and churches, as construction belonging to the so-called *cultural heritage*. Landslide and soil movements, church response and displacements, mechanisms of possible damage and related damage level criteria, are dealt with, by the proposal of a procedure of analysis aimed at correlating slope stability conditions to strain and damage levels suffered by the structure.

Churches are quite different from masonry buildings that have been previously and extensively studied in literature: irregular geometry (like arches, vaults and wide opening), material heterogeneity and its strongly non-linear behaviour, make this structural typology different from others, especially if taken into account to evaluate the effects of movements of a slope. Hence, in order to consider the importance of studying the behaviour of churches exposed to landslides, over 40 surveys in Liguria Region (Northern Italy), have been planned and performed. Regarding landslides, active rotational and translational slide have been considered, in particular those characterized by slow movements (i.e. rate of the order of some mm/year).

One of the most important issue for studying the effect of landslides on churches concerns the definition of displacement patterns to which the building can be subjected. For this reason, it is important to assess the horizontal and vertical components of the landslide movements; another aspect of particular relevance is the definition of the slope stability conditions, to be related to the movements.

In the Thesis, Chapter 1 offers an overview of the state of the art regarding on one hand the typologies of landslide and different methods for their modelling, on the other hand the damageability criteria available in the geotechnical and structural literature for the evaluation of the damage levels of buildings affected by soil displacements. Finally, an overview of different methods for the development of fragility curves is proposed, as these curves can be an useful predictive tool for defining the potential expected damage connected to the evolution of the slope stability conditions, once an "intensity parameter" is defined as the input data of the fragility curve.

Chapter 2 presents the methodology adopted for the choice of a set of churches in Liguria region affected by slow-moving landslides. The inspection method is described in detail as well as the damage analysis carried out on the churches. The introduction of four general damage mechanisms is finally presented.

Chapter 3 proposed the procedure for the analysis and prediction of the effects of slow-moving landslides via numerical approach: Finite Element Method analyses have been performed to assess soil displacements referring to the infinite slope model and Limit Equilibrium analyses have supplied the values of the relevant

slope safety factors to be combined with these displacements. Then a new hazard factor, assumed as intensity parameter, is introduced in order to link slope displacements with slope stability conditions.

Chapter 4 applied the methodology of Chapter 3 on different set of slopes, with particular geometry obtained from the analysis of real slope of the sample described in Chapter 2. Several numerical analyses were performed in order to correlate soil displacement, both vertical and horizontal to the new hazard factor. For each case deformation values were calculated as well. Each couple of value led to the definition of a damage level, by the application of the theory proposed by Son and Cording (2005). Chapter 4 have allowed the definition of a numerical data base where deformation referred to particular slope geometry and footprint of the church were correlated with the damage level

In Chapter 5 fragility and vulnerability curves were then proposed. This chapter focused on the development of the fragility curves with the assumption of the hazard factor FH of the slope as the intensity parameter, in order to give a simple tool for use, as it can be obtained by a limit equilibrium analysis. The procedure was applied on a case study.

INDEX

ii

1. STATE OF THE ART

In this Chapter, an analysis of the state of the art with respect to the topics of the thesis is proposed. Firstly, the typologies of landslides are described as well as the different methods for modelling landslide behaviour and its effect. Secondly, an overview of damage assessment is proposed: classification and criteria for predict damage on buildings and churches subjected to different natural hazard are analysed. Lastly, different method for the definition of fragility curves are proposed.

1.1 LANDSLIDES: TYPOLOGIES, MODELLING AND EFFECTS.

In recent years, the assessment of landslide hazard and the associated risk has become a topic of major interest for both geoscientists and engineering professionals as well as for the community and the local administrations in many parts of the world. The reasons for the increasing international interest in landslides are twofold: firstly, an increasing awareness of the socio-economic significance of landslides and secondly, the increased pressure of development and urbanization on the environment. As development increases on sloping urban areas, a higher incidence of slope instability and landsliding is reported. This is the case of slow-moving landslides whose huge detrimental consequences are expected to grow in the near future due to the increase of the demographic pressure and the effects of climate changes (EEA, 2012). Therefore, studies aimed at detecting the areas affected by slope movements and predicting the related damage to exposed facilities are of great interest for the authorities in charge of the land use planning and the management and protection of cultural heritage. Consequently, a thorough knowledge of the landslide phenomena (e.g. extension and intensity), the exposed structures and their interaction is fundamental. In this regard, this chapter gives an overview of the types of landslides, their modelling and effects.

1.1.1 SLOW-MOVING LANDSLIDES

Landslides are natural dangers whose inherent complexity required and still requires many endeavours from the scientific community. According to many authors (Varnes 1978, Cruden 1991, Fell et al 2008) landslide corresponds to any "movements of a mass of rock, debris or earth down a slope" activated or triggered by causes that can be either external or internal (Terzaghi 1950). Different classification systems have been proposed in the scientific literature; among them, the most widely adopted by both scientific and technical communities are those proposed by Skempton (1953), Hutchinson (1968), Varnes (1978), Hutchinson (1988), WP/WLI (1993), Cruden and Varnes (1996), Leroueil et al. (1996), Hungr et al. (2001) and Hungr et al. (2014). All of these have in common the classification of the characteristics of the soils / rocks involved, the morphometric and kinematic aspects (type of movement) and the stage of the movement.

Varnes (1978) considered two main variables: the type of material involved, which usually is apparent on inspection or preliminary boring and the type of movement, which usually may be determined by a short period of observation or by the shape of the slide and arrangement of debris. Two types of material were considered (bedrock and soils) and four classes of movements were developed (falls, slides, flows, complex). Varnes's classification proposed in 1978 (Figure 1), has expanded and deepened the one previously proposed. First, the Author introduced three classes of involved materials instead of two: "rock" (a hard or firm mass that was intact and in its natural place before the initiation of movement), "earth" (material in which 80% or more of the particles are smaller than 2 mm) and "debris" (contains a significant proportion of coarse material, 20% to 80% of particles are greater than 2 mm and the remaining are smaller than 2 mm). Then, the Author considered five types of movements namely: falls, topples, slides (rotational and translational), lateral spreads and flows; an additional class, including the complex movements, is used to define any combination of more than one type of movement.

TYPE OF MOVEMENT		TYPE OF MATERIAL		
		BEDROCK	ENGINEERING SOILS	
			Predominantly coarse	Predominantly fine
FALLS		Rock fall	Debris fall	Earth fall
TOPPLES		Rock topple	Debris topple	Earth topple
SLIDES	ROTATIONAL	Rock slide	Debris slide	Earth slide
	TRANSLATIONAL			
LATERAL SPREADS		Rock spread	Debris spread	Earth spread
FLOWS		Rock flow (deep creep)	Debris flow (soil creep)	Earth flow
COMPLEX		Combination of two or more principal types of movement		

Figure 1 - Landslide classification based on type of movements and involved materials (Varnes, 1978)

Hungr et al. (2001), for instance, starting from Varnes (1958, 1978) and Hutchinson (1968, 1988) classification, have provided more precise definitions for flow class of landslide. Many other Authors have developed further modifications to the type of soil or to the type of movement characterizing the landslide (i.e. Keefer and Johnson 1983, Hoek and Bray 1981), this denotes the interest in this topic and the need to adapt the terminology adopted in function of the researcher's need. As an example, if the interest is concerned with the runout of the event, then the overall term "debris flow" is appropriate. If the main focus is the pre-failure mechanism in the source area, then "debris slide" or "slope deformation" may be more relevant (Hungr et al. 2014). Consequently, the system of characterization should be flexible enough to accommodate all such uses.

Another important component of great utility for the study of landslides and their effect on facilities is the knowledge/prediction of the maximum value of the velocity attained by the displaced mass during the post-failure stage. In particular, according to Cruden and Varnes (1996), it is possible to identify seven velocity classes (Figure 2) by the association with a destructive significance, like for the Mercalli'scale based on the descriptions of the local effects of an earthquake. As for "slow to extremely slow-moving landslides", the category addressed in this Thesis, typical velocity values do not exceed 1.6 m/year (velocity classes 1,2 and 3); whereas "fast-moving landslides" are characterised by maximum velocity values larger than 1.8 m/hr (velocity classes from 5 to 7).

Velocity Class	Description	Velocity (mm/sec)	Typical Velocity	Probable Destructive Significance
7	Extremely Rapid			Catastrophe of major violence; buildings destroyed by impact of displaced material; many deaths; escape unlikely
		5×10^3	5 m/sec	
6	Very Rapid			Some lives lost; velocity too great to permit all persons to escape
		5×10^1	3 m/min	
5	Rapid			Escape evacuation possible; structures; possessions, and equipment destroyed
		5×10^{-1}	1.8 m/hr	
4	Moderate			Some temporary and insensitive structures can be temporarily maintained
		5×10^{-3}	13 m/month	
3	Slow			Remedial construction can be undertaken during movement; insensitive structures can be maintained with frequent maintenance work if total movement is not large during a particular acceleration phase
		5×10^{-5}	1.6 m/year	
2	Very Slow			Some permanent structures undamaged by movement
		5×10^{-7}	15 mm/year	
	Extremely SLOW			Imperceptible without instruments; construction POSSIBLE WITH PRECAUTIONS

Figure 2 - Proposed landslide velocity scale and probable destructive significant (Cruden and Varnes, 1996)

Cruden and Varnes (1996) also summarized a number of related descriptors, such as advancing, enlarging, retrogressive, multiple, or successive. Illustrations of some of these terms are shown by Hutchinson (1988). Such terms are a useful supplement to landslide type names. The term "progressive" is often misused in landslide literature and should be reserved for the specific phenomenon of progressive failure, used in stability or deformation analyses (e.g., Morgenstern 1992; Leroueil et al. 2012). Another useful group of supplementary terms proposed by Cruden and Varnes (1996) relates to the post-failure activity of the landslide, including re-activated, dormant, and relict. In this post-failure stage, the velocity of soil mass first increases and then decreases. The last stage of movement corresponds to the reactivation;

in this stage, the soil mass (moving along one or several pre-existing shear zones) can exhibit active or occasional reactivation styles. In particular, active (slow-moving) landslides show seasonal variations of the rate of movement that are controlled, both in the accelerating and decelerating phases, by pore-water pressure fluctuations strictly correlated, in turn, to the net rainfall regime and/or snowmelt. Slow-moving landslides, topic of this thesis, are diffused in many geological and geomorphological contexts over the world. As regards to the Italian territory, many areas from the north to the south of the country are affected by landslides, as demonstrated by well-documented case studies in the scientific literature and shown in Figure 3 (Guzzetti, 2000).

Date	Location	Region	Deaths and missing people	Type of failure and secondary effects
22/9/1419	Passer Valley	Trentino-Alto Adige	400	Failure of a landslide dam and subsequent debris flow
1580	Giffoni Valle Piana	Campania	Few hundreds	Several landslides
4/9/1618	Piuro	Lombardia	1200 (ve)	Rock avalanche
27/7/1642	Antronoapiana, Monte Pozzoli	Piemonte	150 (ve)	Rock avalanche
15/10/1691	Castiglione del Genovesi	Campania	70	Large landslide
15/8/1692	Borta, Monte Auda	Friuli Venezia Giulia	53 (>)	Rock avalanche
2/1698	Pisticci	Basilicata	Several hundreds	Large slide
14/8/1748	Valle di Vanoi, Canale di Sotto	Trentino-Alto Adige	72	Debris flow
1/1/1762	Cetara	Campania	50	Large landslide
15/11/1762	Primaluna, Gero and Barcone	Lombardia	100 (c)	Rock fall (?)
24/6/1765	Roccamontepiano	Abruzzo	600 (ve)	Very large slide
2/6/1789	Groscavallo (various sites)	Piemonte	275 (c)	Landslides and debris flows
21/4/1814	Monte Antelao	Veneto	314 (ve)	Rock avalanche
1/5/1826	Valle di Vanoi, Remesori	Trentino-Alto Adige	52	Failure of a debris-cone dam and subsequent debris flow
1840	Verres	Valle d'Aosta	80	Failure of a natural dam and debris flow
22/1/1841	Gragnano, Rione Trivioncello	Campania	116	Landslide
24/10/1910	Costiera Amalfitana (various sites)	Campania	247 (c) (ve)	Landslides and debris flows
26/3/1924	Costiera Amalfitana (various sites)	Campania	237 (c) (ve)	Landslides and debris flows
17/2/1925	Cancia, Monte Antelao	Veneto	341	Rock slide
9/11/1932	Ionian coast (3 sites)	Calabria	56 (c)	Landslides and debris flows
16/10/1951	Ionian coast (various sites)	Calabria	70 (c)	Landslides and debris flows
25/10/1954	Costiera Amalfitana (several sites)	Campania	319 (c)	Debris flows
9/10/1963	Vajont	Veneto	1917 (c) (ve)	Rock slide and outburst flood
19/7/1985	Stava	Veneto	269	Failure of two mine ponds and subsequent debris flow
5/5/1998	Episcopio, Quindici, Bracigliano, Siano, San Felice a Castello	Campania	153 (c)	Debris flows

Figure 3 - Major landslide disasters that occurred in Italy from 1400 to 1999 from Guzzetti (2000)

1.1.2 SLOW-MOVING LANDSLIDES MODELLING

In this section, a brief overview of the method commonly used to model landslide is presented. Numerical investigation is a promising way to study the mechanical and hydraulic behaviour of landslides (Hungr 1995, Crosta et al. 2005, Mangeney et al. 2005, Bui et al. 2008). The most commonly adopted numerical methods include the Finite Element Method (FEM) (Zhang et al. 2005), Smoothed Particle Hydrodynamics (SPH) (Bui et al. 2008) and the Discrete Element Method (DEM) (Cundall and Strack 1979).

The Finite Element Method (FEM) has long been employed to investigate the slope stability (Rahman 1997; Griffiths and Lane 1999, Zhang et al. 2005, Huvaj and Maghsoudloo 2013). FEM allows to obtain the following aspects when studying slope stability:

(a) The failure mechanism at the critical equilibrium state can be obtained. The failure mechanism is very important in some cases. For example, if a monitoring system for predicting landslide is to be installed in a slope, it is necessary to know which part of the slope would deform seriously if the land slipping occurred and where the critical slide surface could be.

(b) The process of progressive failure resulting from shear strength reduction can be monitored. Hence, the limited reinforcement can be placed at those places vital to stability.

(c) The influences of different construction procedures on slope stability can be compared.

(d) The pattern of displacements can be evaluated along the slope.

(e) Some more complicated factors influencing slope stability can be taken into consideration, for example, the rainfall process, the constitutive relations more appropriate for the soil mass.

However, the traditional Lagrangian-based FEM is not appropriate for studying landslides with large displacements, because the finite element mesh would rapidly become highly distorted, leading to inaccurate results (Crosta and Clague 2009).

Smoothed Particle Hydrodynamics (SPH) is one type of Lagrangian meshless methods, commonly used to simulate the large deformation of continuum or dispersed materials (Bui et al. 2008). In the SPH, the fluid (or solid) domain is discretized as a series of elements and the material properties are attributed to the element centres, which are then interpreted as material particles. These material particles carry field variables such as mass, density and stress tensor, and move with the material velocity. The governing differential equations for the continuum are converted into equations of motion of these particles and then solved by a Lagrangian numerical scheme. SPH method can be used in studying geophysical flows (Gutfraind and Savage 1998; Cleary and Prakash 2004). As the SPH particles are used to mimic the behaviour of granular solids, they would repel each other when the soil mass is compressed, while they can attract each other if the soil mass expands. However, when the solid material is stretched, the attraction would result in the formation of SPH particle clumps (Swegle et al. 1995). This is commonly called the "tensile instability" problem for SPH in modelling the mechanical behaviour of solids. This problem is negligible for non-cohesive soil with small friction angle but become troublesome for high friction angles. For cohesive soil, the tensile instability is very serious, so that special treatments are needed during the simulations (Dyka and Ingel 1995, Johnson and Beissel 1996). Bui et al. (2008) pointed out that this problem would result in unrealistic fracture at the soil surface at large deformation.

The application of DEM in the simulation of granular flows, as firstly proposed by Cleary and Campbell (1993), appears to be useful for understanding the behavior of dry granular flows and is likely to yield many

insights into this problem, if it can closely mimic the experimental setup (Lacaze et al. 2008). Within the last two decades, it has become a complementary research method to the laboratory experiments, revealing the fundamental mechanical characteristics of landslides (Savage and Hutter 1991, Staron and Hinch 2007; Tang et al. 2009). As Zenit (2005) pointed out, the use of DEM in landslide simulations is very powerful, because all the numerical data are accessible at any stage of the test, including quantities that are very difficult, or even impossible, to be obtained directly from laboratory experiments, such as the individual particle trajectories and transient interaction forces. This information is essential for understanding the underlying physics of dry granular flows.

All these methods require a relatively complete model of the subsoils and their constitutive parameters determined by an extensive programme of laboratory tests. When detailed data are not available, more simplified methods have to be taken into account.

The Limit Equilibrium Method (LEM) is widely used by researchers and engineers conducting slope stability analysis. The method assumes that the shear strengths of the materials along the potential failure surface are governed by linear (Mohr-Coulomb) or non-linear relationships between shear strength and the normal stress on the failure surface. The most common limit equilibrium techniques are methods of slices, such as the Ordinary Method of Slices OMS (Fellenius 1927) and the Bishop simplified, Janbu simplified, Spencer, and Morgenstern-Price methods. The slide-mass is divided into n smaller sliced. Each slice is affected by general system of forces and for this system, there are ($6n-1$) unknowns. The OMS method was developed by Fellenius in 1927, it neglects all interslice forces and fails to satisfy force equilibrium for the slide mass as well as for individual slices. Bishop's simplified method (Bishop 1955) assumes that all interslice shear forces are zero, reducing the number of unknowns by $n-1$. This leaves $4n-1$ unknowns, leaving the solution overdetermined as horizontal force equilibrium will not be satisfied for one slice. Janbu's simplified method (Janbu 1954, 1973) also assumes zero interslice shear forces, reducing the number of unknowns to ($4n-1$). The Author presented a correction factor, f_0, to account for the inadequacy of an overdermined solution that will not completely satisfy moment equilibrium condition. Spencer (1973) proposes a method that rigorously satisfies static equilibrium by assuming that the resultant interslice force has a constant, but unknown, inclination. Morgenstern and Price (1965) proposed a method that is similar to Spencer's method, except that the inclination of the interslice resultant force is assumed to vary according to a portion of an arbitrary function. This additional portion of the selected function introduces an additional unknown, leaving $4n$ unknowns and $4n$ equations.

These are just some of the methods proposed in the scientific literature to model landslides, the choice of which is based on the type of material involved, the type of movement to be simulated and the available information of the soil.

For the goal of this thesis the focus is on shallow landslide, that typically consists of a slip along an interface dividing a shallow upper soil layer from an underlying stronger and often less permeable lower

soil layer or bedrock. The soil is subject to two major opposing influences: the downslope component of soil weight, which acts to shear the soil along a potential failure plane parallel to the hillslope and the resistance of the soil to shearing (known as its shear strength). The relationship between the two influences is expressed as a factor of safety FS. The landslides objected of this thesis are characterized by very low velocity and the induced displacements are very small. For this reason, FEM and LEM modelling will be adopted.

1.1.3 EFFECT OF SLOW-MOVING LANDSLIDES

Slow-moving landslides may cause different consequences to facilities with their interaction such as the break of underground utilities (e.g. water and gas distribution pipelines), interruption of transport infrastructures (e.g. roads and railways) with consequent high cost of maintenances, but also cracking and tilting of buildings. Generally, their occurrence does not cause injury and/or kill people; however, relevant economic losses and damage to both cultural heritages and environmental assets can be recorded. The available information on related economic losses are generally referred to all types of landslides phenomena. For instance, the annual economic losses in Italy, Austria, Switzerland and France are estimated as US$ 1–5 billion while United States exceed USD 3.5 billion (Dai et al 2002, Kjekstad and Highland 2009). A separate economic estimation for landslides types (fast or slow-moving) is not available.

Concerning the risk of cultural heritage, it is important to remember that after the 31st Session of the World Heritage Committee (2007), the UNESCO's List includes 851 sites forming part of the cultural and natural heritage which the ''World Heritage Committee'' considers as having outstanding universal value. The list of most represented countries reflects this aspect: Italy (41), Spain (39), China (35), Germany (32), France (31), United Kingdom (27), India (27), Mexico (27) are at the top of this inventory. A significant number of the above sites and remains are not in equilibrium with the environment. Among natural phenomena, earthquakes, flooding and landslides are the main causes of disruption to sites of cultural heritage. It is difficult to say the percentage of loss caused by any one type of phenomena but, whilst earthquakes and flooding affect a very large area and a significant number of monuments at the same moment, landslides act more locally, at the scale of the site, thus making statistical analysis rather complicated.

As an example, it is possible to say that among the Italian UNESCO sites documented in the World Heritage List, 25% of them are affected by mass movements. For instance, in Liguria, a region of northern Italy, according to the Italian archive of historical information on landslides and floods (http://sici.irpi.cnr.it, Guzzetti et al. 2004), 1806 landslide events damaged 1233 localities during the period 1800–2001 in the four Provinces of the Liguria Region. The IFFI project (Italian Landslide Inventory), developed by the ISPRA's department for the Geological Survey of Italy and aimed to survey landslides in Italy (Trigila et al 2008), shows that in the Liguria region 13.475 landslides occurred between 1164 and 2017. In particular,

in 2017 an area of 536 km^2, equal to 10.1% of the regional territory, was affected by landslides (Trigila et al 2018). In a territory with such a high number of landslides, the assessment of the effects of landslides on the regional cultural heritage is a current and social issue to which scientific research must offer a contribution. Therefore, developing methods to analyse and predict the induced damage to buildings by slow-moving landslide is of particular concern to adequately assess the tolerability/acceptability of differential displacements in order to plan the most suitable mitigation strategies.

1.2 DAMAGE ASSESSMENT OVERVIEW: CLASSIFICATION AND CRITERIA FOR BUILDINGS AND CHURCHES

The prediction of the effect of landslides is a fundamental issue for the management of the urban system and for the preservation of historical and cultural heritage.

The development of a proper procedure to fulfil this task has to take into account: i) identification of the exposed elements; ii) definition and estimation of relevant parameters able to describe the phenomenon; iii) prediction of the damage severity level. In this Chapter, a brief description of some well-known damageability criteria provided by the scientific literature is proposed.

1.2.1   RISK ANALYSIS

In 2005, the International Conference on Landslide Risk Management was held in Vancouver, following the pilot project proposed by Professor Robin Fell in 1997 in Honolulu (Cruden and Fell 1997). An important work on the use of risk management in landslides were given in the State of the Art papers (Fell et al., 2005a,b; Picarelli et al., 2005; Nadim et al., 2005; Hungr et al., 2005; Roberds 2005; Leroi et al., 2005; Cascini et al., 2005; Wong, 2005). Figure 4 and Figure 5 well describe the overall risk management process. According to the Authors, the risk management includes hazard and consequence analysing, evaluation and mitigation of the risk. Within the risk analysis, the analysis of consequences is comprised of two steps: identification and quantification of the exposed elements and estimation of their vulnerability (Fell et al. 2005, Fell et al. 2008).

For the purpose of this study, historical buildings, with a focus on churches, represent the exposed elements. The first step involves detecting them via image processing and field surveys. It is worth noting that churches are quite different from masonry buildings, largely studied in literature: irregular geometry (like arches, vaults and wide openings), material heterogeneity and its strongly non-linear behaviour make this structural typology different from the others. Carrying out these activities depends on the scale adopted for the analysis. In this case, large (1:25,000 to 1:5,000) and detailed (> 1:5,000) scales were adopted and the single cultural heritage can be accounted for (Cascini et al. 2013; Corominas et al. 2014; Ferlisi et al. 2007; Maquaire et al. 2004; Palmisano et al. 2016; Peduto et al. 2016; Nicodemo et al. 2017). For the definition of risk, in addition to the element at risk and natural hazard, it is essential to define the

vulnerability. The latter is generally defined as the expected degree of loss of a given element, or set of elements, within an area actually or potentially affected by a hazard of a given intensity (Varnes 1984; Wu et al 1996; Glade 2003). Vulnerability relates to the consequences or the results of an impact of a natural force and not to the natural process or force itself (Lewis 1999). Consequences are generally measured in terms of damage and losses (Glade 2003). Its estimation depends on several factors related to both the intensity of the dangerous event (e.g. for slow-moving landslides its kinematics and related displacements) and the exposed facilities. Nevertheless, it is important to remember the existence of several sources of uncertainties (Glade 2003): the peculiarities of factors that predispose/trigger a given phenomenon; the spatial distribution of the intensity parameter and its temporal variability; the vulnerability value that might change from one facility to another even for similar danger intensity.
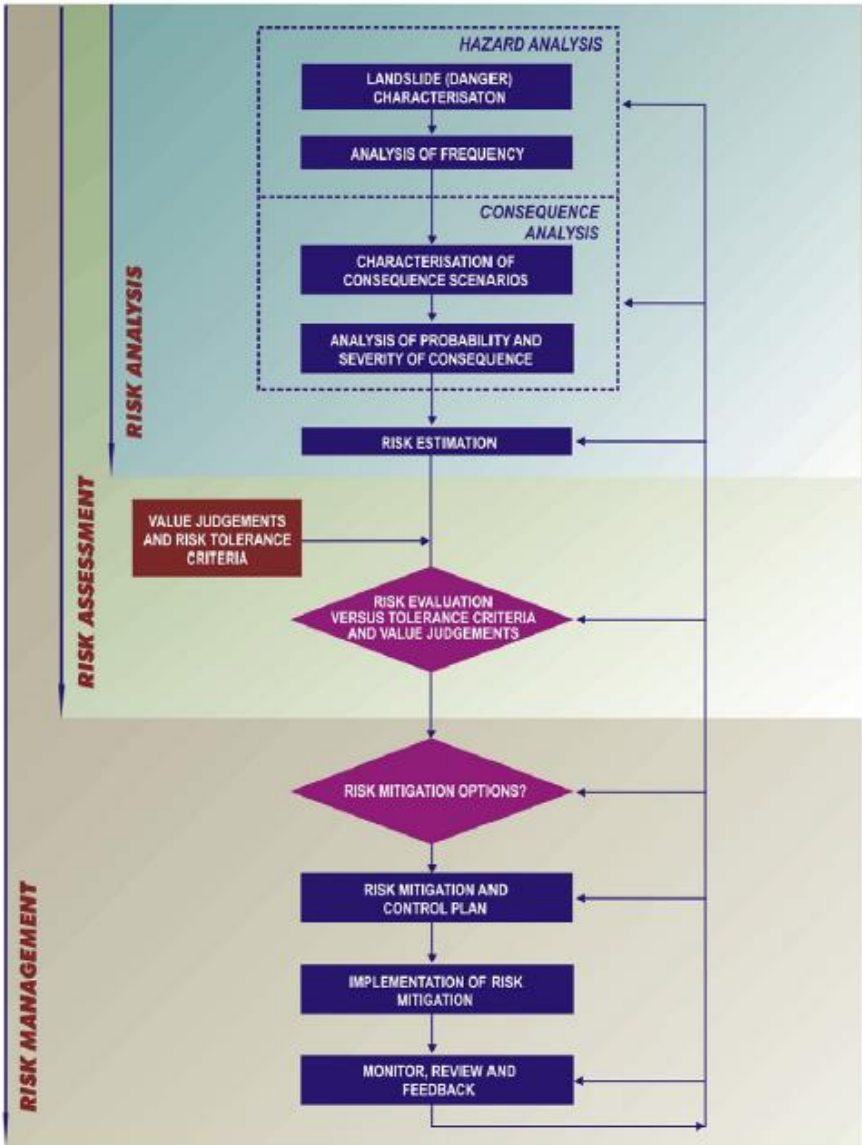

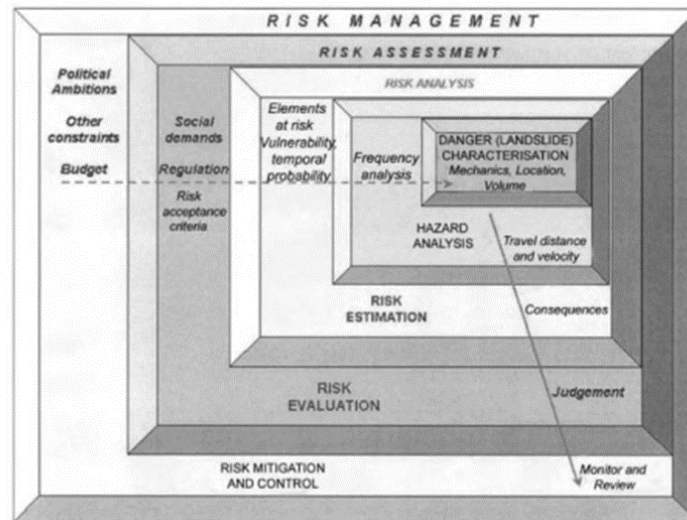Figure 4 - Risk management process

Figure 5 - Risk management process

1.2.2   DAMAGE CLASSIFICATION

Several Authors have attempted the measurement and classification of building damage. Many of the schemes have common features but vary slightly in the parameters and categories. According to Cooper (2008), the way in which damage has been assessed falls into four main types:

1. Quantitative structural deformation schemes that measure in detail the amount of distortion of structures and accompanying damage (NCB, 1975; Bhattachraya and Singh, 1985; Chiocchio et al., 1997);

2. Detailed recording schemes that adopt measurements of damage patterns in buildings and relate them to a pattern of stress that affected the structure (Audell, 1996; Building Research Establishment, 1981; Johnson, 2005);

3. Established earthquake recording schemes used to assess both earthquake damage and earthquake intensity (Wood and Neumann, 1931; Medvedev et al., 1965; Grünthal, 1998);

4. Visual building damage schemes used to record building damage in various geological situations including mining, landslide, shrink-swell clays and general building damage generated by other causes (Burland et al., 1977; Alexander, 1986; Van Rooy, 1989; Geomorphological Services Ltd. 1991; Humphreys and Partners, 1993; Freeman et al., 1994; Palmisano et al., 2016).

Among the visual building damage schemes provided by the scientific literature, the first simple ranking for building damage was proposed by Skempton and MacDonald (1956). The Authors divided the damage into three main categories according to their severity and based upon the structural elements affected by cracks, in absence of any clearly defined threshold values: (i) architectural, damaging the appearance of the facade; (ii) functional, influencing the utility of the structure; (iii) structural, affecting the stability of the building. Burland et al. (1977) proposed one of the most adopted damage classifications in geotechnical

practice. The Authors summarize several approaches to quantify the building damage, starting from those used in Britain and arranged by the UK National Coal Board (NCB), as detailed in the Subsidence Engineers Handbook (National Coal Board, 1975). The proposed system of damage categories is based on the ease of repair (Table 1) and involves three main criteria:

1. visual appearance;

2. serviceability or function;

3. stability.

The Authors established six levels of damage, from 0 to 5 as severity increases. Normally, the categories from 0 to 2 relate to the attainment of aesthetic damages; 3 and 4 to loss of functionality; and 5 to loss of stability. It is important to underline that no distinction of the typology of the structure was made. Palmisano et al. (2016) proposed a method aimed at detecting typological and damage characteristics of ordinary masonry and reinforced concrete buildings. Therefore, these forms are not applicable to 'non-ordinary' buildings, such as theatres, churches, sports facilities, industrial buildings, architectural heritage buildings. The authors defined eight sections for the damage survey forms for ordinary buildings:

• Section 1: building identification.

• Section 2: building description.

• Section 3: structural type.

• Section 4: damage to structural elements and partition walls and existing emergency measures.

• Section 5: damage to non-structural elements (partition walls excluded) and existing emergency measures.

• Section 6: external danger and existing emergency measures.

• Section 7: further notes.

• Section 8: damage grade

Sections 4 and 5 deal with damage to structural and non-structural elements and existing emergency measures. In the forms, four damage levels (from 0 to 3) have been distinguished. The damages to the structural elements and to the partition walls are in the same group, different from that of damages to other non-structural elements. Three levels of damage extension have been defined: • few: not more than 1/3 of the elements are damaged; • many: more than 1/3 and not more than 2/3 of the elements are damaged; • most: more than 2/3 of the elements are damaged. The classification defines six grades of damage, i.e. from 0 to 3c as the severity of the damage increases. Grades 0 and 1 relate to serviceability limit state, grade 2 to serviceability/ultimate limit state, grade 3a to ultimate limit state, grade 3b to ultimate limit state/collapse and grade 3c to collapse. These grades of damages are reported in Figure 6, which illustrates the classification proposed by Grünthal (1998) for seismic action as well.

Burland et al. (1977) Classification		EMS 98 Classification (Grüntal 1998)		Palmisano et al. 2016	
0	Negligible			0	Negligible damage
1	Very slight	1		1	Negligible to slight damage
2	Slight	2		2	Moderate damage
3	Moderate				
4	Severe	3		3a	Substantial to heavy damage
		4		3b	Very heavy damage
5	Very severe	5		3c	Destruction

Figure 6 – Damage classification proposed by Palmisano et al. 2016

Table 1- Damage categories from Burland et al. 1977

Category of damage	Normal degree of severity	Description of typical damage
0	Negligible	Hairline cracks less than about 0.1 mm.
1	Very Slight	Fine cracks which are easily treated during normal decoration. Damage generally restricted to internal wall finishes. Close inspection may reveal some cracks in external brickworks or masonry. Typical crack widths up to 1 mm.
2	Slight	Cracks easily filled. Re-decoration probably required. Recurrent cracks can be masked by suitable lining. Cracks may be visible externally and some repainting may be required to ensure weathertightness. Door and windows may stick slightly. Typical crack width up to 5 mm.
3	Moderate	The cracks require some opening up and can be patched by mason. Repainting of external brickwork and possibly a small amount of brickwork to be replace. Door and windows sticking. Service pipes may fracture. Weathertightness often impaired. Typical crack widths are 5 to 15 mm or several up to 3 mm.
4	Severe	Extensive repair work involving breaking-out and replacing sections of walls, especially over doors and windows. Windows and door frames distorted, floor sloping noticeably[1]. Walls leaning[1] or building noticeably, some loss of bearing in beams. Service pipes disrupted. Typical crack widths are 15 to 25 mm but also depends of the number of cracks.
5	Very severe	This requires a major repair job involving partial or complete rebuilding. Beams lose bearing, walls lean badly and require shoring. Windows broken with distortion. Danger of instability. Typical crack widths are greater than 25 mm but deepens of the number of cracks.

1.2.3   DAMAGEABILITY CRITERIA

Analysing the scientific literature, many criteria to predict building damages due to foundation displacements exist and a large number of parameters are adopted by different Authors. In this work, the terminology and definitions that will be used are those provide by Burland (1995) according with the reference schemes shown in Figure 7. According to these reference schemes, the following deformation parameters are defined:

1. *Settlement Sv*, defines the vertical movement of a point (positive values indicate downwards movement);

2. *Differential or relative settlement* δSv, is the difference between two settlement values;

3. *Rotation or slope* θ, describes the change in gradient of the straight line defined by two reference points embedded in the structure;

4. *Angular strain* α, produces sagging or upward concavity when positive, while hogging or downward concavity is described by a negative value;

5. *Relative deflection* Δ, describes the maximum displacement relative to the straight line connecting two reference points with a distance L;

6. *Deflection ratio DR*, is defined as the ratio of relative deflection and the corresponding length:

DR = Δ/L;

7. *Tilt* ω, describes the rigid body rotation of the whole superstructure or a well-defined part of it. It is difficult to determine as the structure normally flexes itself;

8. *Relative rotation or angular distortion* β, is defined as the rotation of the straight line joining two reference points relative to the tilt.

9. *Average horizontal strain* εh, develops as a change in length δL over the corresponding length L: $\varepsilon_h = \delta L / L$.

As far as the damageability criteria are concerned, Negulescu and Foerster (2010) distinguish among three main categories of methods, namely:

- empirical (e.g. Skempton and MacDonald, 1956; Polshin and Tokar, 1957; Sowers, 1962; Bjerrum, 1963; Rüsch and Mayer, 1964; Beeby and Miles, 1969); which aim at establishing criteria of serviceability by relating the deformation observed from field surveys to the damage;
- analytical (e.g. Burland and Wroth, 1974; Boscardin and Cording, 1989; Boone, 1996; Finno et al., 2005; Bird et al., 2005a,b);
- numerical (e.g. Potts and Addenbrooke, 1997; Burd et al., 2000; Son and Cording, 2007).

Regarding the first category, Skempton and MacDonald (1956) were the first to derive recommendations on allowable settlements of structures based on empirical methods. These recommendations were obtained by treating data collected from settlements and damage observations on 98 buildings mainly reinforced concrete framed buildings, deforming under the own weight. The damage criterion that they used is the "angular distortion" defined as the ratio of the differential settlements and the distance between two points after eliminating the influence of the tilt of the building. Based on their observations, they reported a range of limit values depending on the type of building or foundation, they propose a limit value of 1/300 for "angular distortion" corresponding to a threshold for crack initiation in walls and finishes. They note also that a value greater than 1/150 would cause structural damage. These threshold values have also been reported in the Eurocode EC7.
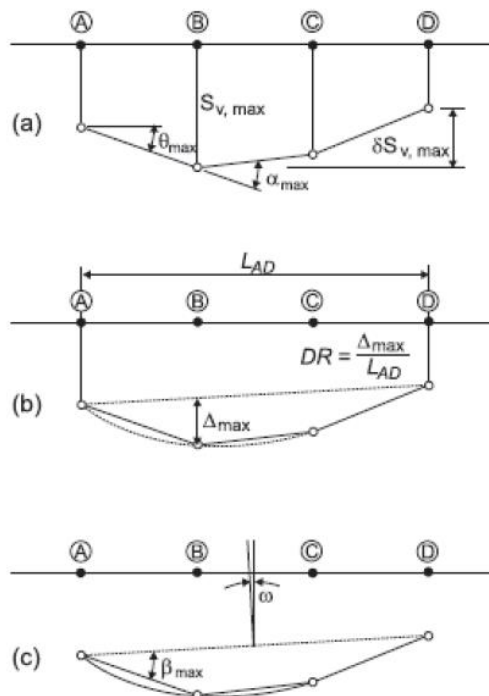

Figure 7 - Terminology and definitions provide by Burland (1995)

Polshin and Tokar (1957) recognise different modes of deformation for different types of buildings, so that they treat separately unreinforced load bearing walls and frame structures. They defined some limit criterion which depend on the "slope" (i.e. difference of settlement of two adjacent supports relative to the distance between them), the "relative deflection" (ratio of deflection to the deflected part length) and the average settlement under the building.

As for analytical methods, the most important is the one proposed by Burland and Wroth (1974). The Authors analysed the building damage due to foundation movements by neglecting the interaction between the structure and the underlying ground. Using the elastic deep beam theory (Timoshenko, 1955), they

replace a simple structure by an equivalent uniform, weightless, elastic beam of length L, height H and unit thickness (Figure 8). Assuming that the equivalent elastic deep beam can deform according to the ground surface settlement trough in "greenfield" conditions (i.e. without the building) and setting the horizontal strains equal to zero, then, they impose the obtained displacements on a structural model of the building in order to assess the expected damage. Burland and Wroth (1974) derived the relationships between the deflection ratio (Δ/L) and the maximum tensile strain for the equivalent elastic deep beam subject to either pure bending or pure shear deformation. In pure bending, ($\varepsilon_{b,max}$) is horizontal; whereas, in pure shear, the maximum tensile strain ($\varepsilon_{d,max}$) is oriented at 45° (Figure 8).

The relationships between the maximum tensile strain and Δ/L for specified deformation modes is obtained using the following equations, where y is the distance of the neutral axis from the lower edge of the beam:

$$\frac{\Delta}{L} = \varepsilon_{b,\max} \frac{L}{12y}\left[1 + \frac{18EI}{L^2 HG}\right]$$
(1.1)

$$\frac{\Delta}{L} = \varepsilon_{d,\max}\left[1 + \frac{L^2 HG}{18EI}\right]$$
(1.2)

Where E is the Young's modulus, G is the shear modulus and I is the second moment of the transversal area of the beam. A limit of this theory lies on the selection of the equivalent beam characteristics (e.g. stiffness parameter values), especially when dealing with a multi-storey structure. From this point of view, recently studies carried out on this topic by Son and Cording (2007), Losacco (2011), Losacco et al. (2014) led to the definition of an "equivalent solid" whose bending and shear stiffness can be estimated taking into account the existence of openings (windows, doors) on buildings.

Boscardin and Cording (1989) complemented the criteria proposed by Burland and Wroth (1974) by including the effects of horizontal strains that, in turn, depend on the lateral stiffness of the structure. Based on the results of their studies, they categorized the damage to buildings by developing relationships between the horizontal strain and the angular distortion (Figure 9).They defined the critical tensile strain ε_{crit} as:

$$\varepsilon_{crit} = \varepsilon_h \cos^2 \theta_{\max} + 2\varepsilon_d \cos \theta_{\max} \sin \theta_{\max}$$
(1.3)

Where ε_h is the horizontal strain. ε_d is the diagonal strain, θ is the angle from the horizontal.

Figure 9 shows curves for the case of ε_{crit} equals to 0.00075 and horizontal strain equals to 0.0005. Notice that for L/H less than about 1, first observable cracking will be controlled by shear related deformations.

Furthermore, these analyses were performed assuming that the beam was composed of an isotropic material such that E = 2(1 + v) G and v is assumed to be as 0.3. In reality, masonry is an orthotropic material,

and the relationship of Young's modulus, E, to shear modulus, G, depends on a number of factors. Typically, the E/G ratio for a solid masonry beam would be expected to be somewhat greater than the E/G ratio for an isotropic material. In addition, the presence of openings in the wall would further increase the E/G ratio. Substituting various ratios of E/G into the equations for Δ/L versus L/H shows that the more flexible the structure is in shear (larger E/G ratio), the greater the range of L/H where shearing distortion and diagonal tension will control cracking. Refer to the case where E/G is equal to 12.5 versus cases where E/G equals 2.6 in Figure 10.
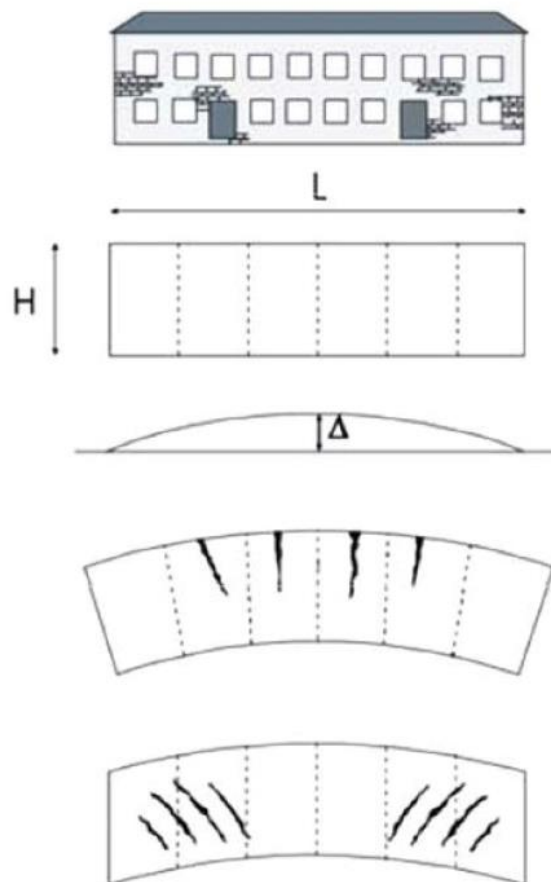
Figure 8 - Equivalent uniform, weightless, elastic beam of length L, height H and unit thickness proposed by Burland and Wroth (1974)
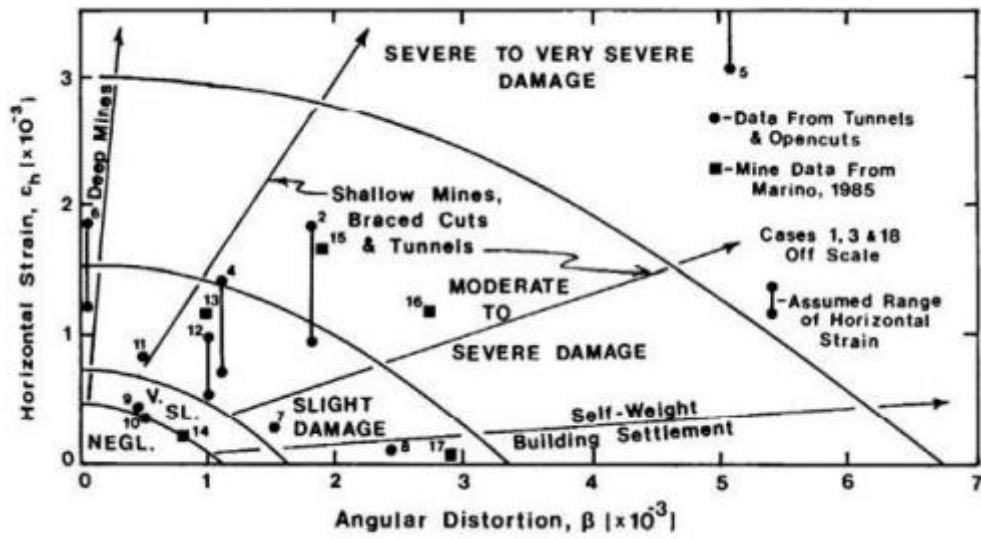
Figure 9 - Relationships between the horizontal strain and the angular distortion and related damage grade from Boscardin and Cording (1989)
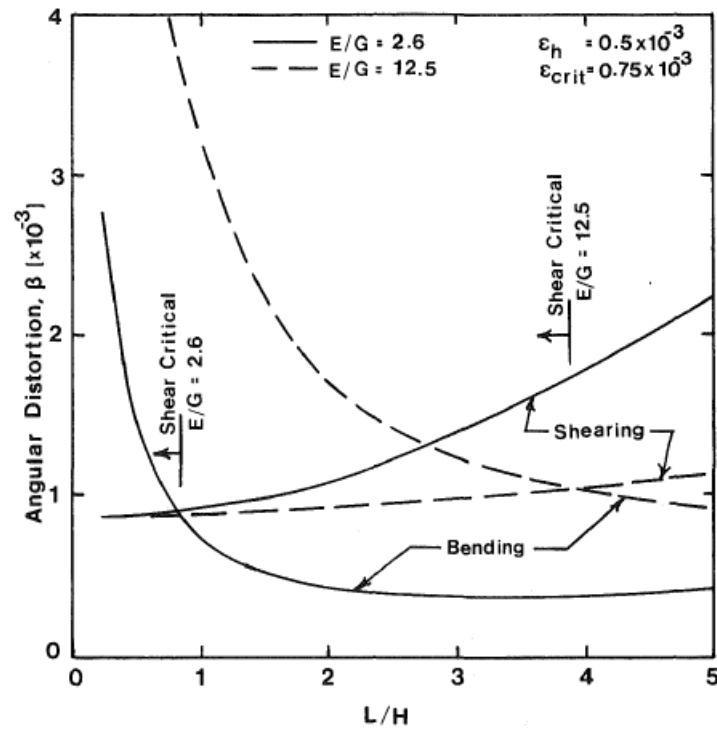

Figure 10 - Relationship between angular distortion and L/H for rectangular beams deflecting due to combined bending and shear after Burland and Wroth, 1974.

The damage criterion developed by Boscardin and Cording (1989) considered angular distortion β and horizontal strain ε_H. The criterion was based on the state of strain of a simple deep beam with L/H=1, E/G=2.6, and neutral axis at the bottom of the beam. Son and Cording (2005) proposed some changes from

that established by Boscardin and Cording (1989). The generalized damage criterion is based on the state of strain at a point (Figure 11), which is not dependent on L/H, E/G, and the position of neutral axis (Cording et al. 2001, Son 2003). unit is evaluated. The ground movements are imposed on the base of the structure, producing lateral strain (extension in the outer portion of the settlement trough) and angular distortion, or shear strain, as shown in Figure 12. A building unit can be a section between two columns or cross walls, two different building geometries or stiffnesses, or two different ground displacement gradients.

Because ground movements are imposed at the base of the structure, lateral strains resulting from the imposed lateral displacements are greatest near the base of the structure. Bending may produce higher lateral strains in the upper portion of the structure, which can only occur for low building length/height ratios if vertical cracks or weaknesses extend over the height of the wall.

The criterion is based on the concept that a structure is deformed by the combination of angular distortion and lateral strain, and the maximum strain on the structure can be decided by a principal strain formed by both the angular distortion and the lateral strain. The maximum principal strain is compared with the critical strains for each different damage category.

The critical tensile strains for different damage levels were determined from the results of field observations. The combination of angular distortion β and lateral strain ε_L at a point or in a building unit results in a maximum principal tensile strain ε_p as follows;

$$\varepsilon_p = \varepsilon_L \cos^2 \theta_{max} + \beta \cos \theta_{max} \sin \theta_{max} \qquad (1.4)$$

Where ε_L is the lateral strain, β is the angular distortion, θ_{max} is the direction of crack formation and the angle of the plane on which ε_p acts, measured from vertical plane. For example, if β is zero, $\varepsilon_p = \varepsilon_L$ acts on the vertical plane ($\theta_{max} = 0$) and a crack forms along the vertical plane, and if ε_L is zero, $\varepsilon_p = 1/2\beta$ acts on the plane at $\theta_{max} = 45°$ and a crack forms at $\theta_{max} = -45°$.

In Figure 12, the critical tensile strain boundaries of the zone classified as "very slight" damage were taken as $0.5*10^{-3}$ and $0.75*10^{-3}$, which are the strains suggested by Burland and Wroth (1974) and Polshin and Tokar (1957) for the formation of a first visible crack.
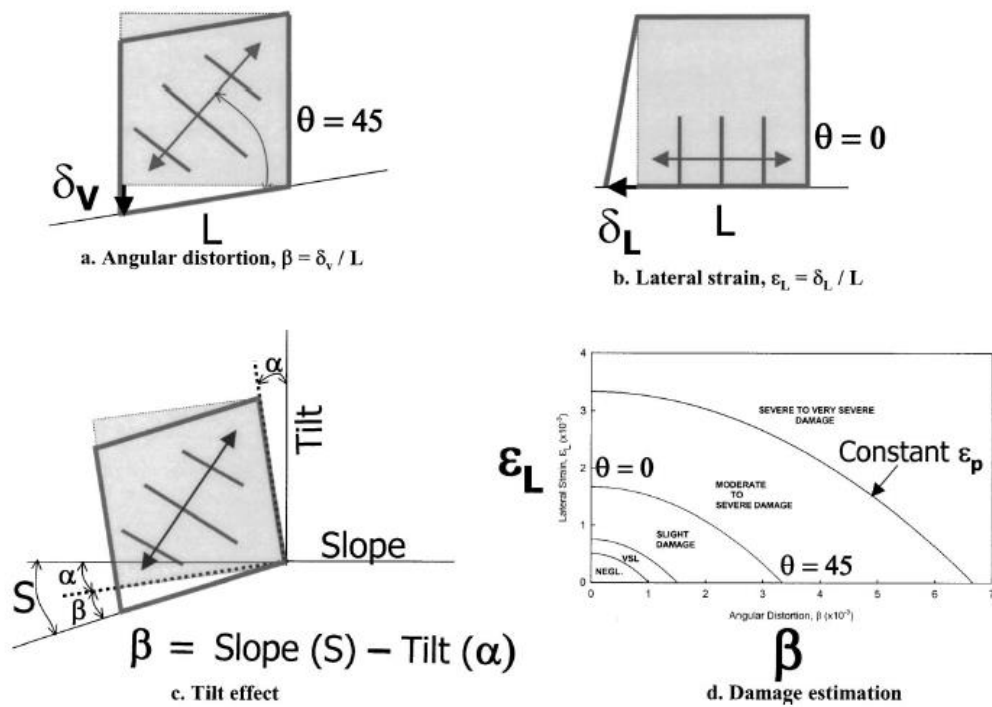
Figure 11 - State of strain at point or average state of strain in distorting portion of structure (from Son and Cording 2005)
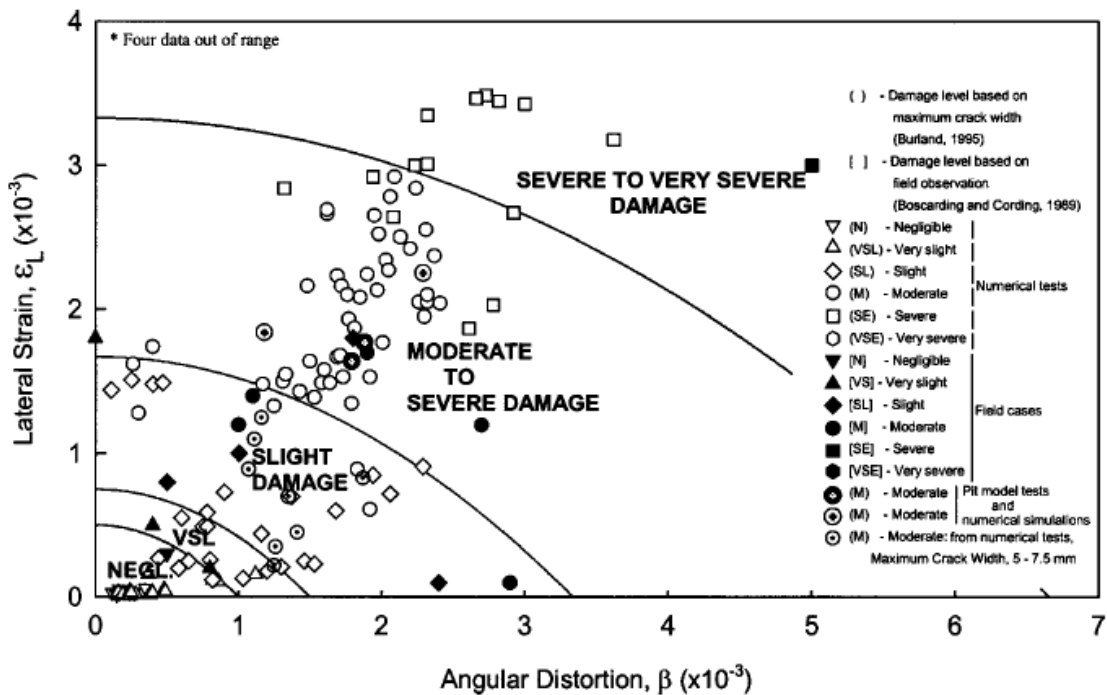

Figure 12 - Comparisons between damage estimation criterion and damage levels resulting from field observations, physical model tests, and numerical parametric studies. (From Son and Cording 2005)

Lastly, an important approach for analytical methods is the one proposed by Bird et al. (2005a,b) who suggested the use of analytical solutions to assess the expected damage to existing buildings (RC frame) due to liquefaction-induced differential ground movements. In particular, the authors derived the equations representing the deformational capacity of critical columns by applying principles of the displacement-based design; the column deformational demand related to ground motions was obtained on the basis of geometrical considerations. The structure deformation was idealized in four representative cases, hypothesizing differential vertical settlements and lateral movements associated with horizontal and vertical components. The study provides interesting conclusions regarding the damage mechanisms due to ground failure and the displacement demand of the floor columns for the RC framed structures, for which the displacement demand is concentrated to the ground floor columns while the upper stories generally rotate as a rigid body. Evolutions of the deep beam model were proposed by Finno et al. (2005) who proposed the use of the ratio EI/GA (instead of the ratio E/G first suggested by Burland and Wroth, 1974) to model the deformational behaviour of the building. The Authors argued that concrete floor slabs provide the main contribution to the bending stiffness of a framed structure building. Walls and diaphragms, instead, offer the main contribution to the shear stiffness.

The limiting values of some parameters that describe the foundation displacements were incorporated in the technical standards and represent today a good starting point for technicians and specialists in charge of either designing new buildings or predicting the response of existing buildings to changes in boundary conditions (e.g. due to anthropic activities). For instance, the Eurocode (EC7) establishes limiting values for foundation movements of new ordinary constructions (CEN, 2007b). A limitation of the Eurocode is that it refers to new constructions while no advices are provided for existing buildings.

As for numerical approaches, the proper use of advanced methods – such as finite element method (FEM) – allow estimating the values of parameters associated to ground and foundation movements via the adoption of appropriate constitutive models. Analyses can be uncoupled (the soil and the structure are studied separately, and the settlement trough is then imposed to the FE building model) or coupled (soil-structure interaction is modelled).

Interesting are the results obtained by Burd et al. (2000) via FE coupled analyses. The Authors highlight that: the building weight tends to increase the general magnitude of settlements that develop underneath; the building stiffness may reduce the differential settlements; depending on the building deformation mode (e.g. sagging or hogging), the soil-structure interactions effects may be more or less pronounced; the lateral restraint offered by the ground may reduce the extent of tensile stresses in the building; differential settlement values obtained as output of coupled analyses are lower than those of uncoupled analyses, which lead to inaccurate predictions. However, coupled analyses might be too complex and time consuming for practical vulnerability analyses. 2D FE analyses were also carried out by Liu, Houlsby, and Augarde (2000),

who investigated the effects of both the weight and stiffness of a masonry façade (with openings) and of its horizontal location with respect to the tunnel axis on the resulting damage.

What is important to underline is that all of these methods are referred to ordinary masonry and reinforced concrete buildings. Therefore, in literature, there are not applicable forms to 'non-ordinary' buildings, such as churches subjected to landslide.

1.3 FRAGILITY AND VULNERABILITY CURVES

The development of vulnerability information in the form of fragility curves is a widely practiced approach when the information is to be developed accounting for a multitude of uncertain sources involved. Fragility curves provide the probability of reaching or exceeding a given damage state as a function of the intensity of the natural event (Figure 13a), and they are usually modelled by lognormal functions. A very important point is that fragility curves clearly take into account that not all buildings of the same type will suffer the same level of damage for a given event intensity. Vulnerability curves (Figure 13b) are relationships between the mean amount of damage for a given type of building and the value of the event intensity. Vulnerability curves may be deduced from fragility curves with Eq. (1.4):

$$\mu_D = \sum P_k D_k \qquad\qquad\qquad (1.5)$$

where μ_D is the mean damage for a given intensity, P_k is the probability of a damage grade D_k, and k is the range of damage category (e.g. from 0 to 5 in the EMS-98 damage scale, Figure 6).
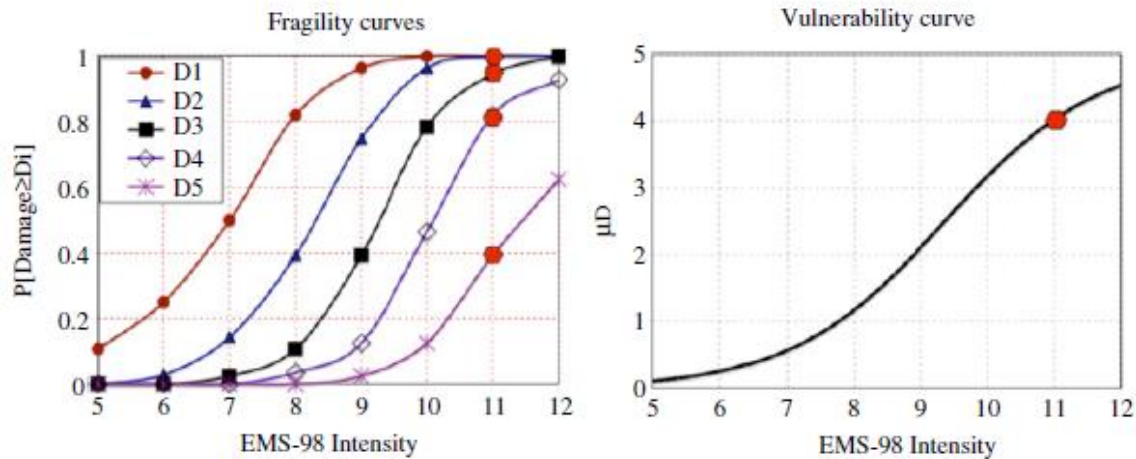

Figure 13- Fragility (a) and vulnerability (b) curve for seismic action

These predictive tools represent a good compromise between the accuracy of the results and the amount of time and money required for the studies; accordingly, they allow providing in a short time the due solutions to the issues related to the occurrence of abovementioned natural hazards whose detrimental effects are worldwide dramatically increasing. Depending on the scale of the analysis and on the basis of

the quality and quantity of available input data, both vulnerability and fragility curves can be generated via the statistical treatment of data collected via heuristic, empirical, analytical or hybrid approach (Saeidi et al. 2009; Negulescu and Foerster 2010; SafeLand Deliverable 2.5, 2011; Mavrouli et al. 2014). In particular, heuristically-based curves come from the expert judgment of people carrying out the related activities; empirical curves are based on data collected during post-event in-situ surveys; analytical relationships are obtained on the basis of results of numerical analyses performed on structural models; hybrid relationships combine observed data and analytical estimations in order to compensate the lack of observational data, the subjectivity of judgmental data and the modelling deficiencies of analytical procedures by combining observed data and analytical estimations. The generation of fragility and vulnerability curves usually requires a previous classification of the buildings in order to identify similar expected damage mechanisms on the basis of the parameters governing the building response (e.g., the building typology and geometry, the foundation type, the mechanical parameters of constituting materials, the type of resistant system and the efficiency of the connections). Moreover, generating analytical fragility/vulnerability curves based on numerical modeling can be extremely computationally intensive and time consuming; accordingly, this kind of curves cannot be easily developed for different areas or countries where, however, different construction techniques might be adopted. It is worth observing that fragility curves take into account that not all buildings of the same type will suffer the same level of damage for a given intensity of the dangerous phenomenon, while vulnerability curves are representative of the expected average damage for a given type of building for a given value of the danger intensity.

Vulnerability and fragility curves use the following three main types of input data:

1. A damage scale

2. A building typology

3. An intensity criterion.

In particular, the building damage severity can be classified using limiting values associated to global and local mechanical parameters of the structure; the building typology can be defined according to the parameters governing the resistance of the buildings against the considered danger (e.g. the building materials, age and the quality of construction, foundation type, etc.); the intensity parameter can be selected in relation to the analysed hazard, (e.g., for the earthquakes might be the pick ground acceleration PGA; for the slow-moving landslides might be differential displacement at the building foundation level).
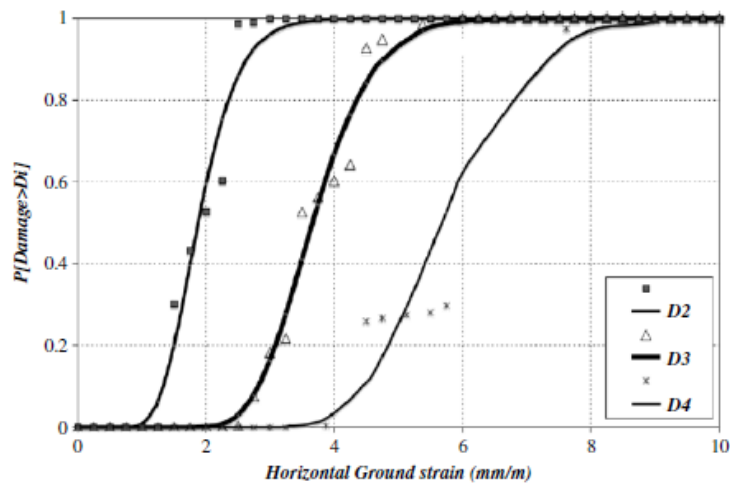
Figure 14 – Fragility curve from Saeidi et al. 2009 for subsidence

In the scientific literature there are many example and methods in the field of the earthquake engineering for the building vulnerability analysis via the generation of fragility and/or vulnerability curves (Sabetta et al. 1998; Rosetto et al. 2003; Lagomarsino et al. 2006, 2013; Cattari et al. 2004; Rota et al., 2006; Bilgin and Korini, 2012; Penna et al. 2013; Karapetrou et al. 2015, 2016; Zuccaro et al. 2015). Few examples can be recovered with reference to fragility and/or vulnerability curves generated for buildings in subsidence and slow-moving landslide-affected areas.

As for subsidence phenomena, the contributions of Saeidi et al. (2009, 2012) can be mentioned. The Authors generated fragility (Figure 14) and vulnerability curves on the basis of the use of empirical and analytical methods, tested and validated with a set of case-histories occurred in Lorraine in the period 1990-1996 and concerning masonry buildings and reinforced masonry buildings with lengths ranging from 10 to 20 m and heights from 7 to 10 m.

As for slow-moving landslides, the contributions of different authors (Negulescu and Foerster 2010; Fotopoulou and Pitilakis 2013a,b; Mavrouli et al., 2014, Pitilakis et al., 2015) are based on the adoption of numerical approaches. For instance, Negulescu and Foerster (2010) generated fragility curves, by assuming the differential displacement as the intensity parameter, with a methodology that consist in using a 2-D parametric non-linear static time history uncoupled analysis for a simple one bay - one storey cast in-place RC frame. Fotopoulou and Pitilakis (2013a,b) generated fragility curves for low-rise reinforced concrete buildings affected by slow-moving landslides triggered by earthquakes using an extensive numerical parametric study (with different idealized slope configurations, foundation typologies and soil settings as well as different distances of the structure to the slope's crest). Mavrouli et al. (2014) provide a general methodology for calculating the vulnerabilities of reinforced concrete frame structures via numerical

fragility curves; in particular, they considered three types of slope instability, namely: slow-moving landslides, rapid flow-type slides and rockfalls.

Scientific contributions on the generation of empirical fragility and vulnerability curves for buildings in slow-moving landslide-affected areas are proposed by Peduto et al. 2017, Peduto et al. 2019. The Authors presents a two-scale (medium and large) procedure for vulnerability assessment of buildings located in areas affected by slow-moving landslides. Their intensity derives from Differential Interferometric Synthetic Aperture Radar (DInSAR) satellite data analysis, which in the last decade proved to be capable of providing cost-effective long-term displacement archives. The analyses carried out on two study areas of southern Italy (one per each of the addressed scales) lead to the generation of both empirical fragility and vulnerability curves for buildings in slow-moving landslide-affected areas.

For the structural typology of churches, literature provides several methods for the evaluation of fragility curves in the field of the earthquake engineering. What is important to underline is the lack of methods for the development of fragility curves for churches subjected to landslides.

In this work, an innovative procedure is proposed for the identification of an appropriate intensity parameter able to describe the effects of slow-moving landslides in the perspective of obtaining fragility curves.

2. ANALYSIS OF THE CASE STUDIES, DEFINITION OF RECURRENT DAMAGE AND DAMAGE MECHANISMS

This Chapter introduces the results of a systematic damage survey investigation of historic masonry churches subjected to slow-moving landslides. According to Cruden and Varnes 1996, this type of landslides is characterized by soil displacements with a speed of some mm/year. Despite such displacements inducing differential vertical and horizontal displacements which are small in their instantaneous value, they can lead to severe damage and even collapse over time.

The first aim of this Chapter is to describe the criteria for the definition of the set of churches that have been the objective of the surveys. Secondly, the damage suffered by churches, in terms of crack patterns and deformations, is introduced as well as the identification of four global damage mechanisms.

The focus of this work is on Liguria, a region of Northern Italy that covers an area of 5418 km^2 and is confined within a narrow strip of land bounded to the North by the Alps and Apennines and to the South by the Ligurian sea. Due to its geographical location, orography and morphological and geological settings, landslides and floods frequently affect Liguria. According to the Italian archive of historical information on landslides and floods (http://sici.irpi.cnr.it, Guzzetti et al. 2004), 1806 landslide events damaged 1233 localities during the period 1800–2001 in the four Provinces of the Liguria Region. The IFFI project (Italian Landslide Inventory), developed by the ISPRA's department for the Geological Survey of Italy and aimed to survey landslides in Italy (Trigila et al 2008), shows that in the Liguria region 13.475 landslides occurred between 1164 and 2017. In particular, in 2017 an area of 536 km2, equal to 10.1% of the regional territory, was affected by landslides (Trigila et al 2018). According to the classification systems most widely adopted in the literature (Varnes 1978, Cruden and Varnes 1996, IUGS/WGL 1995), landslides can be categorized based on the kinematics of their movement, the type of material and the velocity. For the purpose of this work, only landslides characterized by slow movements (i.e. with a speed of the order of some mm/year) were considered. In a territory with such a high number of landslides, the assessment of the effects of landslides on the regional cultural heritage is a current and social issue to which scientific research must offer a contribution. In this respect, for each slope a set of parameters have been collected.

The activity presented in this Chapter is part of the National Research Program PRIN 2015 "PERICLES-Protecting the Cultural Heritage from water-soil interaction related threats" (grant n. 2015EAM9S5 from Ministry of Education, University and Research) carried out in collaboration with Prof. Chiara Calderini and Ph.D. candidate Chiara Ferrero from University of Genoa, Department of Civil, Chemical and Environmental Engineering.

Much of the content of Chapter 2 is published in:

2.1 CRITERIA FOR THE DEFINITION OF CASE STUDIES

2.1.1   CHURCHES LOCATED ON ACTIVE LANDSLIDES

The methodology adopted to identify the set of churches to assess the damage induced by slow-moving landslides is presented in this section.

Regarding slope movements, it is important to highlight that in Italy the identification and classification of the areas exposed to slow-moving landslide threats are closely related to environmental planning. With the law L. 18 maggio 1989, n.183 "Norme per il riassetto organizzativo e funzionale della difesa del suolo", Italy was divided in a series of hydrographic basins. For each basin, a Basin Authority was established, with the main task of developing the basin management plan. The latter had to include maps containing geological, morphological and hydrographic information regarding the area of interest as well as data concerning landslide, hydraulic and geological risk. Since the law n.183 provided only an indication of the contents of the basin plan, each basin authority adopted different criteria to develop its maps, with the result that they are not currently standardized at national level. This applies also to the maps providing information about zoning, classification, typology and state of activity of the landslides, which differ from one hydrographic basin to the other.

Regarding the Liguria region, its territory is divided in three different basins (Figure 15): Tyrrhenian basins for the portion of the Tyrrhenian drainage basins located in the Ligurian territory (the other portion belongs to the Tuscany region), Magra River basin and Po River basin. Different types of maps identify landslides areas in the three basins: landslide susceptibility maps for the Tyrrenian and Magra river basins and the "Atlante dei rischi idraulici e idrogeologici" for the Po river basin.

Different criteria are adopted in each map for zoning purpose and to identify landslides. In the case of the Tyrrhenian basin, the entire territory is divided in five classes of landslide susceptibility on a scale from Pg0 to Pg4. Pg4 class is characterized by the presence of active landslide, thus corresponding to the highest level of landslide susceptibility. Pg3 class is divided in two subclasses, Pg3a and Pg3b, respectively denoting areas with dormant landslide and territories with indirect indicators of movements (i.e. bent trees, damage on retaining wall, etc.) or stabilized landslides. The other three classes, Pg2, Pg1 and Pg0, only indicate the existence of geomorphological indicators, such as springs or cracks in the ground, but are not

actually affected by landslides. For the Magra basin, the same criteria adopted for the Tyrrhenian basin are used to define the classes of landslide susceptibility, but only the areas classified as Pg2, Pg3 and Pg4 are indicated in the landslide susceptibility maps. Regarding the Po River basin, the territory is not classified according to landslide susceptibility levels, but only the areas affected by active, dormant or stabilized landslides are reported in the "Atlante dei rischi idraulici e idrogeologici". In this case, landslides are represented either with their actual extension or with a dot when their perimeter is unknown.

Figure 15 identify landslide areas in the Ligurian territory based on the classification adopted in the maps of the three different basins. Note that these maps (hereafter named landslide maps) were downloaded from the website of each Authority basins, updated on 2017/18. It is also shown the location of the sample of the churches analysed, that will be defined in the following paragraphs.
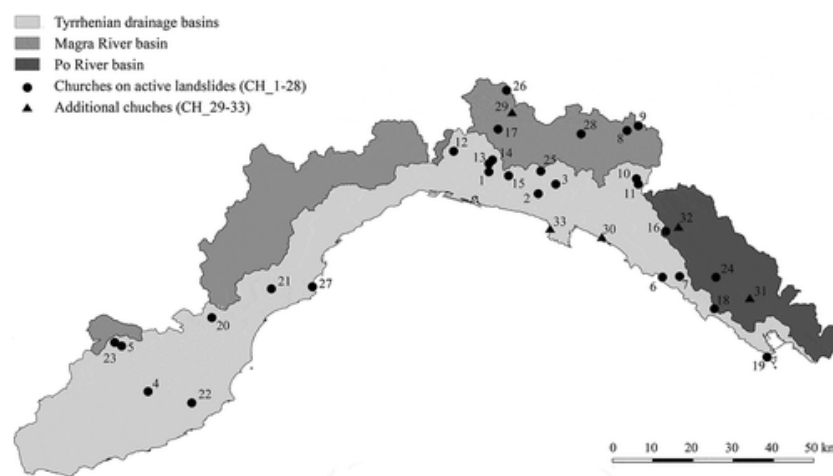

Figure 15 - Maps of landslide areas for the Tyrrhenian basins, Magra River basins and Po River basin and identification of the churches located on active landslide areas in the Liguria region.

With reference to the cultural heritage located in the Ligurian territory, the identification of the churches to analyse was carried out starting from the list of protected heritage buildings according to the Legislative Decree n.42 of 22/01/2004 (*Codice per i Beni Culturali e del Paesaggio*).

The map of the assets belonging to this list is available online (Figure 16). All the churches belonging to the list, as well as all the other religious buildings such as sanctuaries, oratories and chapels, were selected. It is to be highlighted that this approach takes into consideration only listed buildings, neglecting the presence of other churches that could be potentially exposed to landslide threats. However, with the aim to apply the methodology here presented, it is reasonable to select a limited number of case-studies at an early stage of the investigation.
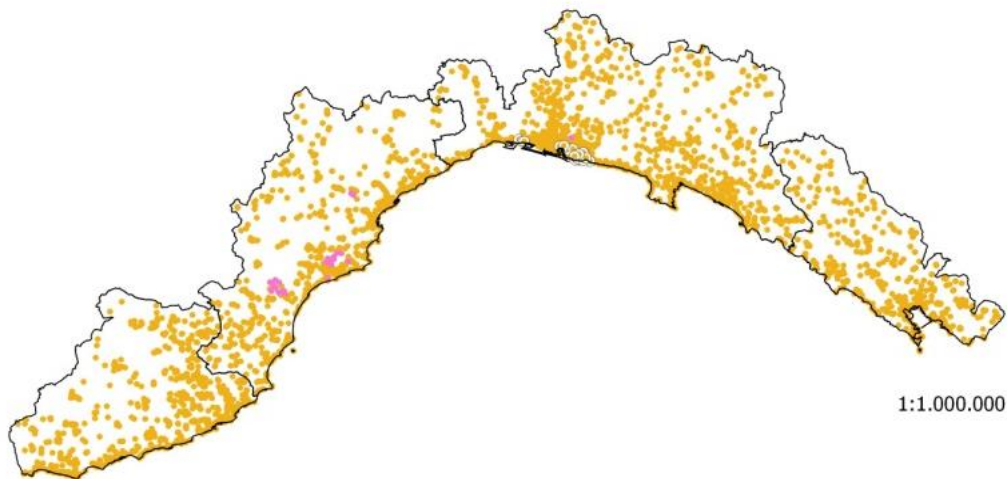
Figure 16 – Listed buildings in Liguria region

Once information about the location of both landslides and churches was collected, the case-studies to investigate were identified superimposing landslide maps on the regional map of the considered listed churches. This overlapping was performed by means of the QGIS software, which allows one to manage a large amount of data spread throughout a territory. Due to the different classification of the landslide areas present in the maps of the three basins of the Liguria region, different criteria were used to select the churches to study. Regarding the Magra River basin and Tyrrhenian basins, the churches located in the areas characterized by the highest landslide susceptibility, identified as Pg4, were considered. In the case of the Po River basin, the churches situated in areas affected by "active landslides" were selected. When landslides were represented in the maps by means of a dot and without borders, the choice fell on the buildings placed within a 50 m radius. The latter was defined based on the extension that usually characterizes landslide areas in the Liguria region. An example of superimposition of the two different maps is presented in Figure 17 for Sant'Olcese church in Sant'Olcese. Extended to the entire Liguria region, this approach led to the identification of 28 churches located on active landslide areas. These buildings, listed in

Table 2, were then selected as case-studies to be investigated in this work. The position of each church within the Ligurian territory is illustrated in Figure 15.

Figure 17 - Identification of churches located on active landslide areas: the case of Sant'Olcese church (GE).

Table 2 - Set of case-studies located on active landslides

Id	Church name	Municipality, locality, province
CH_1	San Pietro Apostolo di Pino	Genova (Loc. Pino Soprano) (GE)
CH_2	Santo Stefano	Lumarzo (Loc. Pannesi) (GE)
CH_3	San Rocco parish church	Neirone (Loc. Ognio) (GE)
CH_4	San Pietro in Vincoli parish church	Borgomaro (Loc. Ville San Pietro) (IM)
CH_5	Santa Caterina	Mendatica (IM)
CH_6	Santa Maria Assunta	Moneglia (Loc. Lemeglio) (GE)
CH_7	Sant'Anna parish church	Deiva Marina (Loc. Piazza) (SP)
CH_8	San Rocco oratory	Rezzoaglio (Loc. Alpepiana) (GE)
CH_9	San Bernardo da Mentone	Santo Stefano d'Aveto (Loc. Ascona) (GE)
CH_10	Santa Maria Assunta	Borzonasca (Loc. Prato Sopralacroce) (GE)
CH_11	San Giacomo oratory	Borzonasca (Loc. Prato Sopralacroce) (GE)
CH_12	San Martino	Ceranesi (Loc. San Martino di Paravanico) (GE)
CH_13	Sant'Olcese	Sant'Olcese (GE)
CH_14	San Giovanni Battista oratory	Sant'Olcese (GE)
CH_15	San Martino di Struppa	Genova (Loc. Struppa) (GE)
CH_16	San Pasquale Baylon	Maissana (Loc. Disconesi) (SP)
CH_17	San Pietro Apostolo	Savignone (GE)

CH_18	Santa Maria del Soviore sanctuary	Monterosso al Mare (Loc. Soviore) (SP)
CH_19	San Pietro	Portovenere (SP)
CH_20	Madonna della Neve	Erli (SV)
CH_21	San Bernardo chapel	Calice Ligure (Loc. Eze) (SV)
CH_22	Santa Margherita	Diano Arentino (IM)
CH_23	Santi Nazario e Celso parish church	Mendatica (IM)
CH_24	Nostra Signora di Roverano chapel	Carrodano (SP)
CH_25	San Tommaso di Boasi	Lumarzo (Loc. Boasi) (GE)
CH_26	Santi Cosma e Damiano	Vobbia (Loc. Arezzo) (GE)
CH_27	Nostra Signora Addolorata chapel	Noli (SV)
CH_28	Cassingheno parish church	Fascia (Loc. Cassingheno) (GE)
Loc. = locality; (GE) = Genova; (IM) = Imperia, (SP) = La Spezia; (SV) = Savona		

Once the churches to be investigated were identified, firstly further information about landslide and geotechnical soil characterization in the surrounding areas was collected and analysed.

Regarding landslides, useful data were found in the "Atlante dei Centri Abitati Instabili della Liguria" (hereafter called Atlante) (Federici et al., 2001), a monograph collecting the studies carried out on the historic centres of the Ligurian territory that were affected by phenomena of slope instability. For each centre, the Atlante provides maps, updated between 2001 and 2007, showing geological conformation, state of activity and type of movement of the landslide, i.e. falls, topples, slides, lateral spreads, flows and complex landslides (Varnes, 1978). In order to evaluate any potential evolution of the landslide areas over time, the maps of the Atlante and the ones of the basins plan, more recent since updated on 2017/2018, were superimposed, as illustrated in Figure 18. Furthermore, the landslide direction was estimated on the basis of the orientation of the symbols used in the maps of the Atlante to represent the different typologies of landslide (Figure 18). When the churches were located in areas not included in the maps of the Atlante, landslide maps together with the contour levels of the slope were used to identify a potential direction of the landslide movement. Lastly, in order to have a more complete characterization of the landslide area, geotechnical data based on geological surveys, in situ tests, inclinometers or piezometers installed in the landslide area, when available, were searched for and analysed.

Then, an accurate research was carried out in the Archives of the Soprintendenza Archeologia, Belle arti e Paesaggio per la Citta' metropolitana di Genova e le province di Imperia, La Spezia e Savona (Italian National Trust) in order to obtain any useful material or information regarding the churches (i.e. historical information, geometry, past alterations). For some churches, a detailed documentation was found including,

for instance, historical information, surveys, past crack surveys and description of past interventions. However, not every church had all these documents available: in many cases, even plans and elevations were not existing or were incomplete, so this involved their elaboration or verification during the inspections. When available, this material was integrated with any additional source (i.e. bibliographical references, informational brochure, Curia website).
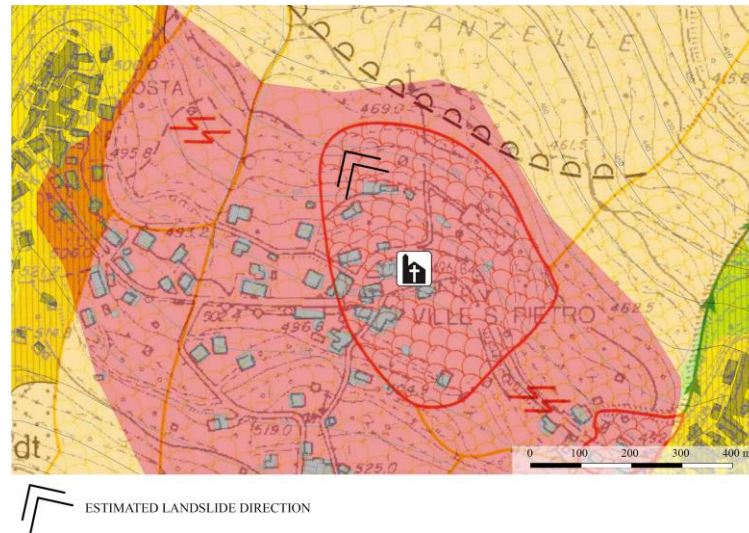

ESTIMATED LANDSLIDE DIRECTION

Figure 18 - Superimposition of the Atlante with the landslide susceptibility maps

2.1.2   ADDITIONAL CHURCHES

During the activity of identification of the churches to investigate, some cases of churches that experienced damage, potentially due to soil displacements were reported. Checking the position of these churches on landslide maps (Figure 19), it was observed that two churches were located close to active landslides, one was situated on a Pg3 area and two were located near Pg3 areas. The distance of each church from the nearest active or dormant landslide is reported in Table 3. For the purpose of this work, these five additional churches were included among the case-studies (that are thus 33 overall) to be investigated in order to compare their damages with the cracking pattern exhibited by churches located on active landslides.

HYDRAULIC AND HYDROGEOLOGICAL RISKS
■ Active landslides   ■ Areas prone to falls

LANDSLIDE SUSCEPTIBILITY LEVEL
■ Pg2 - Moderate   ■ Pg3 - High
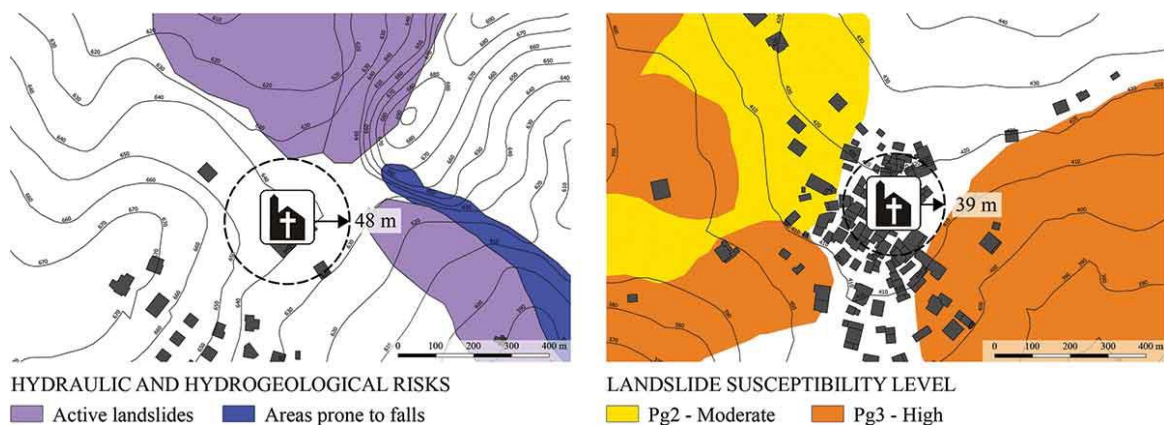
Figure 19 – Position of additional churches on landslide maps: a) Bastia Sanctuary located close to active landslides,
b) San Martino church in Cembrano located close to a Pg3 area.

Table 3 - Additional churches: identification and position on landslide maps

Id	Church name	Municipality, locality, province	Position on landslide maps
CH_29	Nostra Signora della Bastia sanctuary	Busalla (Loc. Bastia) (GE)	48 m from active landslide*
CH_30	Nostra Signora delle Grazie sanctuary	Chiavari (GE)	Pg3 (34 m from Pg4)
CH_31	San Lorenzo	Follo (Loc. Sorbolo) (SP)	Pg3
CH_32	San Martino di Cembrano	Maissana (Loc. Cembrano) (SP)	Pg0 (39 m from Pg3)
CH_33	San Nicolò di Capodimonte	Camogli (Loc. San Rocco) (Ge)	Pg2 (70 m from Pg4)
Loc. = locality; (GE) = Genova; (IM) = Imperia, (SP) = La Spezia; (SV) = Savona; * = Po River basin			

2.2 SURVEY METHODOLOGY

The methodology adopted for the inspection and damage survey of the 33 churches selected as case-studies is here presented. Firstly, the damage observed in each church was surveyed and mapped in detail. When a geometric survey was available, cracks and distortions were marked on it, otherwise simple sketches of plans and elevations were traced on site using laser distance meters and measuring tapes. All the information collected were then converted into a digital format. Three levels of width were considered: 1) thin for a width up to 1 mm (the latter included); 2) medium for a width included between 1 mm and 5 mm; and 3) large for a width equal or larger than 5 mm. Crack width was accurately measured by means of crack scales and calipers for cracks that were easily accessible, while it was only estimated for cracks located at a significant height from the ground level. Regarding the damage of the floor, a further distinction was made between cracking of tiles and gaps among tiles (further explanation is provided in the paragraph about damage). Finally, construction joints were identified and distinguished from other damage signs since they are related with the construction process of the building.

In addition to the cracking pattern, out-of-plumbness in the vertical elements and sinking of the floors were surveyed and, when possible, measured by means of electric bubble levels or out-of-plumb wires.

Lastly, as shown in Figure 20, for each church an inspection of the surroundings was performed in order to detect any potential evidence of the presence of soil movements: cracks and distortions in neighbouring buildings, cracking of the retaining wall of the embankment on which the church parvis is resting, cracking in road surfaces, inclined lampposts or trees.

Appendix 1 shows the crack pattern for each church analysed (Ferrero et al. 2020).
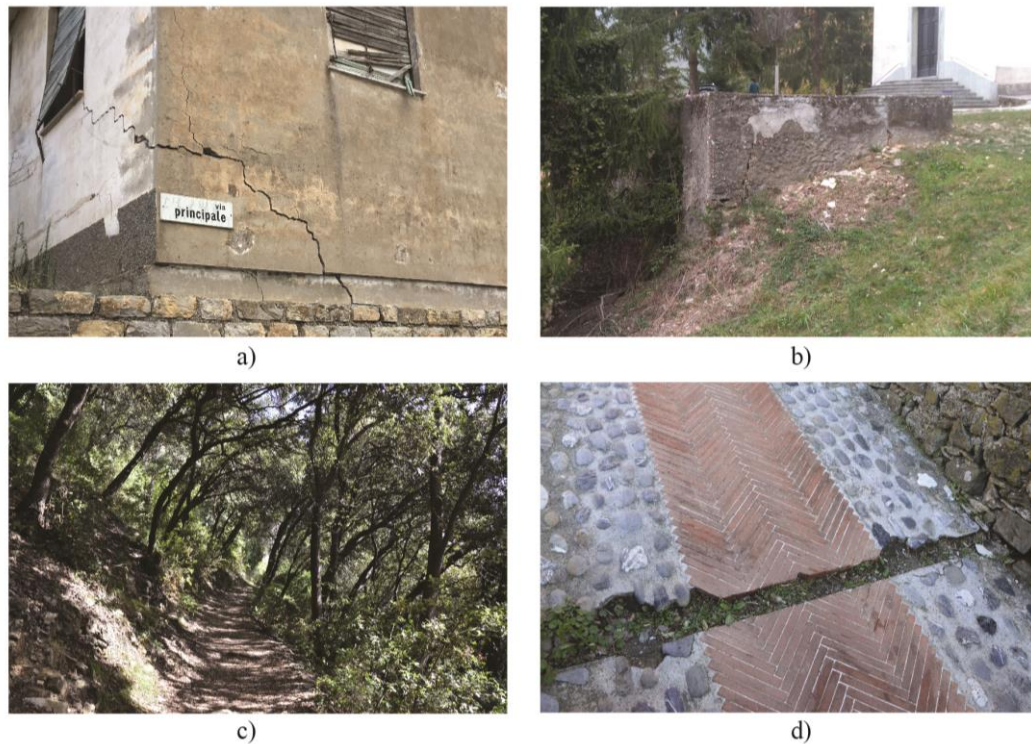

Figure 20 - Inspection of the surroundings to detect the presence of soil movements: a) cracks in neighbouring buildings, b) cracks in the retaining wall of the embankment on which the church parvis is resting, c) inclined trees, d) cracking in road surfaces.

2.3 GEOTECHNICAL DATA ANALYSIS

For each case study, in addition to the structural information and the survey of the damage experienced by the church, information regarding the landslide were collected. From the website of Liguria region (geoportal.regione.liguria.it/) it is possible to download data about geological surveys, geotechnical investigations, in situ tests, inclinometers or piezometers installed in the landslide area, when available. What came out from this analysis is that landslide and subsoil data and information are often missing or not complete.

Table 4 shows, for each case study, the available soil stratigraphy in the neighbouring of the church, the presence of a monitoring system of the landslide (inclinometers and piezometers), Synthetic Aperture Radar SAR data of the area and the position of the church in the landslide map.

Table 4 shows that the majority of the case studies is characterized by SAR data. The basic concept of Synthetic Aperture Radar is based on the observation that a given target is imaged in a certain number of echoes during the passage of the sensor. All satellites equipped with SAR sensors orbit the earth on a near-polar orbit at an altitude ranging from 500 to 800 km above the earth's surface, depending on the satellite platform hosting the SAR sensor, and follow polar orbits in order to provide a global coverage. SAR Satellite Interferometry is therefore a technique for measuring the superficial displacements of the territory. Through radar images, acquired by satellites in the same area, it is possible to measure displacements with millimetre precision of land and structures. ERS satellite (in orbit from 1992 to 2011) has a resolution of 20x5m, like ENVISAT satellite (in orbit from 2001 to 2012). COSMO SKYMED is in orbit since 2008, is characterized by a higher resolution than ERS and ENVISAT (1x1m). In order to have serviceable information relating to the soil displacements it is necessary that the areas of interest are covered both by ascending and descending orbits (Cascini et al. 2010, Di Maio et al. 2018).

Figure 21 shows an example referred to case CH_32: the targets available for all the SAR satellites are covered by both ascending and descending orbits. For each point, the values of the mean velocity and displacement are available. In summary, the main issues related to the analysed case histories are the following:

- Only few sites of the 33 here considered are "well exposed" to the satellite orbits in order to have useful information about landslide movements;
- Only 3 cases over 33 are covered by ENVISAT, ERS and COSMO SKYMED satellite with both ascending and descending orbit;
- Only after a detailed and specific analysis of these few data, their post processing to get the average velocity and displacement components, some useful results could be obtained;
- For these reasons, the data from SAR can only give general information about the presence of movement and its entity in terms of absolute velocity and displacement.

Table 4 – Landslide/subsoil information available for the case studies

Id	Soil stratigraphy in the vicinity	Inclinometer/ piezometer	SAR Interferometry data	Position on landslide map
CH_1	Yes	No	ENVISAT/ERS	Active landslide
CH_2	No	No	ERS	Active landslide
CH_3	Yes	No	ENVISAT/ERS	Active landslide
CH_4	Yes	Yes	ENVISAT/ERS	Active landslide
CH_5	Yes	Yes	ENVISAT/ERS	Active landslide

CH_6	No	Yes	COSMO SKYMED	Active landslide
CH_7	No	Yes	No	Active landslide
CH_8	No	No	ERS	Active landslide
CH_9	No	No	COSMO/ENVISAT/ERS	Active landslide
CH_10	No	No	COSMO/ERS	Active landslide
CH_11	No	No	COSMO/ERS	Active landslide
CH_12	Yes	No	ENVISAT	Active landslide
CH_13	Yes	Yes	ENVISAT	Active landslide
CH_14	Yes	Yes	ENVISAT	Active landslide
CH_15	Yes	No	ENVISAT	Active landslide
CH_16	No	No	COSMO/ENVISAT/ERS	Active landslide
CH_17	No	No	ENVISAT	Active landslide
CH_18	No	No	No	Active landslide
CH_19	No	No	ENVISAT	Active landslide
CH_20	No	No	No	Active landslide
CH_21	No	No	No	Active landslide
CH_22	No	No	No	Active landslide
CH_23	No	Yes	ENVISAT/ERS	Active landslide
CH_24	No	No	COSMO SKYMED	Active landslide
CH_25	No	No	ENVISAT/ERS	Active landslide
CH_26	No	Yes	No	Active landslide
CH_27	No	No	No	Active landslide
CH_28	Yes	Yes	No	Active landslide
CH_29	Yes	No	No	48 m away from active landslide
CH_30	No	No	No	Pg3 (34 m away from Pg4)
CH_31	No	No	ENVISAT	Pg3
CH_32	Yes	Yes	COSMO/ENVISAT/ERS	Pg0 (39 m away from Pg3)
CH_33	Yes	Yes	No	Pg2 (70 m away from Pg4)

Figure 21 – Target available for all the SAR satellite (CH_32), respectively on the top ascending and on the bottom descending orbits

Table 4 also suggests that few landslides have been monitored (11 over 33) and for only a small sample (11 over 33) stratigraphical information are supplied, sometimes referred to shallow soil strata. When the geotechnical data were available, an attempt of defining a reliable geological/ geotechnical soil model has been made, as shown in Figure 22 for CH_28 (Berardi and Cambiaggi 2019). In other cases, like CH_22 (Figure 23 illustrates the related crack pattern), no stratigraphical, monitoring nor SAR information were available even if the case presented very severe damage condition to prohibit the access to the church. All the previous observations allow to remark that too often geotechnical information and data are not complete or completely missing, making the general study of landslide and their interaction with structures particularly complex.
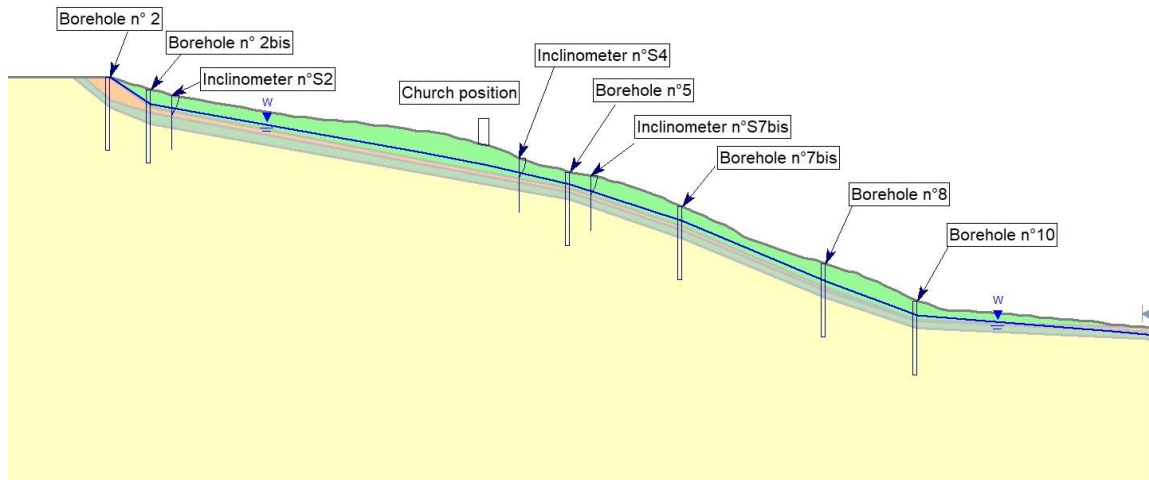
Figure 22 - Geotechnical and instrumentation information for CH28
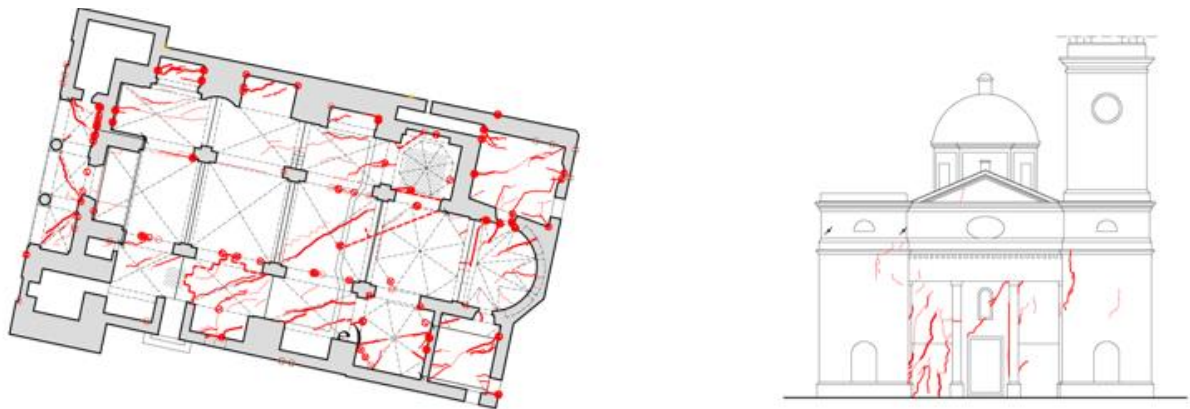
Figure 23- Crack pattern for CH_22

2.4 DAMAGE OBSERVED: STRUCTURAL ANALYSIS

A detailed analysis of the deformation and crack pattern of the 33 churches inspected was performed in order to detect the presence of recurrent types of damage. It is important to point out that not all the damage observed can be attributed to landslide phenomena. It is well known that many factors such as construction process, foundation problems (settlement/ bearing capacity), natural disasters (e.g. earthquakes) and many others can contribute to the damage exhibited by historical masonry structures (Roca et al. 2010). Only a deep knowledge of the building, including materials, geometry, construction details and history, can lead to a correct interpretation of the cracking pattern and its causes. Consequently, the main aim of the research presented in this Chapter is to describe critically the damage detected in the set of churches under consideration and to associate it with slope movements. The deformation and damage patterns observed

during the inspections is described for the different structural elements composing the church: 1) floor; 2) walls and pillars; and 3) arches and vaults.

1) Damage in the floor may arise in the form of cracking of the tiles, gaps among tiles or sinking. The former is usually localized in few tiles and it is especially observed on step treads (Figure 24a). Contrarily, the latter creates a well-defined cracking pattern on the floor, which is usually consistent with the direction of the damage pattern in the vaults (Figure 24b). This fact can be attributed to the occurrence of a global mechanism induced in the church by soil movements. Furthermore, in some cases, a continuity between the cracks on the floors and the ones in the lateral walls is present, which is a peculiar separation mechanism of the church in the transverse direction (Figure 24c). In addition to this type of damage, the presence of dips in the floors is often observed (Figure 24d), this resulting in some cases in buckling of some tiles. Finding a correlation between this type of damage and landslide is not straightforward since other soil movements can produce this effect.
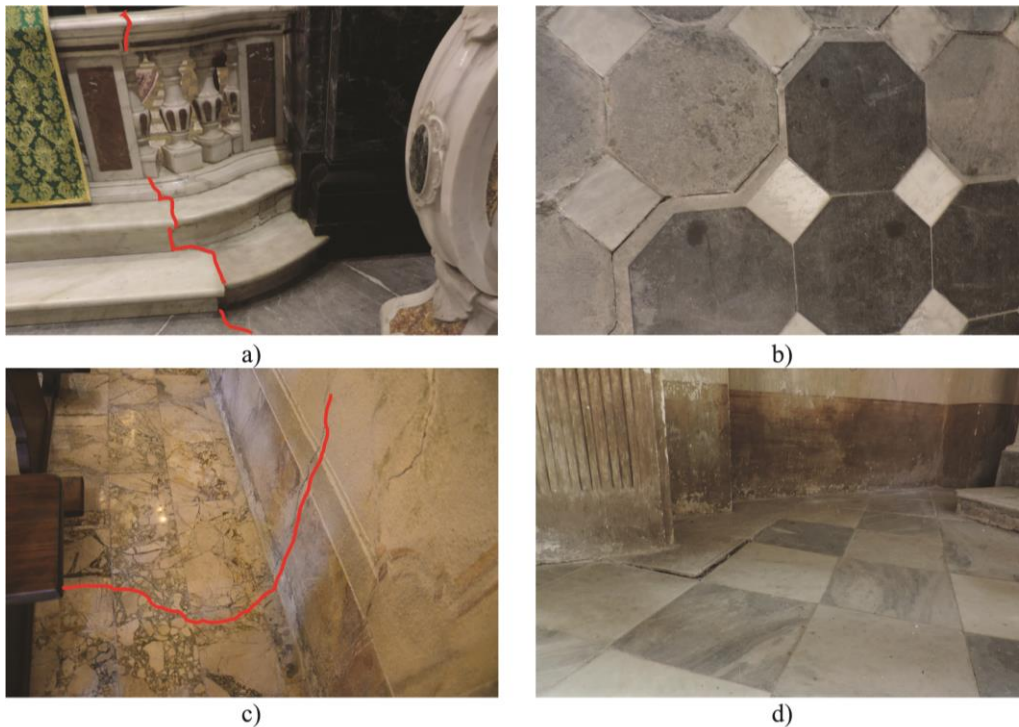
Figure 24 – Damage in the floors: a) cracks on step treads and balustrades bases (CH_17), b) saw-tooth gap among tiles (CH_22), c) cracks propagating from floor to wall (CH_28), d) lifting of tiles due to sinking (CH_22).

2) The majority of the churches are affected by the presence of cracks in the façade as well as in lateral walls. As for the cracking pattern in the façade, shear cracks are usually located close to the openings and inside alcoves (Figure 25a). Regarding the damage experienced by lateral walls, they frequently exhibit cracks extending upwards from the base of the structure, as shown in Figure 25b where crack increase in width with the height of the wall. Cracks can develop in vertical (Figure 25b) or inclined directions (Figure 25c) and, in some cases, they extend along the entire height of the walls and continue from the floor into the vaults within them (Figure 25d). The development of the cracks may be an indication of the predominant soil displacement: vertical in case of inclined cracks or horizontal for vertical cracks. In addition to the cracking pattern described above, significant rotations and out-of-plumbness were observed in the lateral walls and pillars of a number of churches. From Figure 25e it can also be observed that these rotations and out-of-plumbs usually produce large distortions in the arches as well as loss of horizontality in metallic tie-rods, where present.
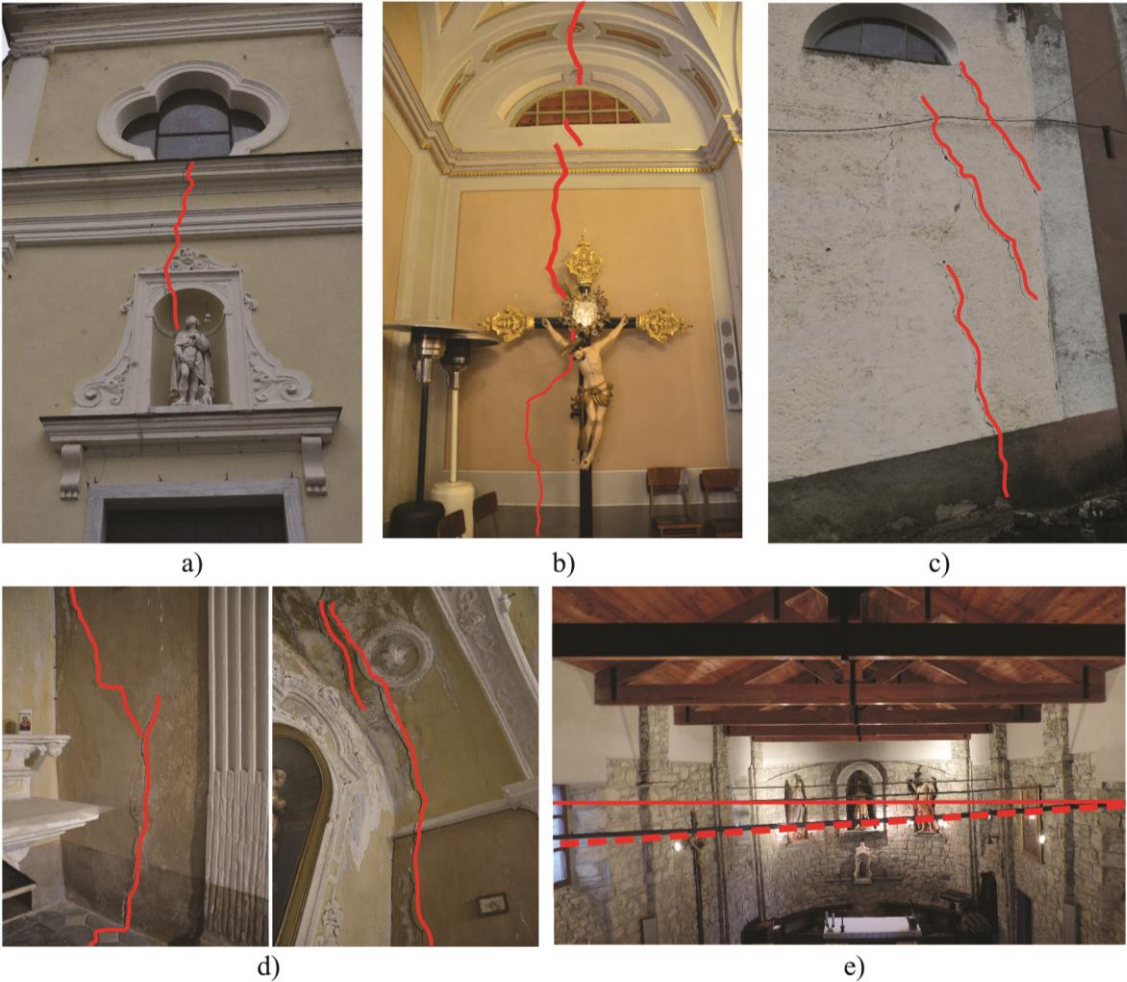
Figure 25 – Damage and deformation in vertical element: a) cracks in the façade wall next to openings (CH_3c) cracks in the apse wall between openings (CH_28), b) vertical cracks in longitudinal walls propagating from the

level of the ground (CH_22),c) diagonal cracks in longitudinal walls propagating from the level of the ground (CH_9), d) vertical cracks in lateral walls extending from the level of the ground and continuing up into vaults (CH_22) e) loss of horizontality of metallic tie-rods (CH_8)

3) Recurrent damage patterns are identified in arches and vaults. As shown in Figure 26a, large deformations are observed in the arches, which are accompanied by the occurrence of some cracks along the section of the arch. The cracking pattern observed in the arches can be in general symmetrical (Figure 26b) or asymmetrical (Figure 26c). This behaviour can be due to the formation of rotational or sliding hinges, which results in an asymmetrical or symmetrical crack distribution respectively. However, it can also be reasonably explained by different combinations of differential vertical and horizontal displacements at the supports. As for the vaults, a different behaviour and type of damage is exhibited by different types of vaults. Barrel vaults, which are made of a continuous series of arches and, hence, are characterized by a bi-dimensional response, usually show a cracking pattern similar to the one exhibited by arches, with the opening of some cracks along their sections (Figure 26d). Conversely, cross vaults, which have a double curvature leading to a tri-dimensional behaviour (DeJong, 2016), mainly present diagonal shear cracks (Figure 26e). It is important to note that these cracks are usually repeated in the different bays of the church, thus composing a well-defined damage pattern that can be related to the direction of the moving landslide.

Figure 26 - Damage and deformation in arches and vaults a) large deformations (CH_13), b) symmetrical crack pattern (CH_4), c) asymmetrical crack pattern (CH_13),d) longitudinal cracks along the vaults (CH_22),e) diagonal cracks along one of the ribs in cross vaults (CH_22)

2.5 IDENTIFICATION OF DAMAGE MECHANISMS

By observing the cracking patterns of the 33 churches as a whole and considering their possible link with landslide direction, it was possible to identify four global damage mechanisms involving the church in its entirety: (i) hogging, (ii) extension, (iii) rigid rotation, and (iv) shear deformation. For each mechanism, Figure 27 and Figure 28 show the associated soil displacement pattern and the damage pattern (3D view, plans and/or elevations) of a specific church exhibiting that mechanism.

As for as hogging (along the length of the nave) is concerned (Figure 27 a), the structure exhibits vertical cracks in the longitudinal walls, which are repeated in each bay in the middle of the wall. These cracks progress over the entire height of the wall, increasing in width with height, and propagate in the vaults oriented perpendicular to the longitudinal walls. No significant cracks or gaps are observed in the floor. This damage mechanism can be attributed to a concave-downward bending (hogging) of both soil and structure (Cooper, 2008), produced by displacements, primarily vertical, in the direction of the longitudinal axis of the church. This mechanism can be clearly observed in CH32.

In the case of the extension mechanism (Figure 27b), a similar damage pattern is present in both vaults and floor. Multiple parallel diagonal cracks are observed in the vaults, oriented in the same direction as the series of parallel gaps in the floor. It is important to note that these gaps indicate that tiles moved apart in the horizontal direction without experiencing any local vertical displacement. In addition, severe vertical cracks occur in the walls in planes perpendicular to the landslide direction. It is observed that these cracks propagate from the level of the ground and cut the structure over its entire height from the floor to the vaults, thus indicating that it suffered extension in the direction of the acting landslide. Despite landslide phenomena tend to produce a combination of downward and lateral movements (Cooper, 2008), the horizontal separation between tiles as well as the occurrence of vertical cracks in the walls indicate that a significant component of horizontal displacement should be present in the extension mechanism. This mechanism can be clearly detected in CH22.

The rigid body rotation mechanism (Figure 28a) is associated with significant out-of-plumbs of the lateral longitudinal walls in the direction of the landslide, distortions in the transverse arches and loss of horizontality of metallic tie-rods. This damage pattern can be produced predominantly by a differential settlement, in the direction of the transverse axis of the church. This mechanism can be observed in CH31.

Finally, in the case of shear deformation (Figure 28b), severe diagonal cracks propagating from the level of the ground are observed in the longitudinal walls at both sides of the church. Differently from the hogging mechanism, these cracks are not repeated in each bay but are localized in a single portion of the wall. A crack/gap in the floor propagates between the cracks affecting the opposite walls. This damage mechanism may be attributed to a differential settlement, in the direction of the longitudinal axis of the church. This mechanism can be observed in CH9.

In conclusion, this first part of the work led to a better understanding of the churches' response to landslide movements. In particular, it was possible to identify recurrent damages that allowed the definition of four global damage mechanisms. Each mechanism is associated with the prevalence of the vertical or horizontal displacement component of the slope movement. In the following Chapter, numerical analyses will be performed in order to better understand the landslide effects in terms of associated displacement patterns.
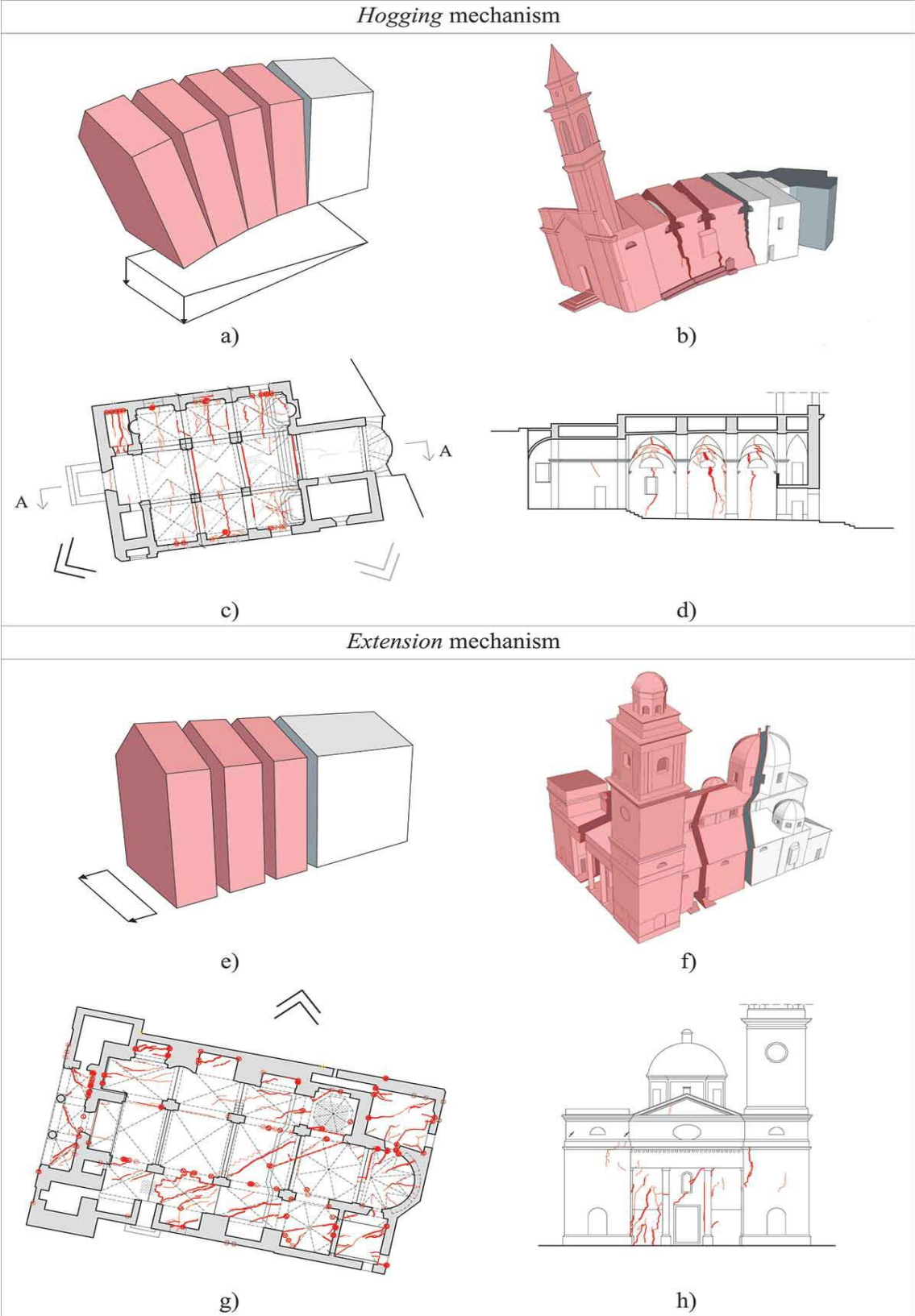
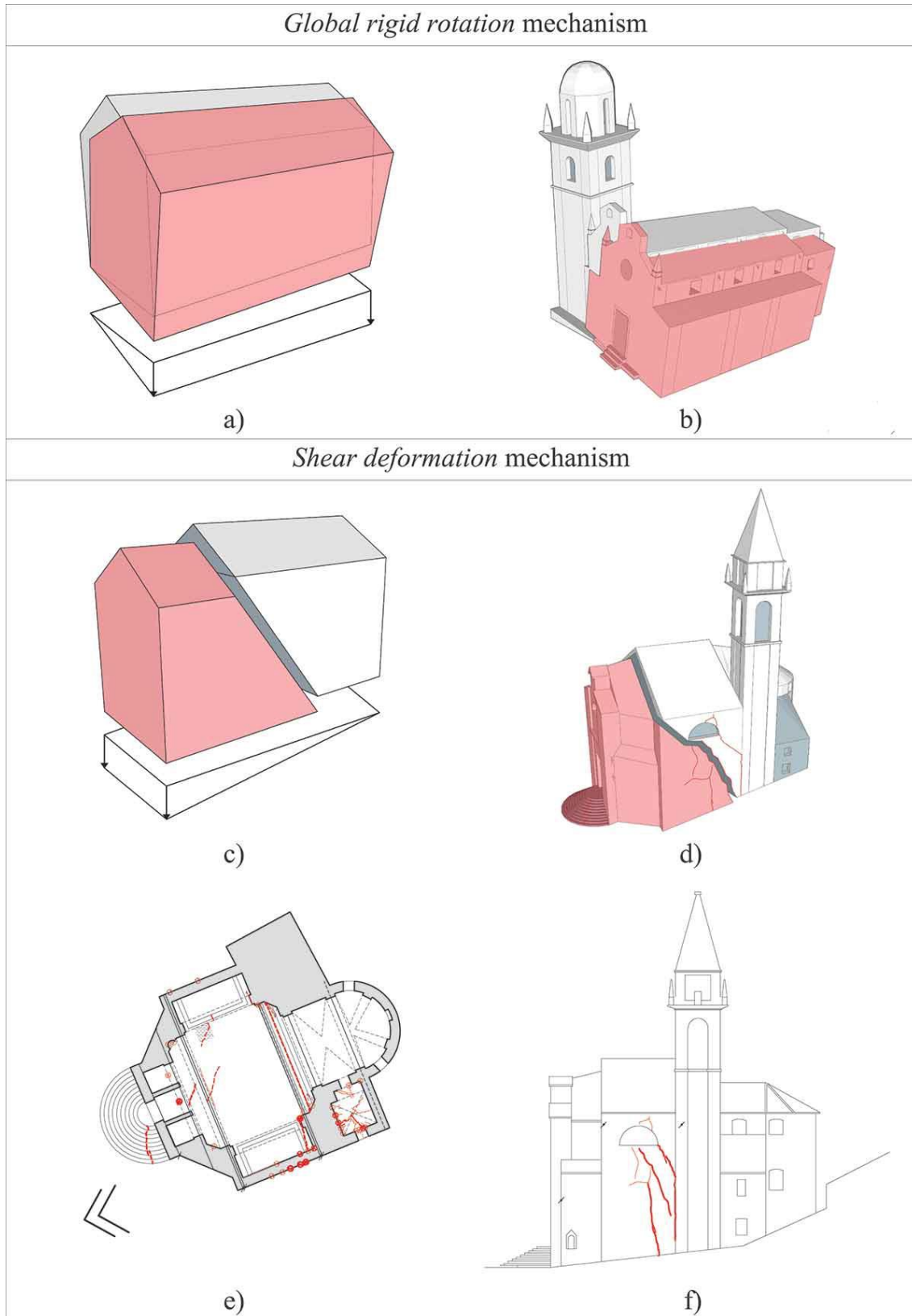Figure 27 - Hogging (a) and extension (b) mechanisms

Figure 28 - Rigid rotation (a) and shear deformation (b) mechanisms

3. PROCEDURE FOR THE ANALYSIS AND PREDICTION OF THE EFFECT OF SLOW-MOVING LANDSLIDE VIA NUMERICAL APPROACH: INFINITE SLOPE MODEL

Since the aim of this research is the development of a procedure for the analysis and the prediction of the effect of slow moving landslide on historical building, in particular churches, this Chapter will show the infinite slope model that have been developed, in order to be able to evaluate the displacement profiles (under free-field condition) and the definition of an intensity parameter. These values will be used as a database for the evaluation of the deformation to which the structure will be subjected, with a fixed geometry of the slope and the introduction of a Hazard Factor. In this Chapter, no data from the real slope of Chapter 2 has been used since the main objective is to develop a procedure for the analysis of the slow-moving landslide in a very generic case.

The contents of Chapter 3 are published in:

Cambiaggi L., Berardi R. Identification and modelling of displacement fields due to slope movements for the vulnerability analysis of historic buildings. *XVII European Conference on Soil Mechanics and Geotechnical Engineering ECSMGE, Reykjavik Iceland 2019 ISBN 978-9935-9436-1-3.*

3.1 MODEL OF THE SLOPE AND PRELIMINARY ANALYSES

The first step involved the modelling of the slope as an "quasi-infinite slope" model, in order to carry out a first set of parametric analyses aimed at the evaluation of the influence of geometric and geotechnical parameters of the slope. The infinite slope model is the oldest and simplest slope stability method that assumes identical conditions occur on any vertical section (Figure 29). Infinite slope equation for the factor of safety (FS) of a homogeneous Soil with both cohesion, c', and internal shearing resistance φ', with seepage parallel to the slope in this case is given by:

$$FS = \frac{(H\gamma \cos^2 i - u)\tan\phi' + c'}{H\gamma \sin i \cos i}$$

(3.1)

where the independent variables have the following meanings:

- H depth of the soil layer to the potential failure surface
- *i* slope inclination
- γ bulk unit weight
- u pore pressure at the base of the slice

- ϕ' angle of internal shearing resistance at the base of the slice
- c' effective cohesion at the base of the slice
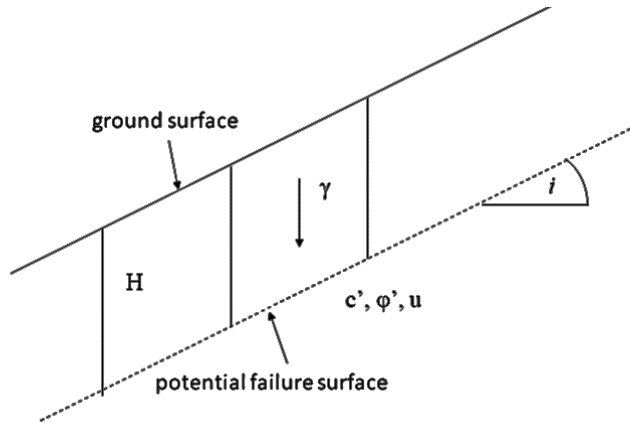
Figure 29 - Infinite slope scheme

As well known, limit equilibrium method (LEM) with the infinite slope scheme, can only provide changes of the safety factor values when soil proprieties, pore pressure and slope inclination change. In order to have indication of the slope displacements, numerical approaches have to be considered and "coupled" with LEM solutions. In this regard, using a plane strain, finite element model (hereafter called FEM) adopting PLAXIS 2D software, slope schematization has been simplified with the purpose of performing several parametric analyses. A typical 2D mesh, composed of 15-noded elements and fine element size, with boundary conditions and two soil layers (typical stratigraphical sequence in a slope: a superficial blanket overlying a stiff and resistant bedrock) is illustrated in Figure 30, that also shows the different sections taken into consideration. Obviously, Section 2,3 and 4 better represent the "quasi-infinite slope" response. The interface between the materials has been modelled as rigid: the interface properties are the same as the soil properties in the data set, no reduced strength will be applied. The initial stress state has been generated by *Gravity Loading* procedure. In this type of calculation initial stresses are generated based on the volumetric weight of the soil.

In order to obtain displacements and failure conditions, a simple elastic-plastic constitutive model with Mohr-Coulomb failure criterion has been adopted for both the two soil layers.

In these parametric analyses, ground properties have been chosen considering the following main criteria:

-        stiffness and strength parameters have to representative of typical and actual soil conditions, often observed in a two-layered slope scheme;

-       the values of the mechanical parameters must correspond to the ones possibly obtained by the available investigation results.
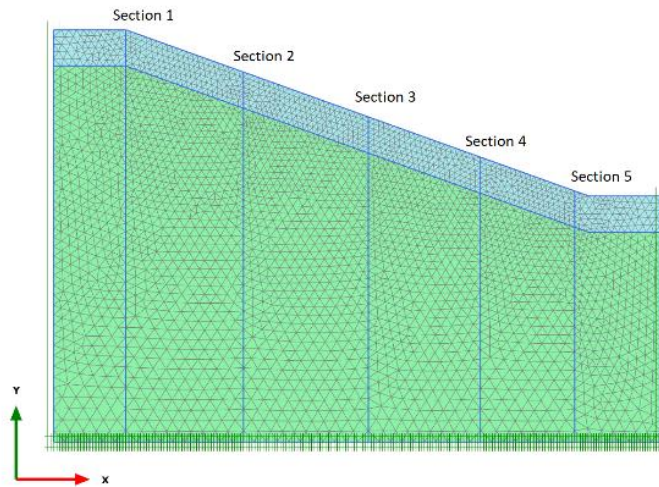
Figure 30 – Mesh and sections analysed

As far as soil modulus is concerned, a literature review has been made to investigate typical values of primary and secondary wave (V_p and V_s) in superficial blanket, to be compared with some results available from performed geophysical test (see section 2.3).

Many Authors have proposed typical P-wave velocities in different materials and ground conditions that could be representative for the analyses here proposed; as an example, Table 5 reports values that well correspond to the ones measured in some of the case histories analysed.

Table 5 – Primary wave velocity, adapted from Lowe and Zaccheo (1991) and Abramson et al. (2002)

Material	Wave velocity V_p (m/s)
Dry silt, sand, loose gravel loam, loose rock, talus, and most fine-grained top soil.	180-760
Talus, loose rock	380-760
Top soil, dry	180-275
Top soil, wet	300-760
Rock, weathered, fractured or partly decomposed	610-3050
Limestone, soft, weathered	1700-4200
Schist, soft, weathered	790-2400

Schist, hard	2750-4700

The evaluation of P-wave and S-wave is given by the elastic theory of wave propagation:

$$V_s = \sqrt{\frac{G_0}{\rho}} \tag{3.2}$$

$$V_p = \sqrt{\frac{\lambda + 2G_0}{\rho}} \tag{3.3}$$

From the expression of Lamè's constant λ, Young Modulus E and Poisson's coefficient ν, it is possible to obtain the correlation between V_p and V_s:

$$\frac{V_p}{V_s} = \sqrt{\frac{2(1-\nu)}{1-2\nu}} \tag{3.4}$$

From Eq.3.2, the value of the initial shear modulus G_0 can be obtained from the shear wave velocity and soil density ρ:

$$G_0 = \rho \cdot V_s^2 \tag{3.5}$$

To account for non-linearity, many stress-strain and stiffness decay curves have been proposed and adopted for practice in the last thirty years (e.g. Seed et al. 1986, Jardine et al. 1986, Vucetic and Dobry 1991, Puzrin and Burland 1996,1998, Goto et al. 1999, Darendeli 2001). All these contributions to the knowledge of soil behaviour allow to assume that "operative" values for soil modulus can be chosen in the range of 0.2-0.3 G_0. Assuming the value of Poisson ratio $\nu=0.2$ and the relationship:

$$E = 2(1+\nu)G \tag{3.6}$$

Table 6 summarizes the values obtained by the procedure just described.

From this analysis, two different representative values of Young modulus have been considered, E=40MPa and E=60MPa.

As far as the strength parameters of the blanket are concerned, a value of 5 kPa has been adopted for the effective cohesion, in order to account for a possible contribution of vegetation (see, e.g. Wu, 2012), slight cementation, fines content and other possible sources of non-frictional shear strength. It is also worth observing that, to avoid complications in the numerical analyses, the adoption of a small value for the cohesion can be advisable. A peak friction internal shearing resistance value of 35° has been chosen, starting from the experience gained in this kind of non-homogeneous material, usually mainly composed by sand and gravel (70-80%) with a non-negligible fines fraction (20-30%).

Table 6. Values of Young Modulus E as Vs varies

Vs (m/s)	240	190	150
G_0 (MPa)	102	64	40
$G=0.2\ G_0$ (MPa)	20	13	8
$G=0.3\ G_0$ (MPa)	31	19	12
E (MPa)	51-76	32-48	20-30

Table 7- Geotechnical parameters adopted in FEM analyses

	Blanket	Bedrock
γ (kN/m^3)	17	26
c' (kPa)	5	10
ϕ' (°)	35	38
ψ (°)	0	5
ν	0.2	0.2
E (MPa)	40-60	1500

Table 7 reports the adopted geotechnical properties chosen in order to depict a typical stratigraphical sequence in the slope: a superficial blanket overlying a stiff and resistant bedrock, is former possibly subject to movements and potential failure along a curved or almost plane surface, the latter being stable, even if its mechanical parameters represent better a weathered and fractured transitional rock layer than a sound rock mass.

The values of the strength parameters are considered appropriate and representative, at least for the purpose of the performed analyses. In fact, the values of the peak friction angle ϕ' and effective cohesion c' so defined, assure initial stable conditions: in the different configurations studied, the initial factor of safety FS_0 (assessed by the FEM analyses as discussed in the following) ranges from 2.31 to 1.28. For these preliminary analyses, in order to simplify the interpretation of the obtained results, no water table (dry conditions) has been taken into account.

Starting from a set of parameters that include the slope angle *i*, the thickness H and the Young modulus E of the blanket, some parameters have been varied, obtained eight different models for the slope. For each of these models, the angle of internal friction φ' and the effective cohesion c' have been progressively reduced, in order to reduce the geotechnical parameter of the slope and investigate the evolution of displacement until failure is reached. For models characterized by *i* equal to 20°, ten steps of decrease have been considered: 100%, 95%, 90%, 80%, 75%, 70%, 65%, 60%, 55% and 50% of the initial values. For models characterized by *i* equal to 30°, five steps (100%, 95%, 90%, 85% and 80%) have been modelled; in those cases, after a reduction of 80%, failure occurs. As a result, 60 different sets of analyses have been obtained. Table 8 shows a summary of the cases analysed.

Table 8. Characteristics of the different cases

Slope parameter	Case analysed							
	A1	A2	A3	A4	B1	B2	B3	B4
i (°)	20	20	20	20	30	30	30	30
H (m)	3	3	5	5	3	3	5	5
E (MPa)	40	60	40	60	40	60	40	60

The values of the Young modulus obviously influence the displacements of the slope and its influence has been investigated. Figure 31 exhibits the horizontal displacements profile for the case B1 and B2, section 3 as the geotechnical properties decrease, from 100% of the initial values to failure condition (80% of the initial values); as the values of the strength parameters decrease the difference between the horizontal displacements of the two cases increase. Figure 32 shows the trend of Eu_x, expressed by:

$$Eu_x = \frac{u_x(E60) - u_x(E40)}{u_x(E40)}$$

(3.7)

At the ground level (y=37.6m), $u_x(E40)$ is higher than $u_x(E60)$ and the maximum difference between their value is equal to 0.55 mm. This difference is reasonable due to the greater deformability of the soil in B1 case than B2 case but does not appear to be of considerable importance for the purpose of the analyses.

In the following, since the horizontal and vertical displacements of the blanket will be normalized to respective maximum computed displacement, only the cases referred to E=60 MPa will be reported.

As far as the unit weight γ, Poisson's ratio ν and dilatancy angle ψ are concerned, they have been always kept constant.
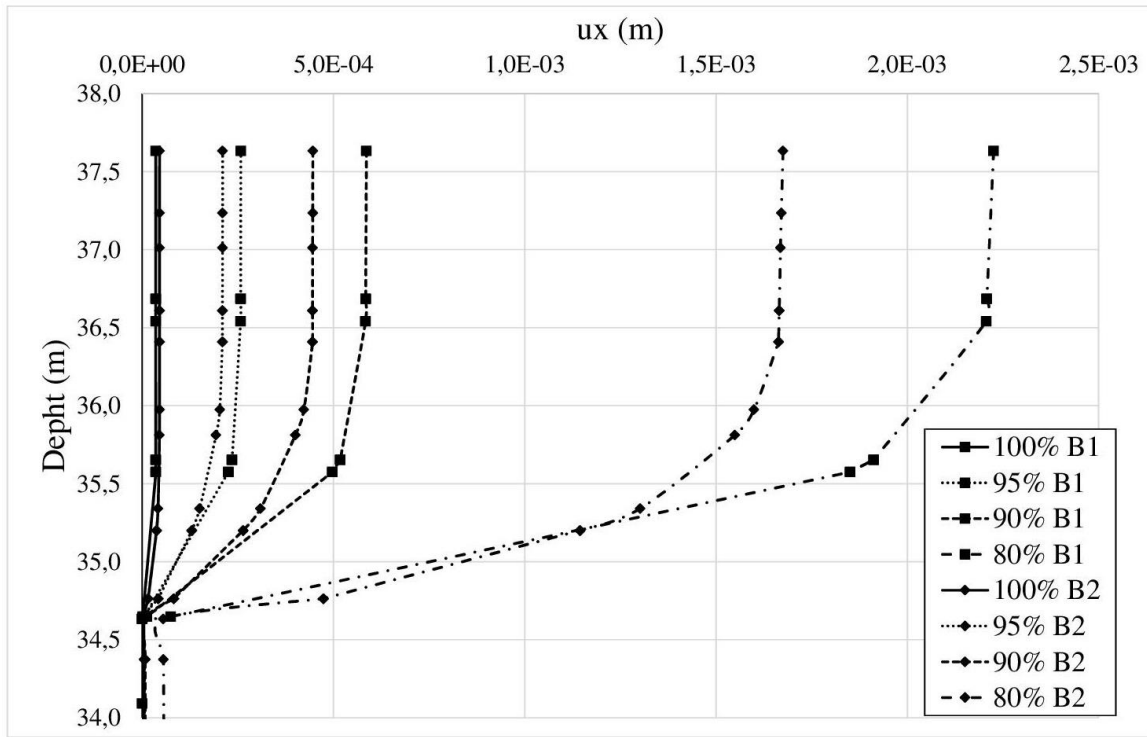
Figure 31 – Horizontal displacements as strength parameters decrease, E=40MPa vs E=60MPa
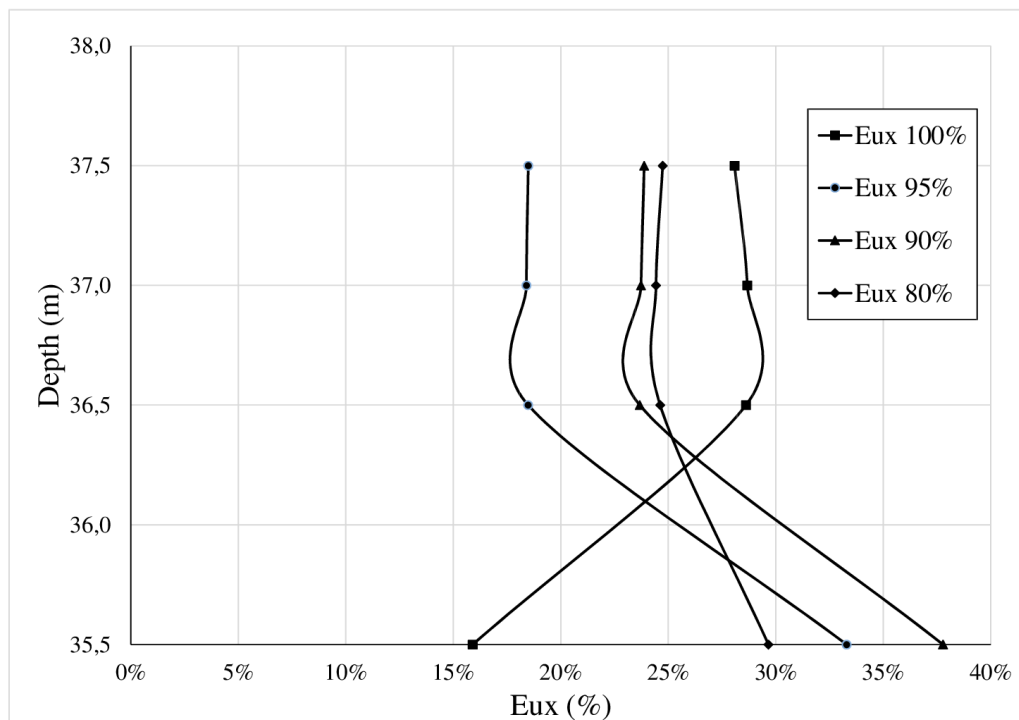
Figure 32- Trends of Eux

After having evaluated the effect of the Young's modulus value on the displacement profiles, a further step has been made by investigating the influence of the adopted constitutive model. Since the focus is on displacements, in addition to stability conditions, the non-linear Hardening Soil model (hereafter called HSM) (Schanza, 1988) has been adopted in comparison with the simpler elastic-plastic Mohr-Coulomb model (hereafter called MCM).

The HSM supersedes the hyperbolic model by far: firstly, by using the theory of plasticity rather than the theory of elasticity, secondly by including soil dilatancy and thirdly by introducing a yield cap (PLAXIS manual 2019). Some basic characteristics of the model are:

• Stress dependent stiffness according to a power law Input parameter m

• Plastic straining due to primary deviatoric loading Input parameter E_{50}^{ref}

• Plastic straining due to primary compression Input parameter E_{oed}^{ref}

• Elastic unloading / reloading Input parameters E_{ur}^{ref}, ν'_{ur}

• Failure according to the Mohr-Coulomb failure criterion Parameters c' and ϕ

A triaxial test was modelled with PLAXIS in order to calibrate the parameters of the HSM. They have been varied to find those that fit better with the parameters chosen for the MCM. For the case E=60 MPa the parameters reported in Table 9 have been chosen:

Table 9 – Hardening soil parameters

E_{50}^{ref}	60 MPa
E_{oed}^{ref}	35 MPa
E_{ur}^{ref}	120 MPa
Power (m)	0.500
ν'_{ur}	0.2
K_0^{nc}	0.4264
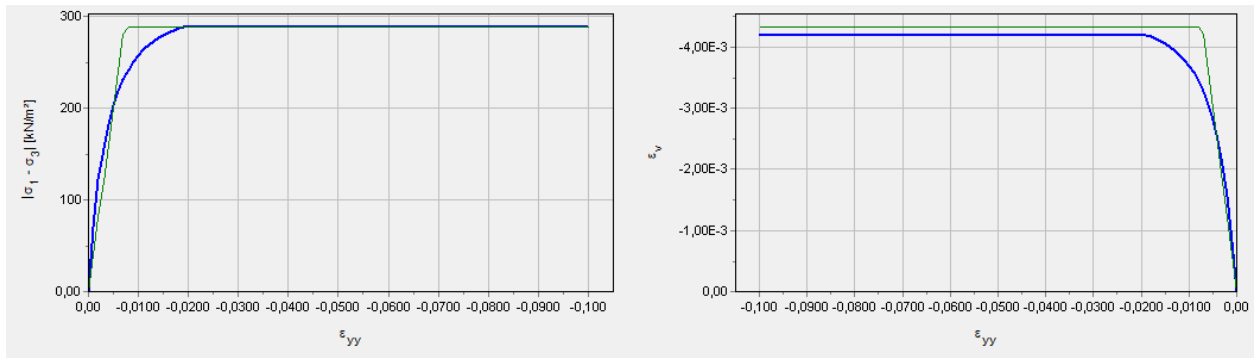
Figure 33 - Triaxial test results, in blu HS model, in green MC model

Figure 33 shows the comparison between the test results (in term of stress-strain curve and volumetric strain vs axial strain) for soil modelled with MC constitutive law and HS constitutive law, which are in good agreement.

Figure 34 shows the pattern of the horizontal displacements in one section of the slope. As it can be seen, no relevant difference occurs between HS model and MC model when strength parameters are 80% of the initial values and failure occurs while, when the slope is not closed to failure condition (from 100% to 85% of the initial values), displacement obtained with MCM are two times bigger than the HSM ones.
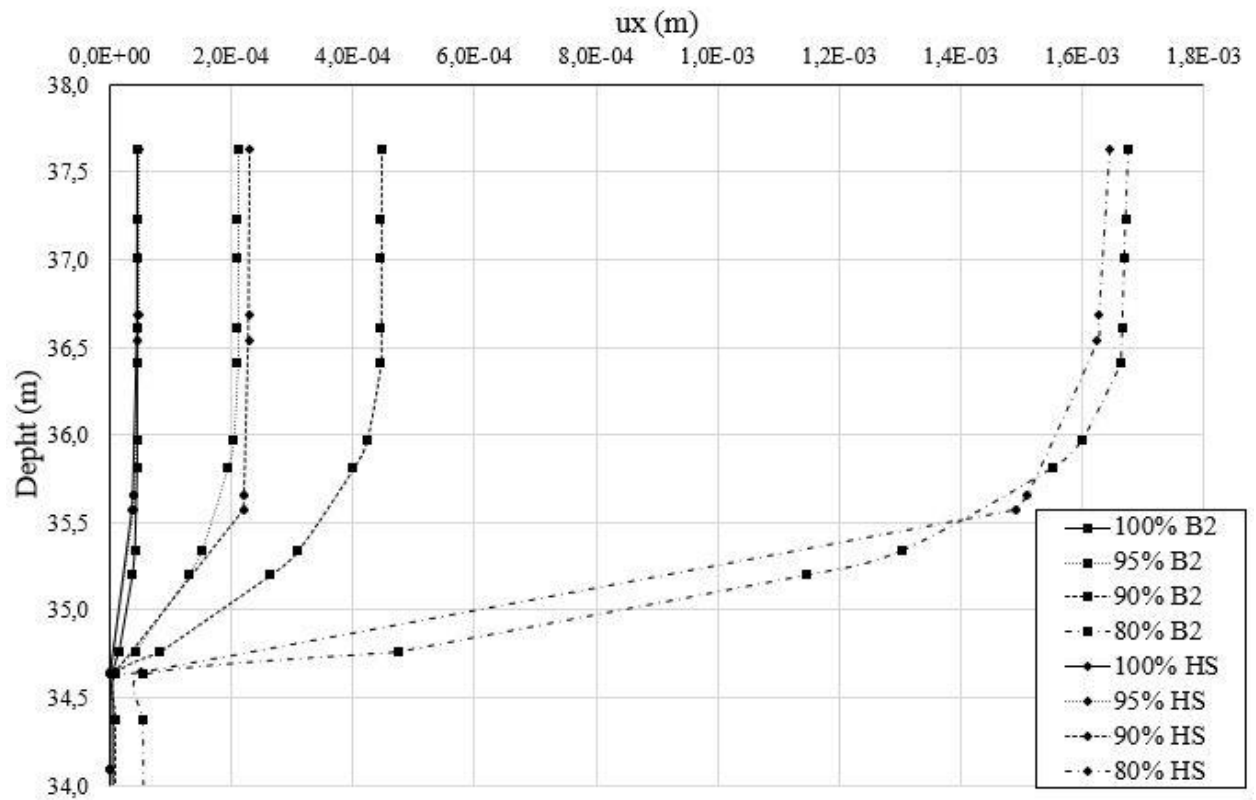
Figure 34 – ux profile: comparison between HSM and MCM

Based on these considerations and with the awareness of making a simplification, however useful for the purpose of this study, the analyses performed in the Thesis have been carried out with MCM, in order to provide results obtained by a simple but robust soil model, consistent with the results of failure analyses as well and characterised by only few parameters.

For each case, the slope safety factor FS has been assessed performing "safety analyses" (often denoted as ϕ'-c reduction analyses), which led to a wide range of FS values (FS= 2.31 to 1.10 for i=20°; FS= 1.37 to 1.09 for i=30°). Figure 35 shows an example of one of these safety analyses, illustrating the potential sliding surface that is associated to the respective safety factor FS.

In this respect, the slope safety factor becomes the reference parameter for the performed FEM analyses, because stability conditions (represented by the FS values) can be associated to the relative displacements, approach not possible starting from limit equilibrium methods.

The slope, so schematized, has been studied through five sections of interest (Figure 30) placed in different positions (one on the top of the slope, three in the middle and one at the bottom), in order to correlate each safety factor FS with the computed vertical and horizontal displacements (u_y and u_x respectively). Figure 36 illustrates a schematization referred to a generic section.
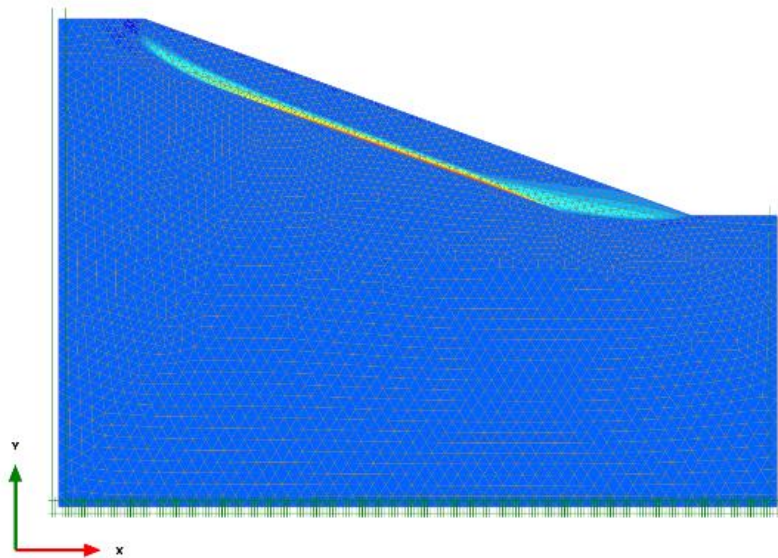
Figure 35 – Failure surface in case B3
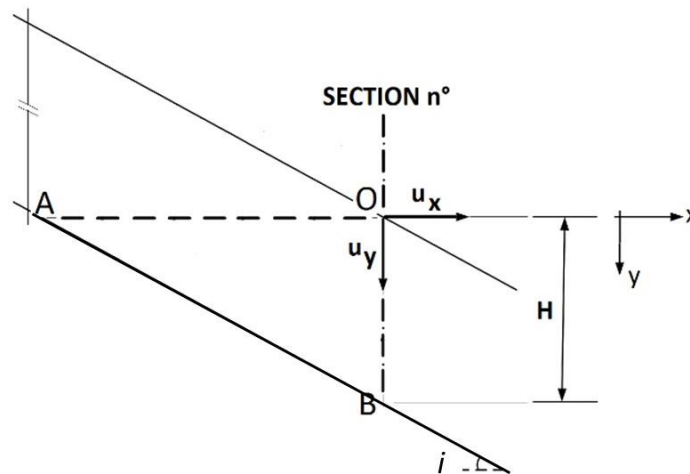
Figure 36 - Schematization of vertical and horizontal displacements in a generic section

3.2 RESULTS

For every section, displacement profiles have been assessed. Both vertical and horizontal displacements, computed for every decrease of strength parameters, have been normalized by the maximum value of u_x or u_y of the case analysed.

Figure 37 and Figure 38 show, for case A3- section 2, the profile obtained for both horizontal (along OA line – Figure 36) and vertical (along OB line – Figure 36) normalized displacements. It is worth observing that the maximum value (with the adopted scheme) occurs near the ground level and remains constant for more than 50% of the relevant length (OA and OB respectively). Beyond, the displacements tend to become negligible. The order of magnitude of the maximum value of u_x and u_y is 1 mm. The Figures mentioned above also clearly, and quite obviously, show that the value of u/u_{max} decreases as the safety factor FS increases.

In the simple free-field geometry here assumed, the displacements u_x and u_y have been related to the imaginary lines OA and OB, in order to obtain deformations referred both to the thickness of the moving blanket (OB) and to a possible foundation plane (OA) of a building placed along the slope.

In order to supply details about the deformations related to the safety condition of the slope, the maximum value of both u_x and u_y, for each section and each reduction of strength parameters, have been collected then vertical ε_y and horizontal ε_x strains and angular distortion β have been defined as:

$$\varepsilon_y = \frac{u_{y,max}}{H} \tag{3.8}$$

$$\varepsilon_x = \frac{u_{x,max}}{H/tani} \tag{3.9}$$

$$\beta = \frac{u_{y,max} - u_{y0}}{H/tani} \qquad (3.10)$$

Where $u_{y,max}$ (m) is the maximum value of u_y, $u_{x,max}$ (m) is the maximum value of u_x, H (m) is the thickness of the blanket layer and i (°) is the slope angle and being $u_{y0} \approx 0$..
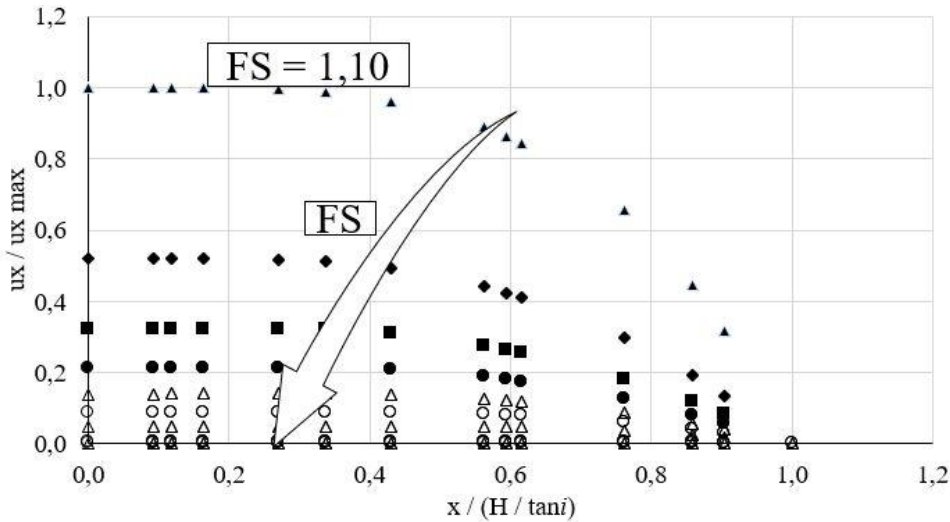
Figure 37 - Horizontal normalized displacement
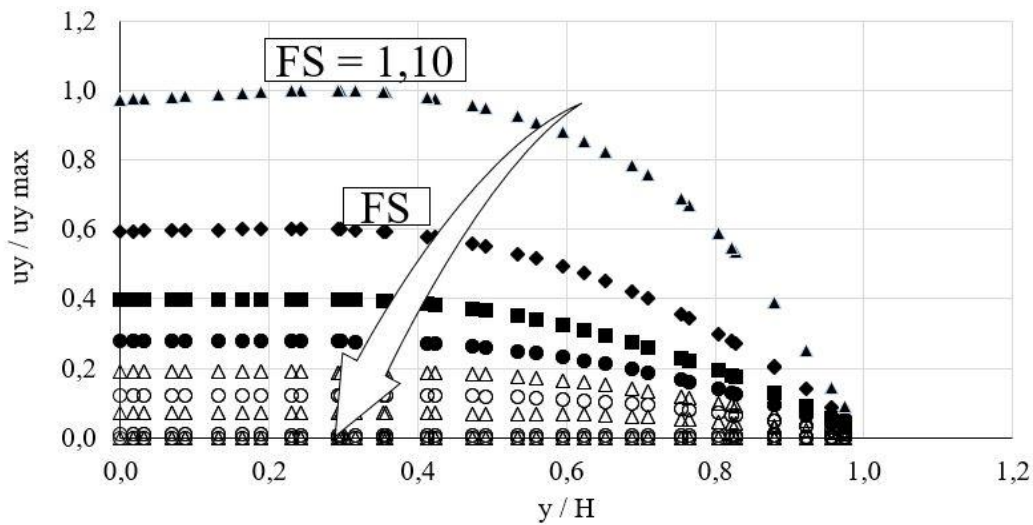
Figure 38 - Vertical normalized displacement

Each couple of value of ε_x and ε_y has been associated with the relative safety factor FS. Figure 39 shows for the central section 3 of case A3 the evolution of FS as the horizontal and vertical strains increase.

This result supplies a first insight of the relation between the evolution of slope safety conditions and slope movements, even if for the simple schematization adopted. The trend towards instability (FS→1),

associated with the increase of horizontal and vertical displacements and deformations are clear and consistent.
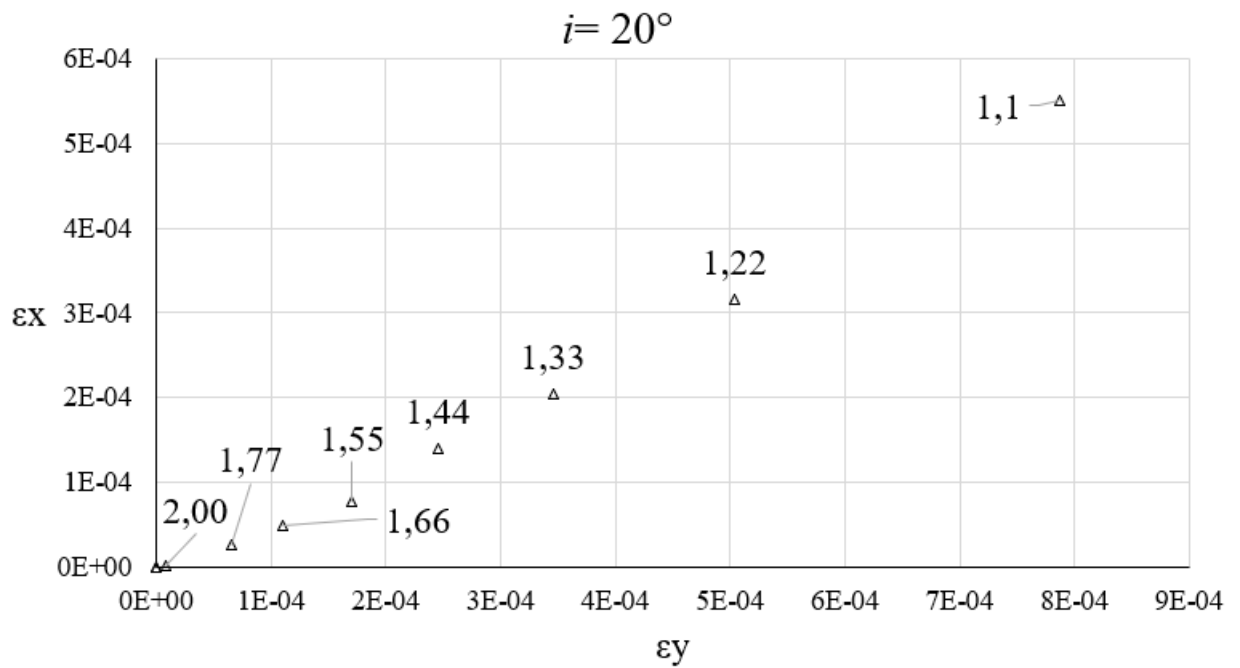
Figure 39 - Case A3 – section 3, i=20°, H=5m, E=40MPa

To generalize and supply useful information about possible deformation levels and correlations between horizontal and vertical strains, Figure 40, Figure 41, Figure 42 and Figure 43 show the links among ε_x, ε_y and β obtained in the different configurations previously described (Cambiaggi and Berardi, 2019).
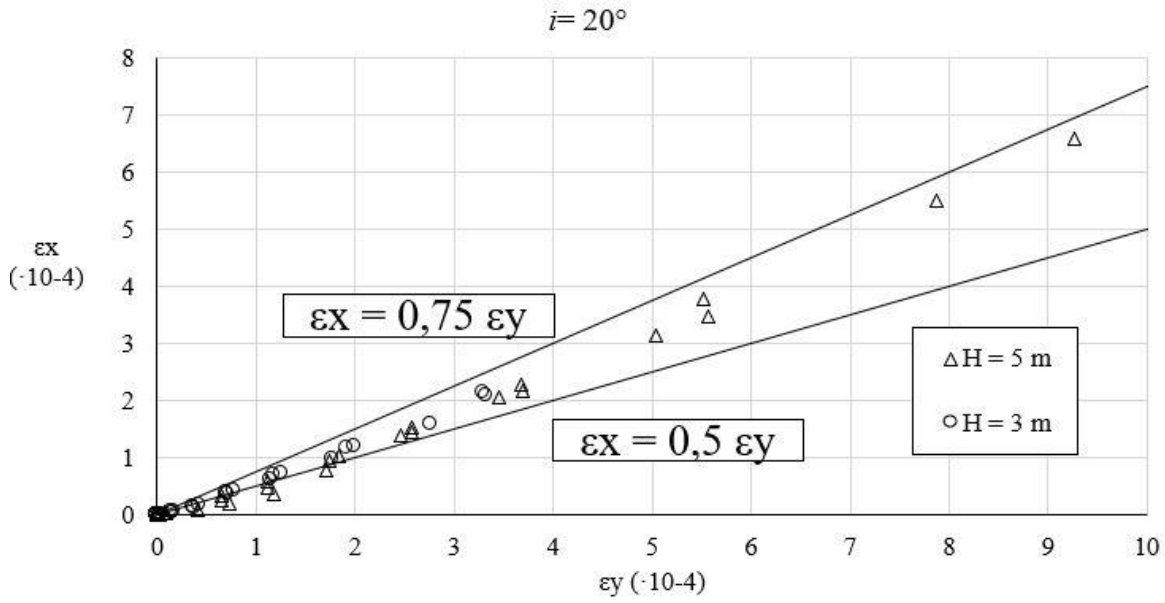
Figure 40 - Horizontal and vertical deformations i=20°, section 3
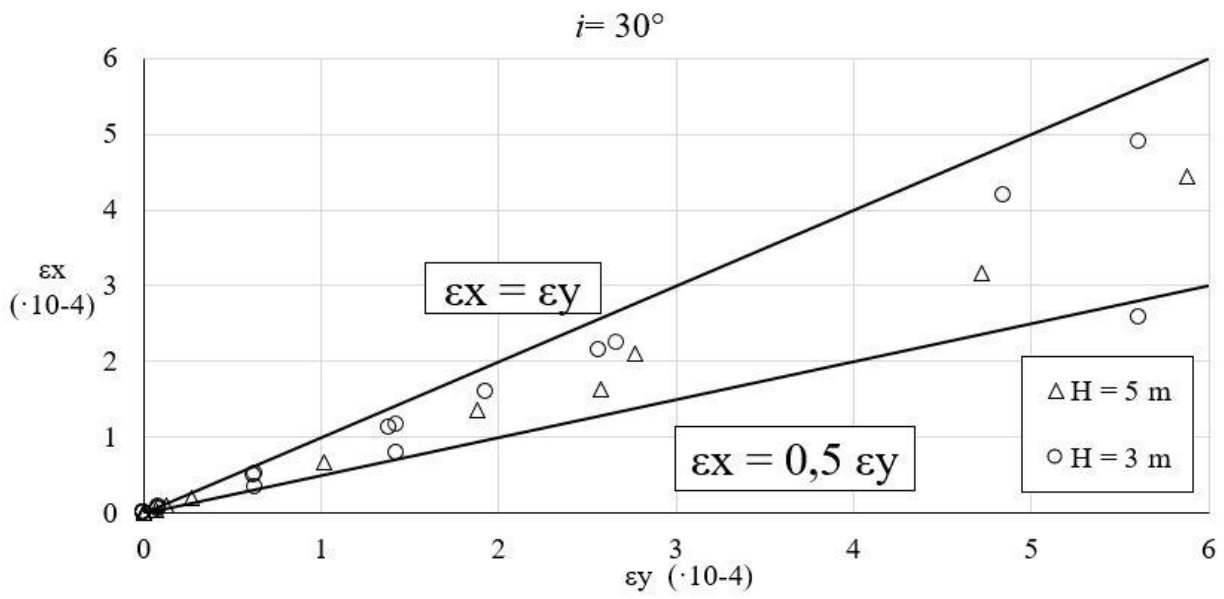
Figure 41 - Horizontal and vertical deformations, i=30°, section 3
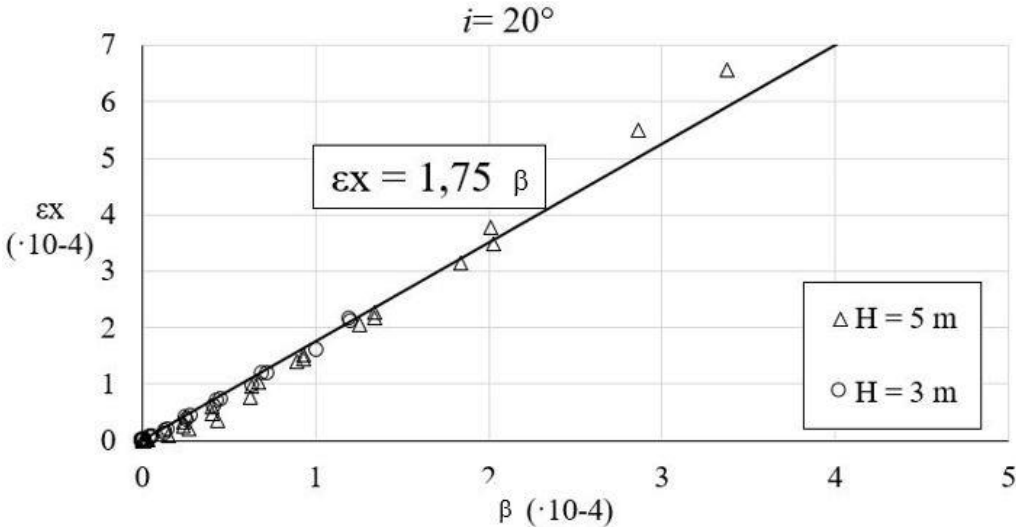
Figure 42. Horizontal deformation and angular distortion, i=20°, section 3
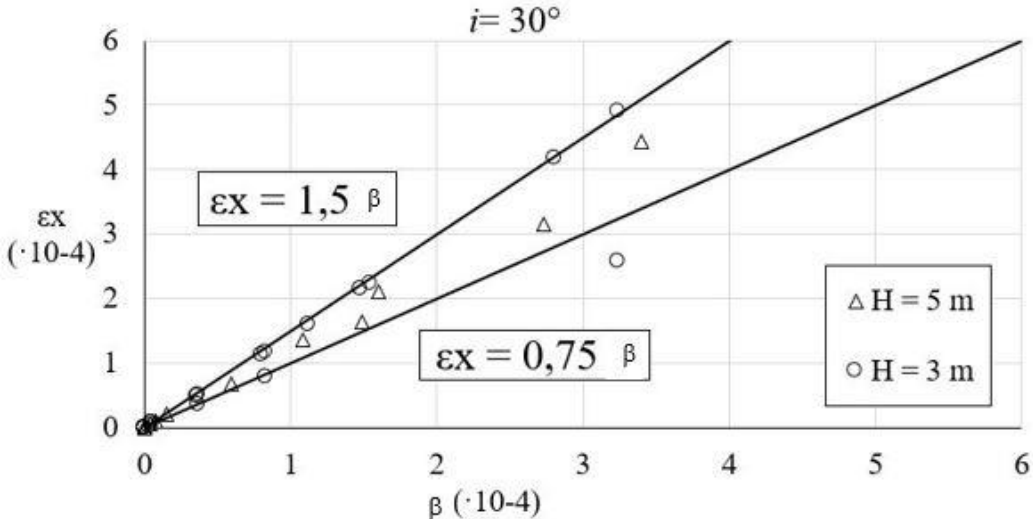
Figure 43. Horizontal deformation and angular distortion, i=30°, section 3

It is possible to observe that well-defined correlations between horizontal and vertical strains can be identified, being in general $\varepsilon_x = (0.5$ to $1)$ ε_x; moreover, the results obtained by the FEM numerical analyses allow to correlate the strain levels with the slope safety factors as well. In fact, larger deformations correspond, obviously, to lower safety factors, and vice versa.

In the following paragraph more realistic analyses are described, introducing also a new "hazard factor" FH suitable for better correlation of the evolution of strain levels with stability conditions (Cambiaggi and Berardi, 2019):

$$FH = \frac{FS_0 - FS}{FS_0 - 1} \qquad\qquad\qquad (3.11)$$

where FS_0 is the initial safety factor of the slope and FS the safety factor associated with a given strain level. The hazard factor here introduced is a parameter useful to depict the evolution of the safety factor from a certain initial value of FS. FH does not have a probabilistic meaning but indicates, when it is close to 1, the approach of the failure conditions for the slope. From the results referred to the infinite slope scheme, it is expected that the strain levels vary with FH as depicted in Figure 44.
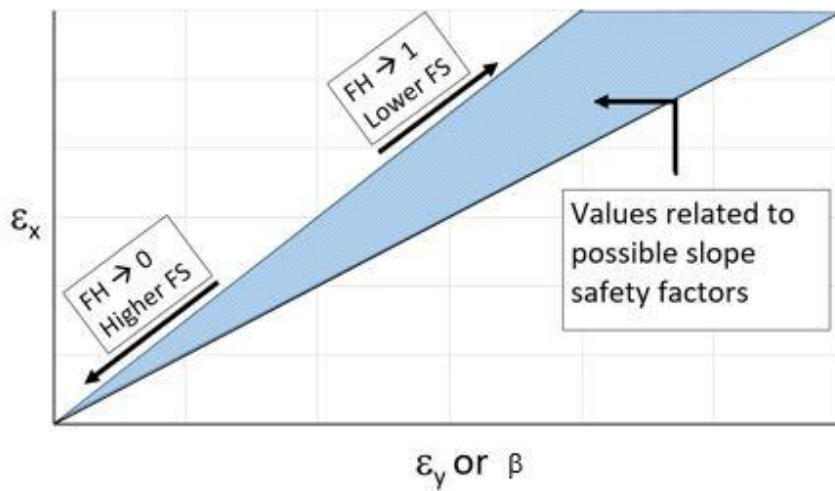
Figure 44. Schematic representation of relationship between strain levels and hazard factor

4. PROCEDURE FOR THE ANALYSIS AND PREDICTION OF THE EFFECT OF SLOW-MOVING LANDSLIDE VIA NUMERICAL APPROACH: FINITE ELEMENT METHOD AND LIMIT EQUILIBRIUM METHOD MODEL

4.1 DEFINITION OF THE SLOPE MODEL

The schematization as an infinite slope led to the introduction of the hazard factor FH and its possible correlation with the strain levels. This work led to the definition of the following methodology:

- choice of sections of interest, definition of stratigraphical sequence and geotechnical parameters;

- assessment of the initial safety factor (FS_0);

- reduction of the initial safety factor up to failure conditions;

- evaluation of the displacement values for each decrease in FS;

- definition of the reference deformations associated with the computed displacements;

- comparison of the computed displacement and strain patterns and levels with the detected ones;

- representation of displacement and deformation evolution by introducing the hazard factor FH.

The next step of the research concerned the modelling of the slope in a more realistic way. For this purpose, over thirty real slopes, characterized by the presence of both active or dormant slow-moving landslides and historic masonry churches in Liguria territory, as described in Chapter 2, have been analysed

Regarding the geometric characteristics of the slopes, by the acquisition of Digital Terrain Model (DTM) data of the areas of interest and its processing by means of QGIS software, it was possible to obtain the plano-altimetric profiles along the landslide direction and the locations of the churches in an accurate way (Figure 45).
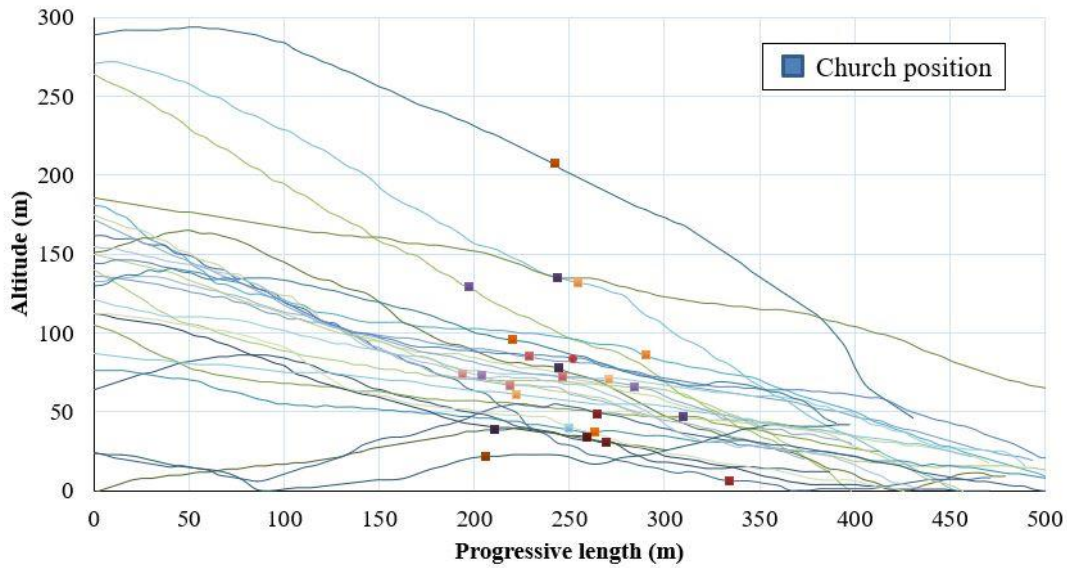
Figure 45 – Plano-altimetric profile of the slopes and churches position

Slope modelling must necessarily go through the adoption of a simplified scheme, characterized by a reduced number of geometric variables. For this reason and for providing a tool suitable with more generic scheme instead of the single case study, the common characteristics of the profile of the slope reported in Figure 45 have been grouped together. Figure 46, Figure 47 and Figure 48 show, for example, slopes characterized by different uphill slope angle, from 15° to 25°. This led to the definition of different geometric parameters that can effectively describe the slope profile.
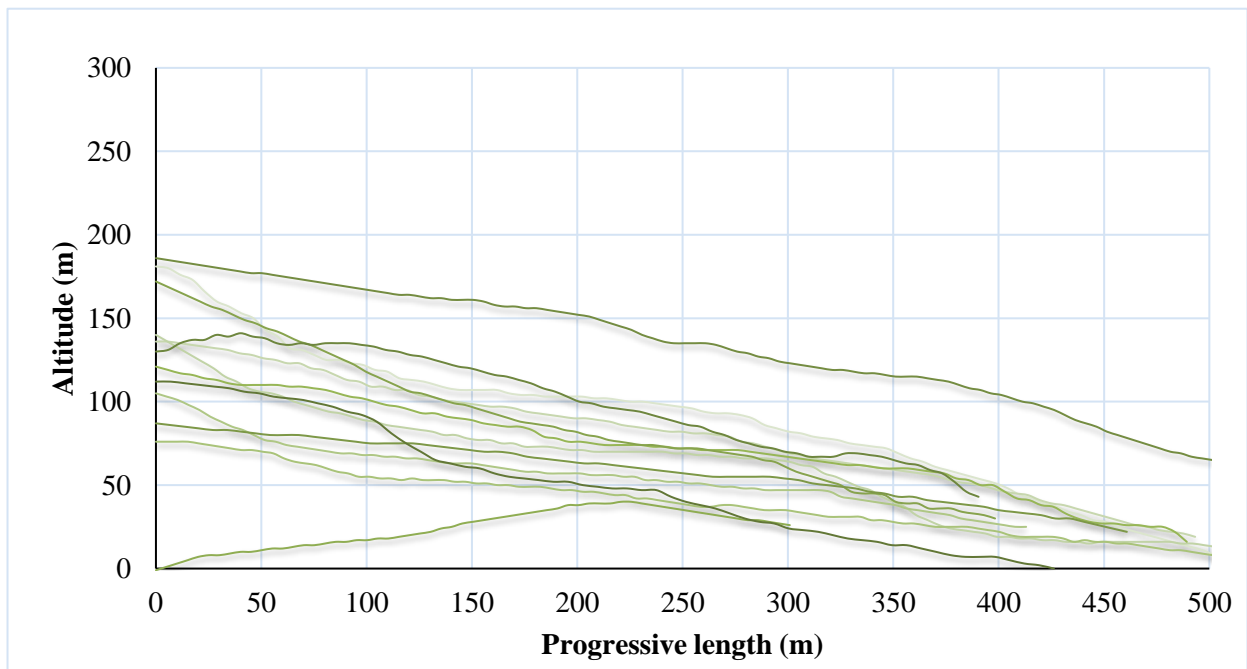
Figure 46 – Set of slopes with uphill angle=15°
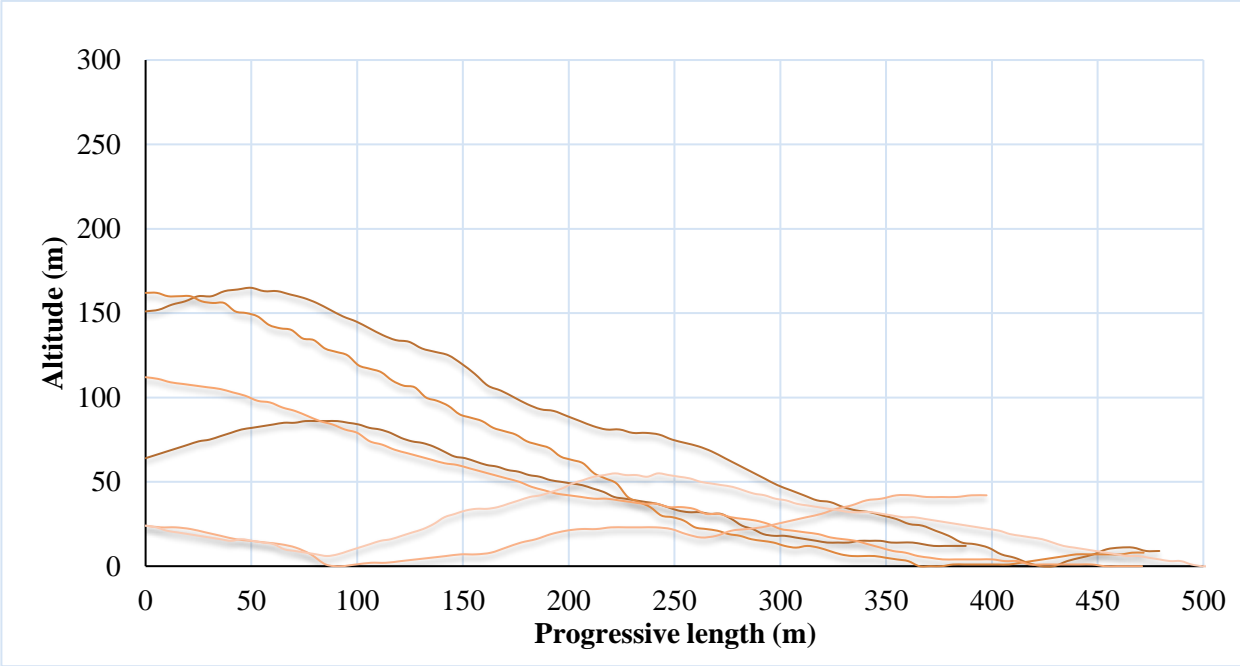
Figure 47 - Set of slopes with uphill angle=20°
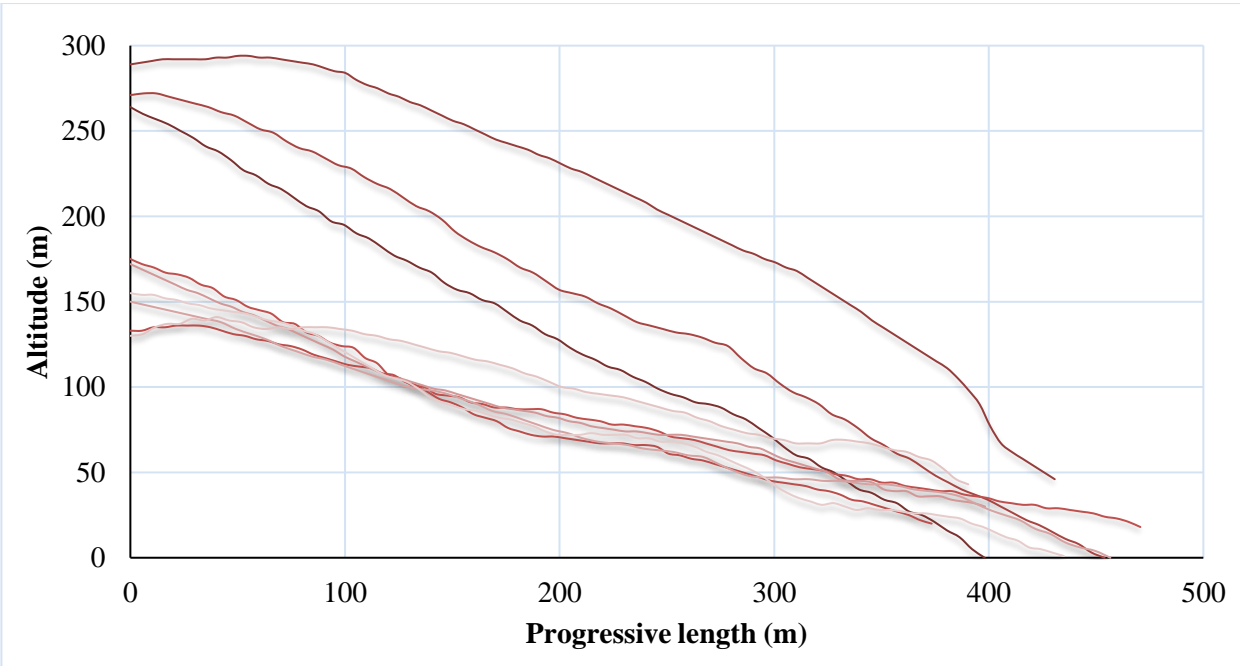
Figure 48 - Set of slopes with uphill angle=25°

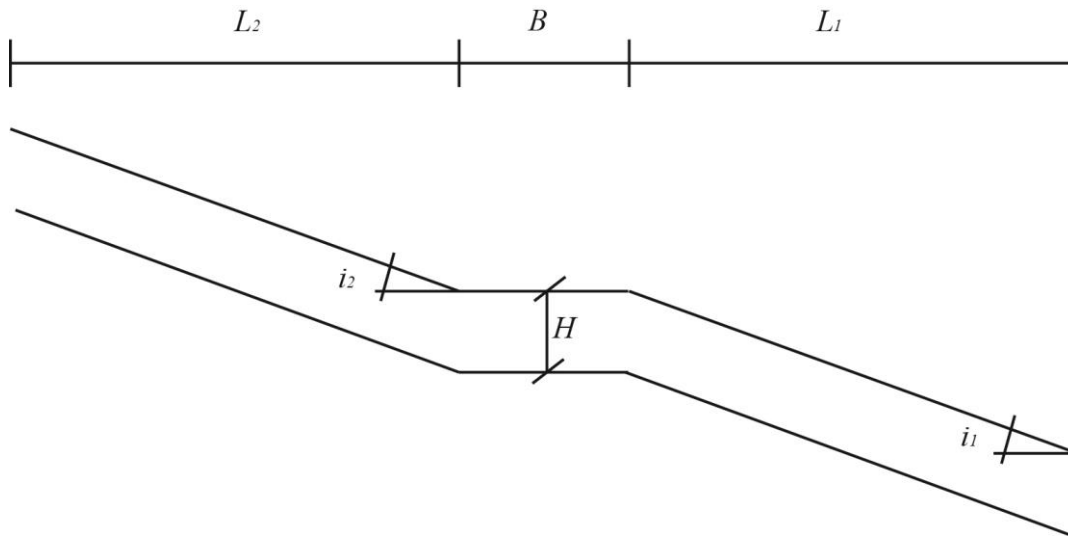The following slope profile has been consequently adopted (Figure 49).

Figure 49 - Scheme of the simplified slope

where the independent variables have the following meanings:

- i_1 downhill angle,
- i_2 uphill angle,
- L_1 length of the slope downhill,
- L_2 length of the slope uphill,
- H thickness of the layer of blanket/depth of the soil layer to the potential failure surface,
- B church footprint on slope.

The analysis of the available data showed that the slope can be characterized by three slope angles, $i=15°$-$20°$-$25°$. In particular, downhill angle i_1 and uphill angle i_2 have been varied resulting in the following combination to be studied:

i_1 (°)	15	15	15	20	25
i_2 (°)	15	20	25	15	15

The length of the slope has been obtained based on the surveys, these values were also evaluated in order to not be affected by boundary effects.

Regarding the depth of the soil layer to the potential failure surface H, analysing the data from the inclinometer readings available for each slope studied (Figure 50 represents an example of the inclinometric data for one of the case studies), it has been observed that its value is ranged from 12 and 30 m below ground level. For this reason, a representative value of H=25 m has been adopted.
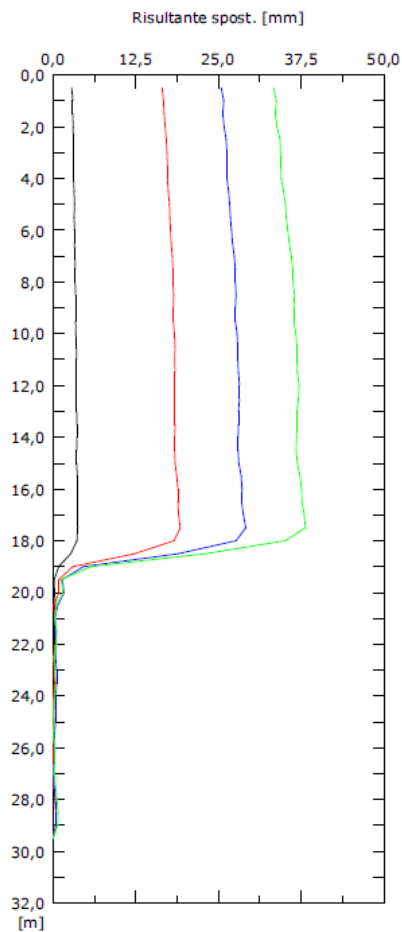
Figure 50 – Example of inclinometer reading

For each church, along the section of the landslide direction, the breadth area in proximity of the church has been evaluated. It is important to note that in some cases the position of the church is on the edge of the slope so B coincides with the width of the church itself. As consequence, two different values of B have been considered: B=10m and B=30m.

Likewise the case of the infinite slope, in order to obtain displacements and failure conditions, a simple elastic-plastic constitutive model with Mohr-Coulomb failure criterion has been adopted. The set of parameters, reported in Table 10, have been considered. As explained in Chapter 3, a value equal to 60MPa has been adopted for the Young Modulus, while the angle of internal shearing resistance for the blanket has been set equal to 30°. This choice has been made in order to reach failure condition with a smaller number of steps of geotechnical properties reduction.

As a result, 10 different set of results have been obtained and for each case angle of internal shearing resistance ϕ' has been progressively reduced for the purpose of reaching slope failure

Table 10 - Set of parameters for FEM analysis

	Blanket	Bedrock
γ (kN/m³)	17	26
c' (kPa)	5	10
ϕ' (°)	30	38
ψ (°)	0	5
ν	0.2	0.2
E (MPa)	60	1500

. Table 11 shows a summary of the cases analysed. It is important to underline that a larger number of step of reduction of ϕ' has been taking when 25°≤ ϕ ≤ 30°, in order to obtain more detailed results when the slope angle is close to 25° or the failure of the slope will take place in very few calculation steps.

Once the variables of the problem were defined, FEM and LEM analyses were performed.

Table 11 – List of cases analysed

	C1	C2	C3	C4	C5	C6	C7	C8	C9	C10
i_1 (°)	15	15	15	15	15	15	20	20	25	25
i_2 (°)	15	15	20	20	25	25	15	15	15	15
ϕ_0 (°)	30	30	30	30	30	30	30	30	30	30
ϕ_1 (°)	29	29	29	29	29	29	29	29	29	29
ϕ_2 (°)	28	28	28	28	28	28	28	28	28	28
ϕ_3 (°)	27	27	27	27	27	27	27	27	27	27
ϕ_4 (°)	26	26	26	26	26	26	26	26	26	26
ϕ_5 (°)	25	25	25	25	25	25	25	25	25	25
ϕ_6 (°)	22	22	22	22	22	22	22	22	22	22
ϕ_7 (°)	20	20	20	20	20	20	20	20	20	20
B (m)	30	10	30	10	30	10	30	10	30	10

4.2 FINITE ELEMENT METHOD ANALYSIS

Using a plane strain, finite element model by means of PLAXIS 2D software, several parametric analyses have been performed. Horizontal and vertical displacements have been evaluated for each case and safety analyses have been performed. Figure 51 shows mesh, geometry and boundary conditions adopted.

Horizontal and vertical displacements have been evaluated in different sections. For horizontal displacement, the values have been taken at 0.3-0.5-0.7 B, while for vertical displacement depth of 1m under ground level has been considered (Figure 52, Figure 53). The trends of the horizontal and vertical displacements have been plotted as the geotechnical strenght characteristics decrease. For the horizontal displacement, the maximum value occurs on the ground level and tends to zero at the interface between the substratum and the blanket, Figure 52. For the vertical displacement, considering a horizontal section at -1m depth from ground level, the maximum value occurs towards the edge of the slope and the trend can be assumed as triangular as shown in Figure 53. Figure 52 and Figure 53 show, respectively, the most significant u_x and u_y profile in case C7 until failure is reached (tables and diagrams for all the cases analyses can be found in Appendix 2). It is worth observing that these values increase as the geotechnical characteristic of the slope decrease as well as the slope angle becomes higher. Figure 54 shows that the difference between sections 0.3B and 0.7B, when B is equal to 10m, are not relevant in terms of displacements. For this reason, the following analyses for B=10m will be referred to the section 0.5B. As can be noted, FS_= is the initial condition of the slope so not movements occurres.
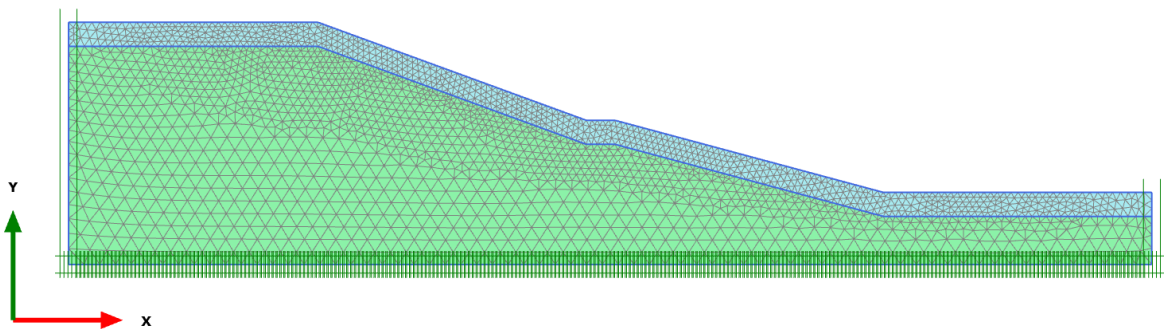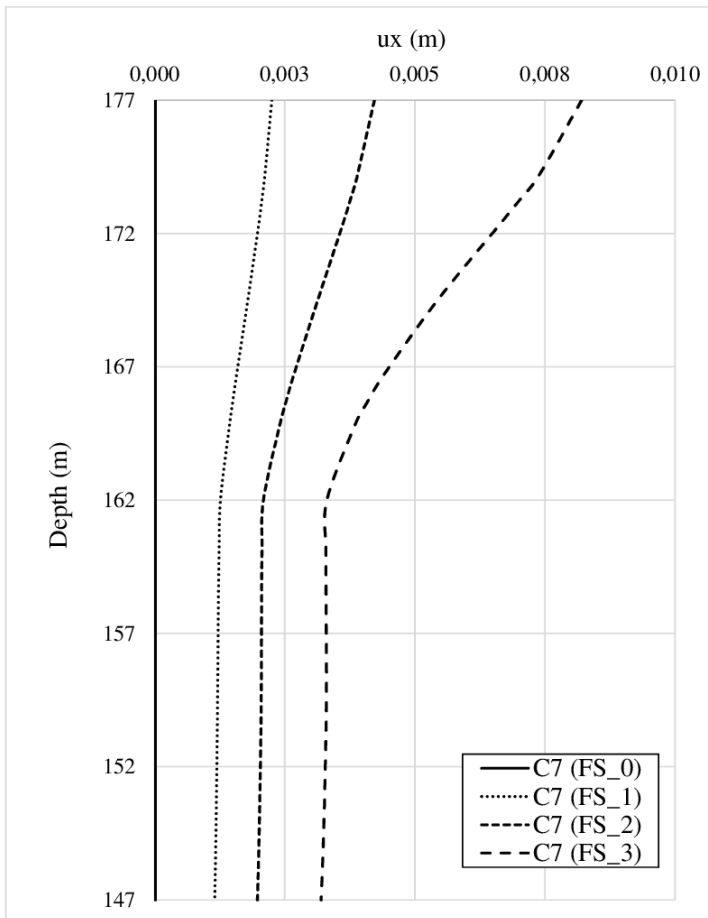

Figure 51 – Mesh adopted for the analysis

Figure 52 – Horizontal displacements for C7 case, $i_1=20°$, $i_2=15°$, B=30, as the geotechnical parameters decrease

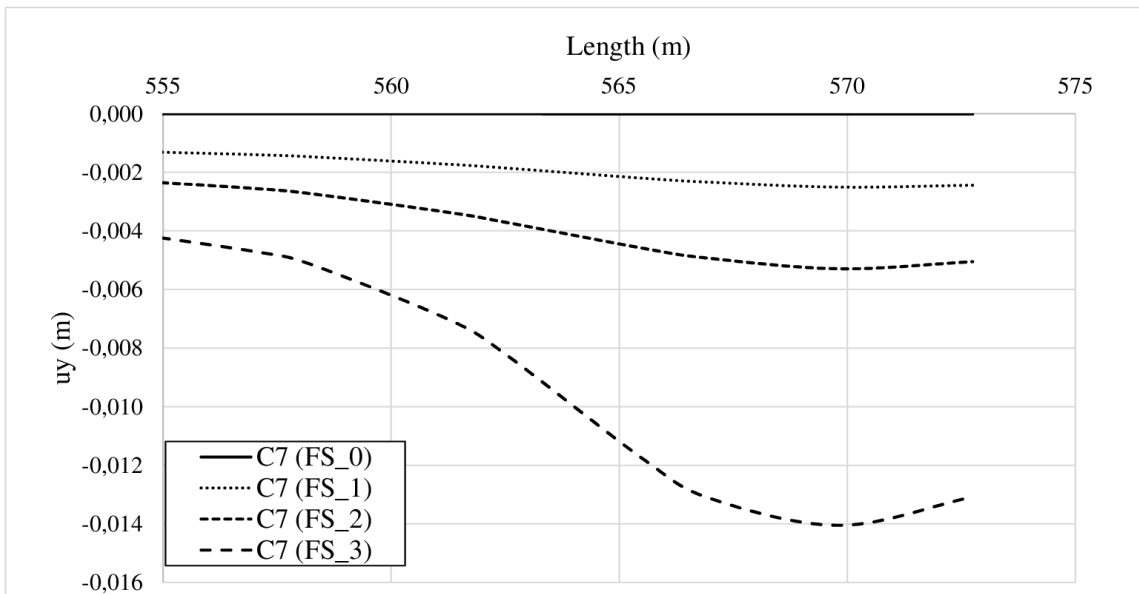
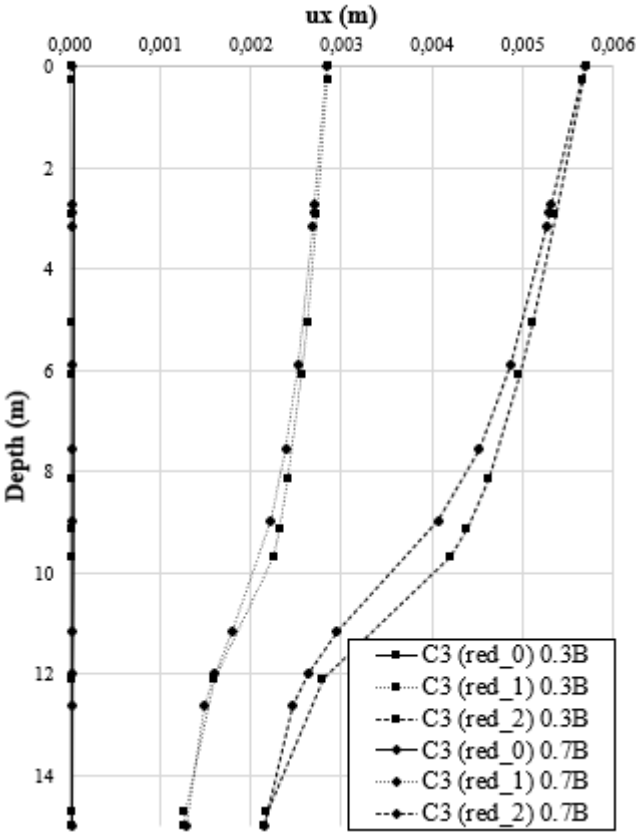Figure 53 - Vertical displacements for C7 case, $i_1=20°$, $i_2=15°$, B=30, as the geotechnical parameters decrease

Figure 54 -Comparison of horizontal displacements for section 0.3B and section 0.7B case C3, $i_1=15°$, $i_2=20°$, B=10

4.3 LIMIT EQUILIBRIUM METHOD ANALYSIS

In PLAXIS software, the safety calculation type is an option to compute global safety factors. In the safety approach, the shear strength parameters $\tan\varphi'$ and c' as well as the tensile strength are successively reduced until failure occurs. The total multiplier M_{SF} is used to define the value of the soil strength parameters at a given stage in the analysis:

$$M_{SF} = \frac{\tan\phi'_{imput}}{\tan\phi'_{reduced}} = \frac{c'_{imput}}{c'_{reduced}}$$

(4.1)

FS is defined as the value of M_{SF} at failure. It is important to underline that when using Safety calculation in combination with advanced soil models, these models will actually behave as a standard Mohr-Coulomb model, since stress-dependent stiffness behaviour and hardening effects are excluded from the analysis.

The safety analyses performed in PLAXIS show the sliding surface with the minimum value of FS. This value, depending on the case studies analysed, does not necessarily correspond to the area of interest, i.e. under the possible position of the church. This reason and the possibility to correlate the horizontal and vertical displacements obtained in the FEM analyses with the safety factor specific for the area of interest, have led to the use of a limit equilibrium approach in conjuction with FEM. The software used for the 2D

stability analyses is SLIDE 6.0 (Rocscience): analyses can be performed adopting both a single user-defined failure surface or searching for the failure surface with minimum FS. Composite surfaces can also be chosen.

The same cases developed in the FEM analyses have been analysed by the LEM approach. For each section, the reduction of the soil strength parameters has been applied in order to gradually promote/induce a failure condition. Once the various analyses were set, the LEM and FEM results have been combined. A first comparison and validation with respect to the FEM analysis concerned both the location of the sliding surface characterized by the minimum FS value and its own numerical value. The results, Figure 55, of the LEM and FEM modelling are in good agreement: LEM analysis shows the failure surface on the upper portion of the slope (C3 case) with a value of FS equal to 1.31; almost the same sliding surface is reported in FEM analysis with FS equal to 1.29. Subsequently, five different sliding surfaces have been identified, two positioned both downhill and uphill, each of those takes into consideration the area where the church could be located. A global failure surface has also been considered. Each surface is thus characterized by a value of the safety factor FS. Figure 56 shows the geometry adopted in LEM analysis and the choice of the sliding surfaces for C3 case while the other cases are reported in the Appendix 2.
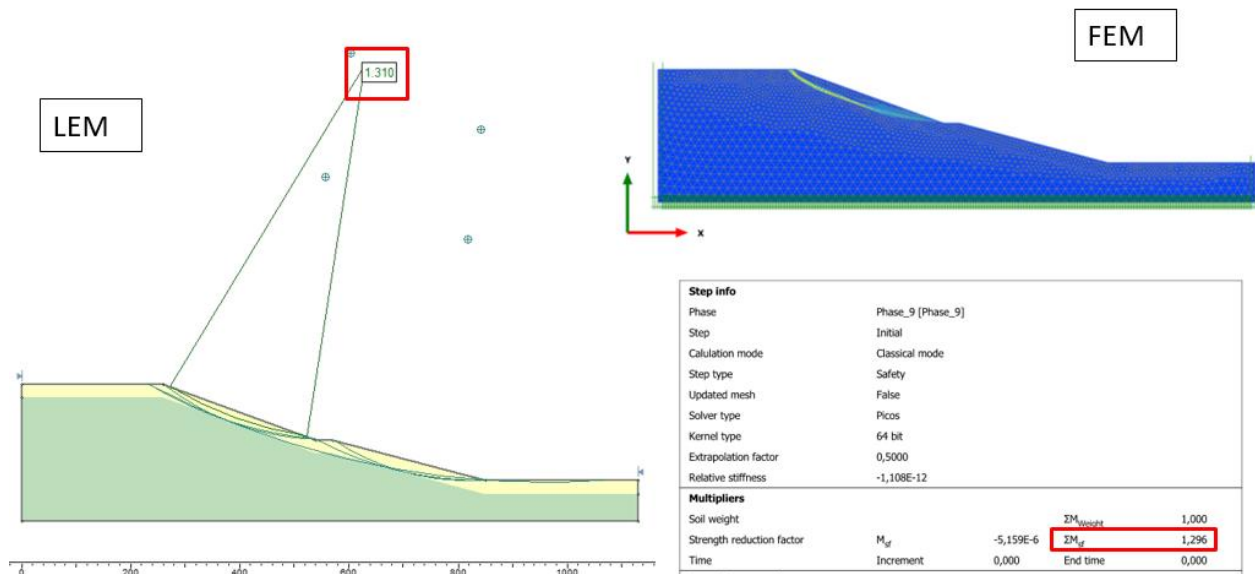

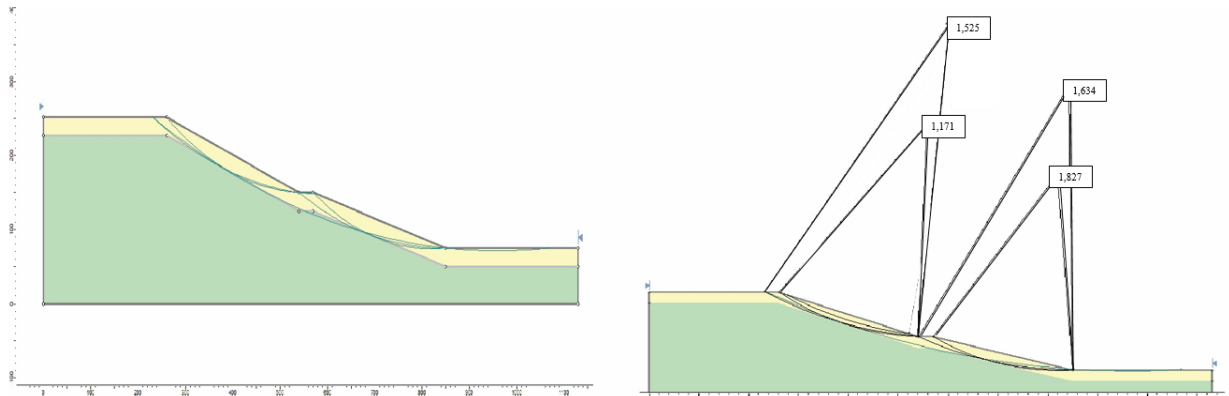Figure 55- Comparison between LEM and FEM analysis

Figure 56- Case C3, i_1=15°, i_2=20°, B=30: geometry (a) and sliding surface selected (b)

4.4 COMBINATION OF LIMIT EQUILIBRIUM METHOD AND FINITE ELEMENT METHOD ANALYSIS

Once the results were obtained both for FEM analyses (in terms of vertical and horizontal displacements for each slope scheme in the different sections) and LEM analyses (regarding the values of the safety factors), the outcomes were combined.

A first step concerned the selection of the failure surface among the five identified in SLIDE. By the examination of the displacement patterns obtained in FEM analyses, the potential failure surfaces that involved the area of interest are the two positioned downhill. Figure 57 shows the comparison between LEM and FEM for the selection of the sliding surface.
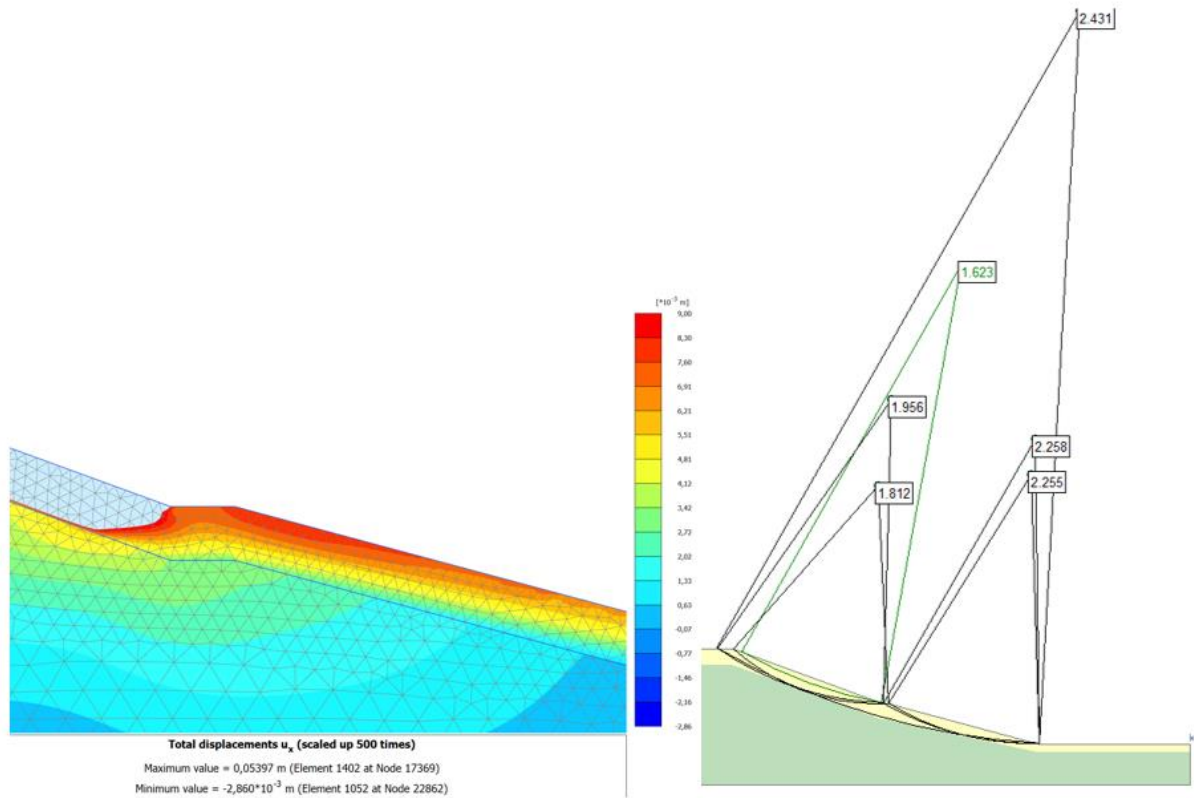
Figure 57 – FEM and LEM comparison for the selection of the sliding surface.

It is worth observing that, by LEM analyses, different methods to estimate safety factor FS are available, as reported in Chapter 1. As an example, Table 12 shows for C3 case the different values of FS, referring to the sliding surface located downhill, obtained by the following methods: Bishop simplified, GLE Morgenstern – Price, Janbu correct, Janbu simplified and Spencer. Table 13 reports the value of FH as defined by Eq. 3.11, as it can be seen, the difference in the values of FH between the different methods is negligible.

Table 12 - Values of FS as a function of the different methods

Case C3		Bishop Simplified	Jambu Simplified	Jambu Corrected	GLE/ Morgenstern - Price	Spencer
FS0	$\phi=30°$	2,42	2,36	2,45	2,43	2,42
FS1	$\phi=29°$	2,36	2,22	2,40	2,30	2,35
FS2	$\phi=28°$	2,12	2,20	2,18	2,15	2,18
FS3	$\phi=27°$	2,06	2,03	2,09	2,06	2,06
FS4	$\phi=26°$	1,98	1,98	2,00	1,98	1,99
FS5	$\phi=25°$	1,88	1,86	1,91	1,89	1,89
FS6	$\phi=22°$	1,63	1,61	1,66	1,64	1,36

Table 13 - Values of FH as a function of the different methods

Case C3		Bishop Simplified	Jambu Simplified	Jambu Corrected	GLE/ Morgenstern - Price	Spencer
FH0	$\phi=30°$	0,00	0,00	0,00	0,00	0,00
FH1	$\phi=29°$	0,04	0,10	0,04	0,09	0,05
FH2	$\phi=28°$	0,21	0,12	0,19	0,19	0,17
FH3	$\phi=27°$	0,26	0,25	0,25	0,26	0,26
FH4	$\phi=26°$	0,31	0,28	0,31	0,31	0,31
FH5	$\phi=25°$	0,38	0,37	0,37	0,38	0,38
FH6	$\phi=22°$	0,55	0,55	0,55	0,55	0,75

For this reason and for sake of simplicity, in the following the exposed results are referred to the safety factor values as obtained by Bishop method.

Once the different values of FH have been evaluated for all the cases as the geotechnical properties vary, they have been assigned to the displacement profiles obtained from FEM analysis case by case. As hypothesis, the maximum values of the horizontal displacements have been taken for the analyses, while for the vertical displacements a linear distribution (u_y varies from the maximum to the minimum value along B, see also Figure 53) has been considered. The objective is to correlate the displacements generated by reaching a certain "limit state" for the slope with the respective factor FH. Figure 58 and Figure 59 show the correlation between horizontal and vertical displacement for B=10m while Figure 60 and Figure 61 are related to the B=30m case. The relative value of FH is shown in each figure as well. As expected, (see also Figure 44) FH increases as the respective displacements increase. The value of the ratio u_x/u_y when B=10m is between 1.4 to 2.7 while for B=30m the ratio u_x/u_y is 1.3 to 2.1. From these results, once the slope geometry has been defined (i.e. i_1, i_2, B values) and given a value of FH representing a possible evolution of the slope stability conditions with respect to its initial-state displacement values can be assessed.

Obviously, if slope angles are small, higher displacements can develop failure conditions being more difficult to reach (higher FH values with larger displacements).
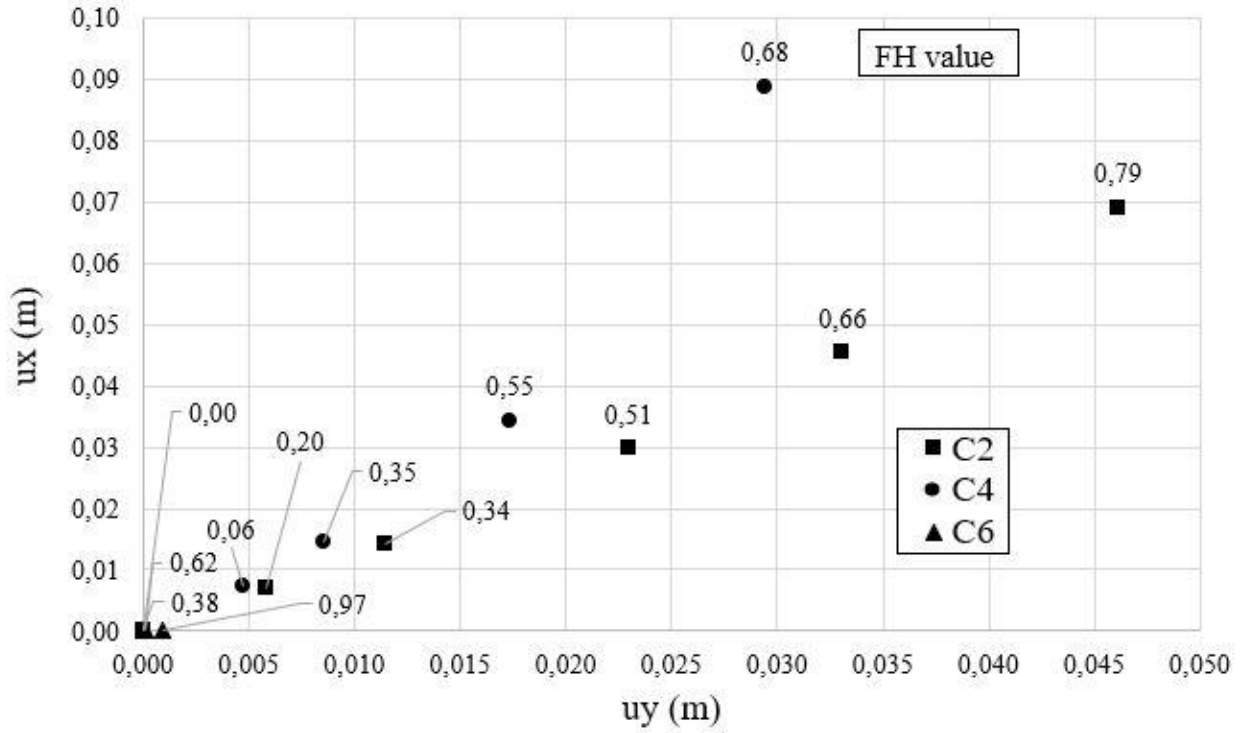
Figure 58 – Horizontal and vertical displacements for C2, C4 and C6 cases
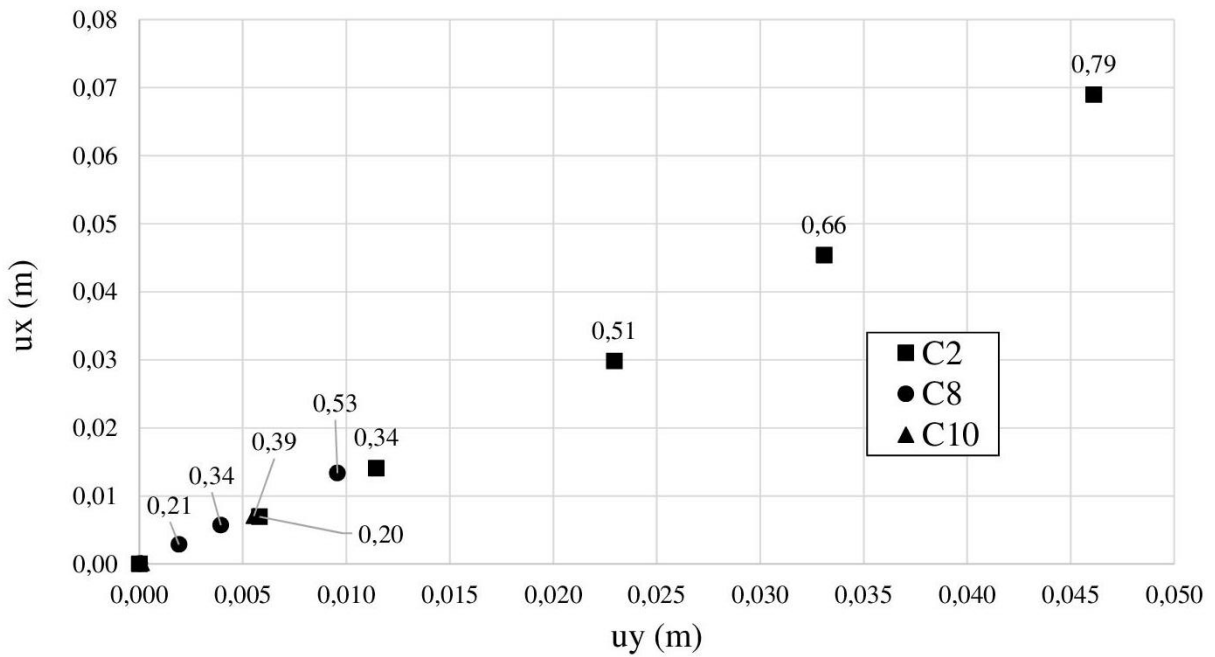

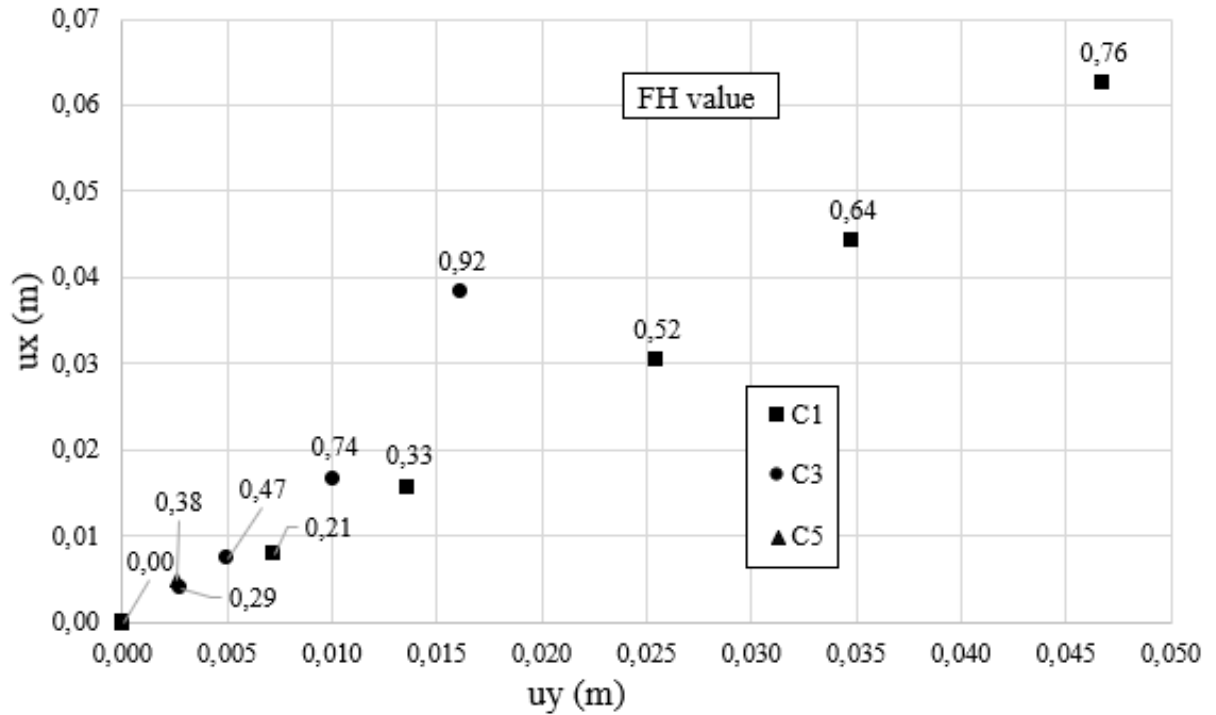Figure 59 - Horizontal and vertical displacements for C2, C8 and C10 cases

Figure 60 - Horizontal and vertical displacements for C1, C3 and C5 cases
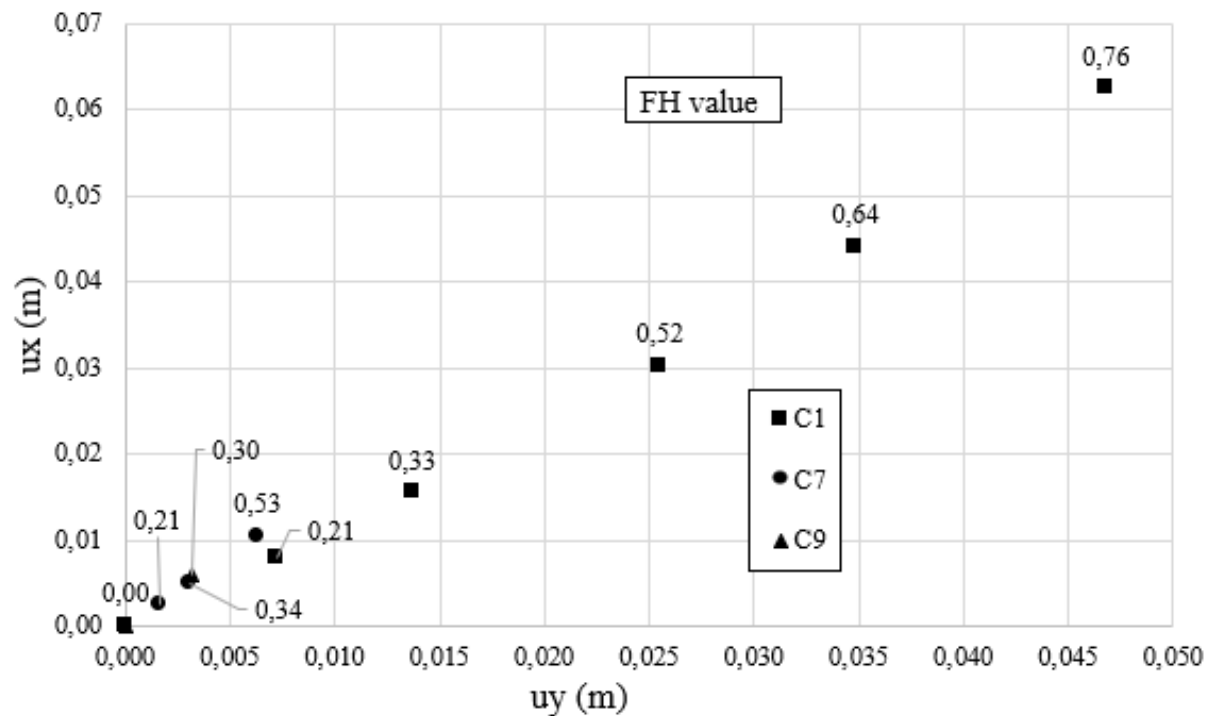

Figure 61 - Horizontal and vertical displacements for C1, C7 and C9 cases

In order to have a useful predictive approach to use even when only limit equilibrium analyses can be performed, for example for a preliminary analysis or when detailed geotechnical parameters are not

available, for each case FH has been correlated with possible strain levels. As suggested by Boscardin and Cording (1989) and Son and Cording (2005), angular distortion and lateral strain (Figure 62) can be simply defined as follows:

$$\beta = \frac{\Delta u_y}{L} \qquad\qquad\qquad\qquad (3.13)$$

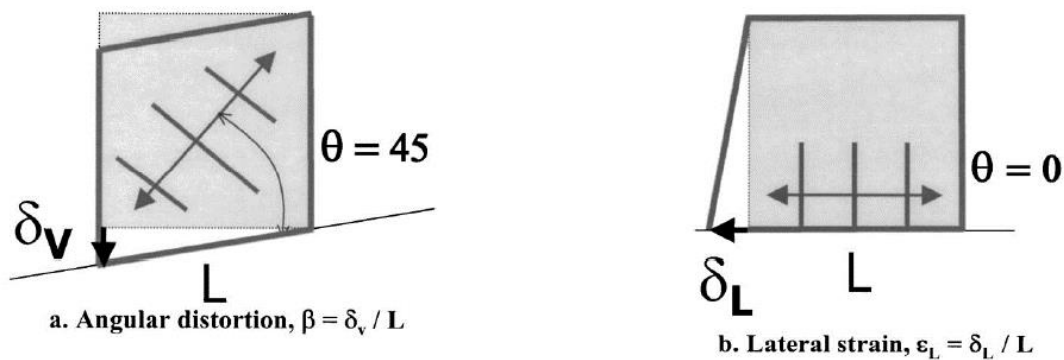$$\alpha = \frac{u_x}{L} = \varepsilon_L \qquad\qquad\qquad\qquad (3.14)$$

Figure 62 – Angular distortion and lateral strain definition by Son and Cording 2005

Following this approach, the obtained results could be applied also to other geometries (especially with regard to B dimension); again, starting from slope angles i_1 and i_2 and from the assessment of the slope initial safety factor FS_0, it is possible to forecast possible strain levels caused by the decrease of stability conditions, represented by the pertinent FH value. Figure 63 illustrates the previously obtained results in terms of the variation of angular distortion β and lateral strain α with FH.

The results obtained by the proposal procedure (Figure 63) aimed at setting up slope displacements with slope safety factors, are compared with the ones provided by Son and Cording 2005, referred to displacements, strain levels and damages caused by deep excavation (Figure 64). It can be noted that, both qualitatively and quantitatively, the agreement is good: the strain levels are of the same order of magnitude as the slope conditions get worse (the hazard factor increases), as it happened for buildings close to deep excavations for which the damage conditions worsen. In addition, the ratio between α and β is very similar to the one obtained by the authors. These considerations confirm the validity of the procedure proposed in this Thesis. Figures from 66 to 75 show the result for each case analysed.
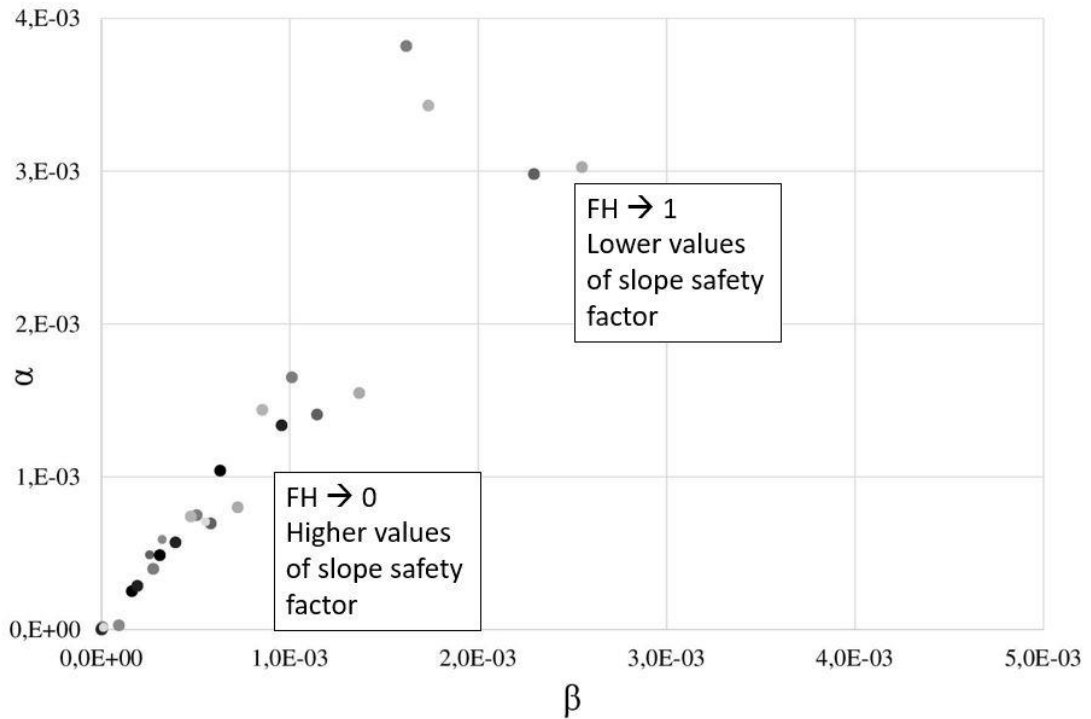
Figure 63 - Relation between angular distortion and lateral strain from the results of the analyses
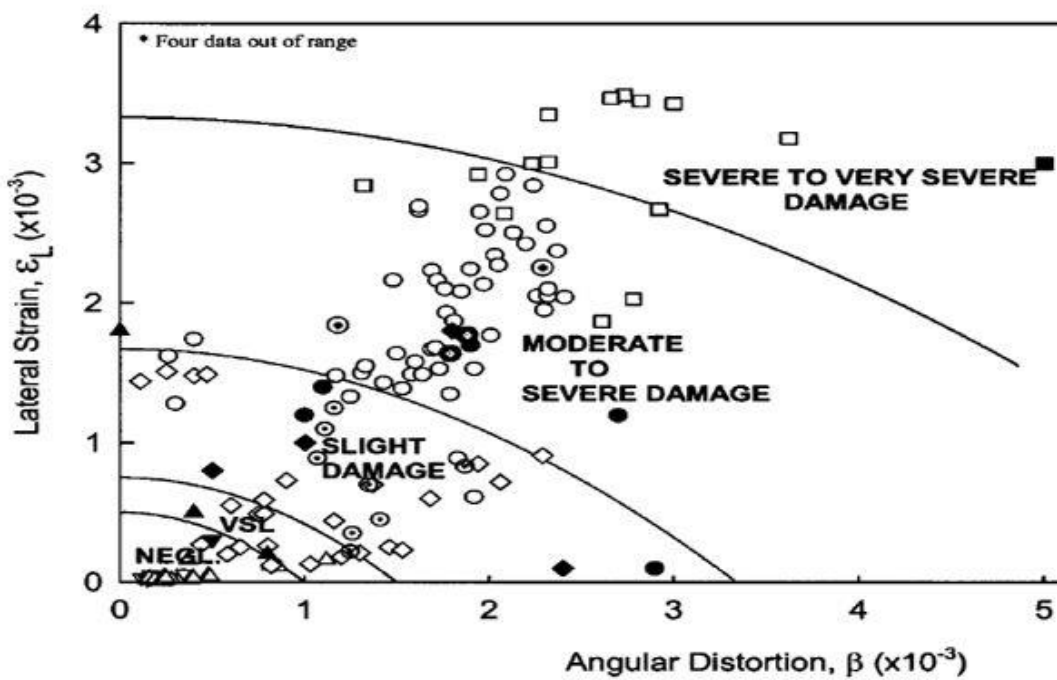

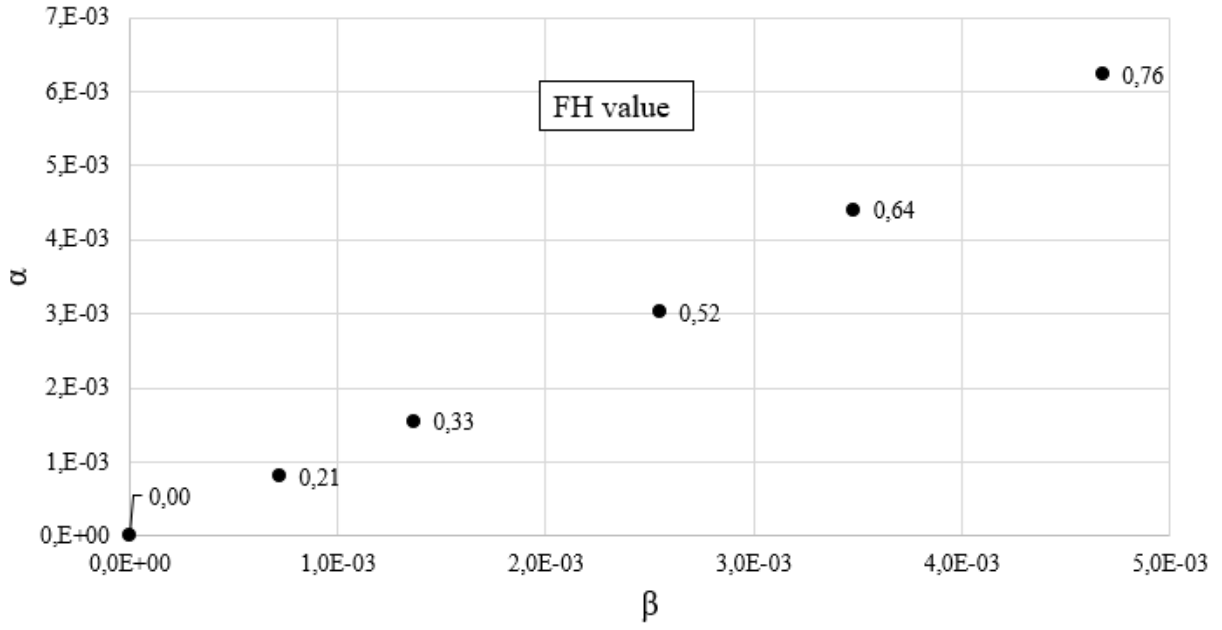Figure 64 – Relation between angular distortion and lateral strain from Son and Cording 2005
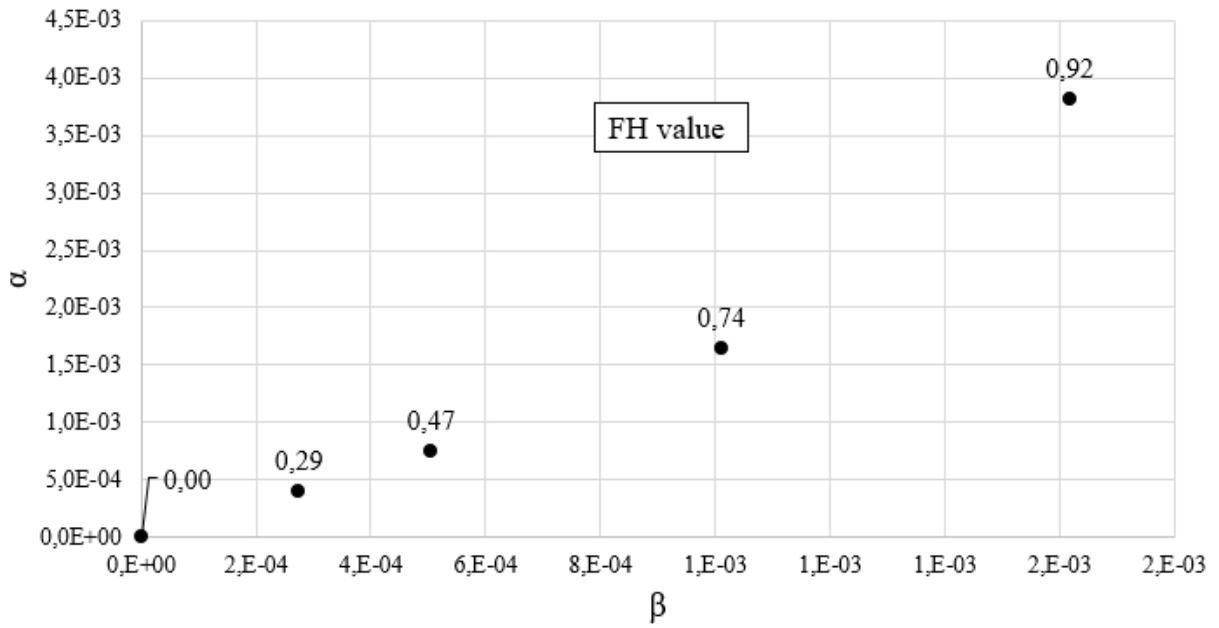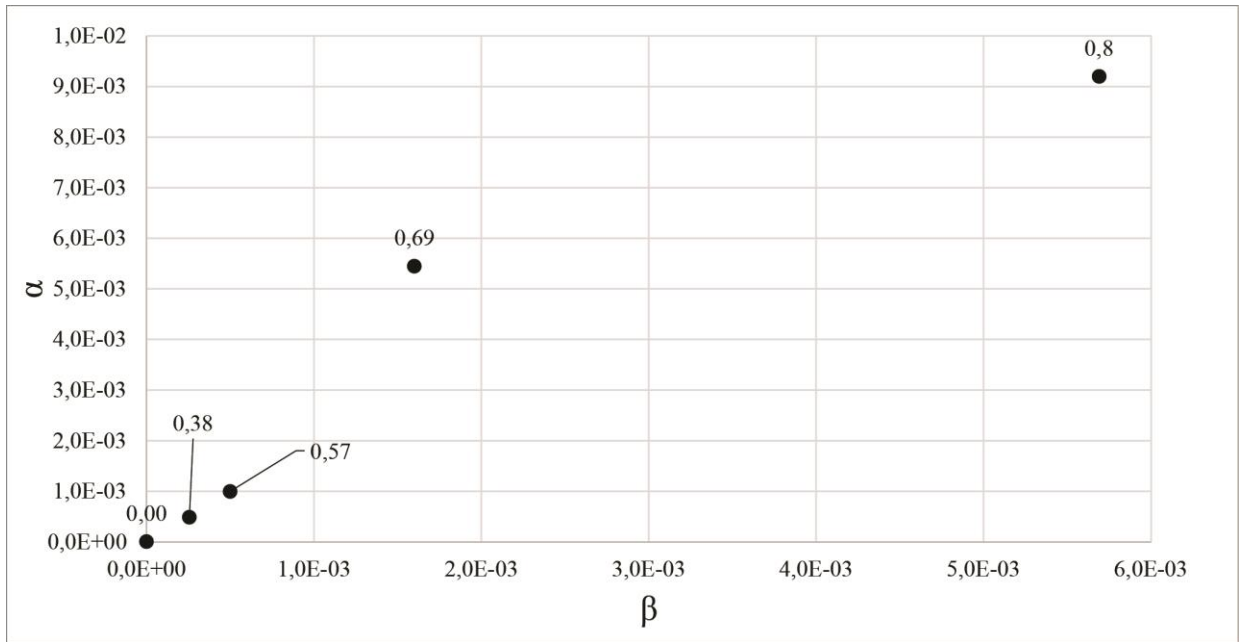
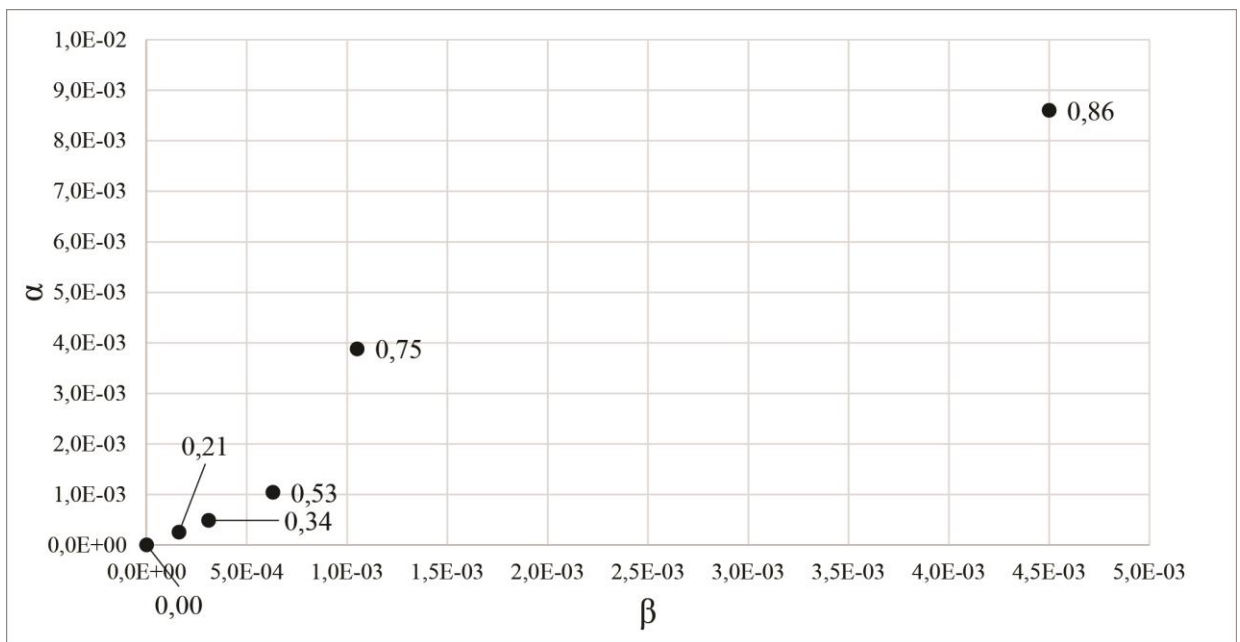Figure 65 – C1 case

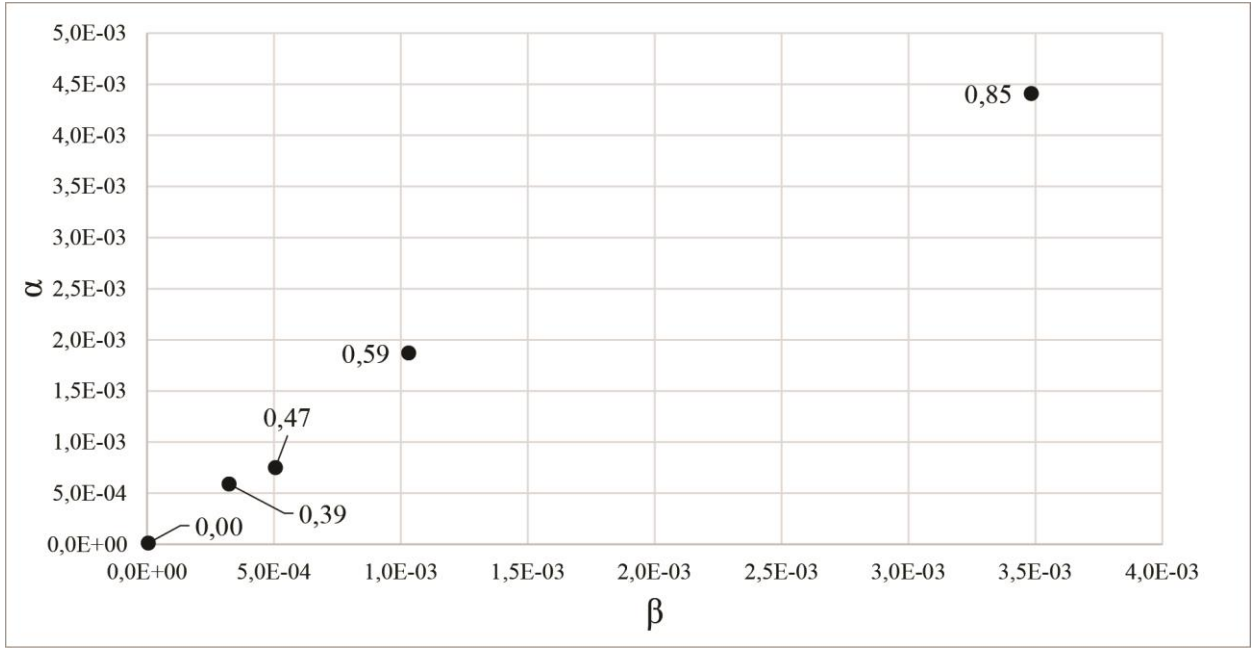Figure 66 - C3 case

Figure 67 - C5 case
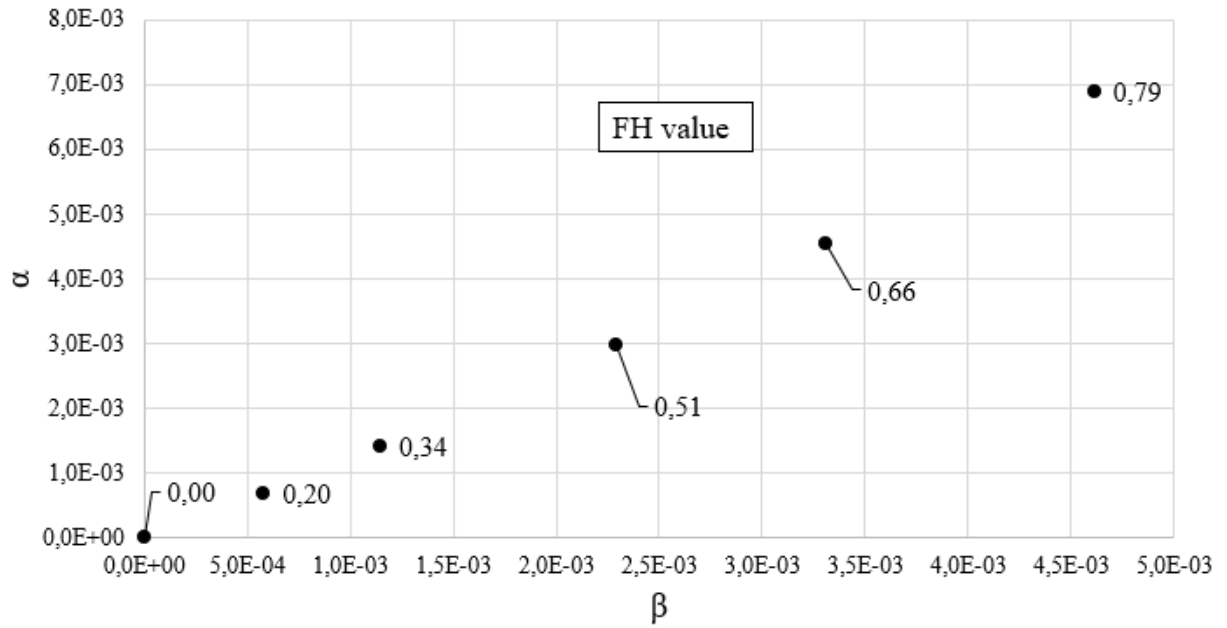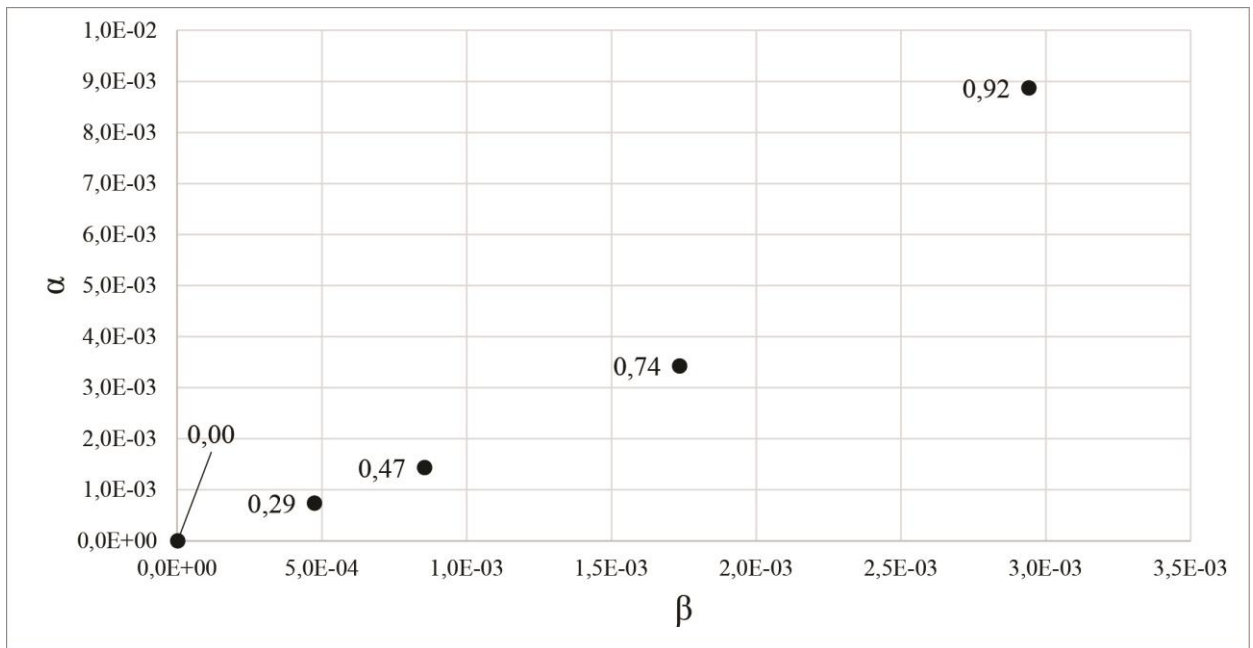

Figure 68 - C7 case

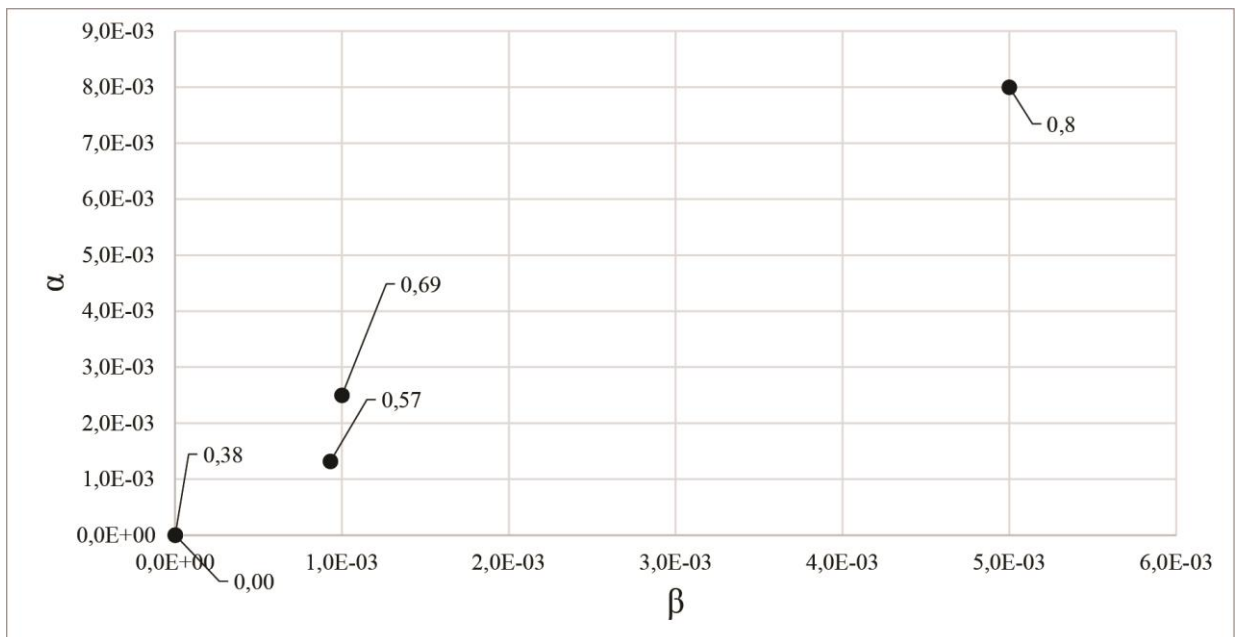Figure 69 – C9 case

Figure 70 - C2 case
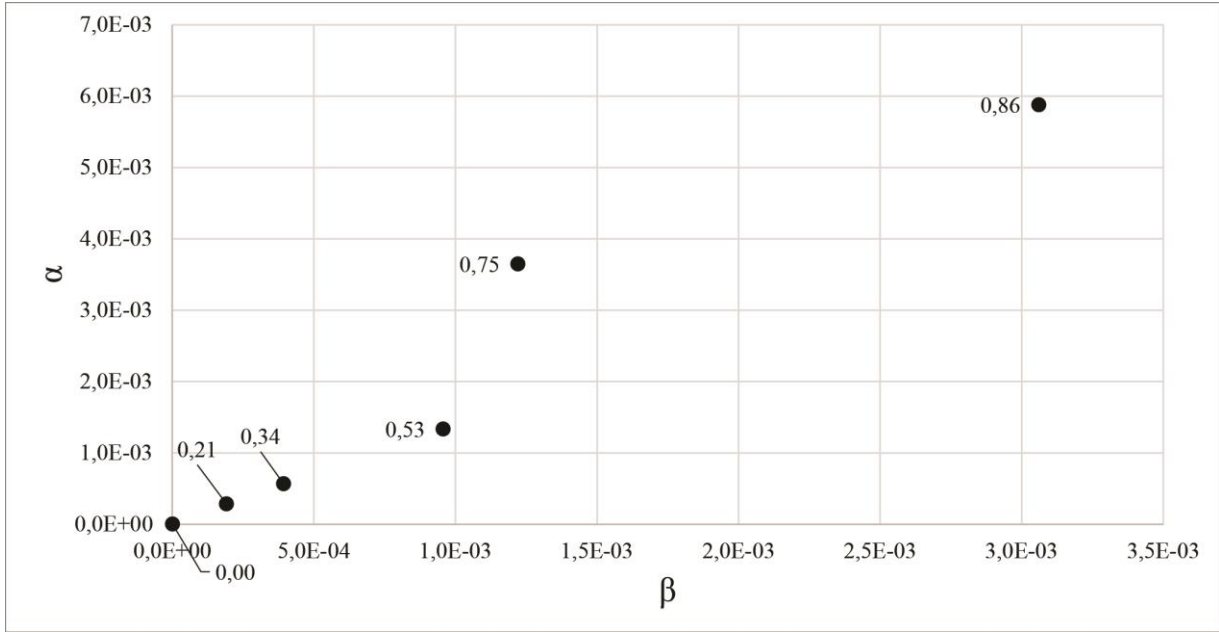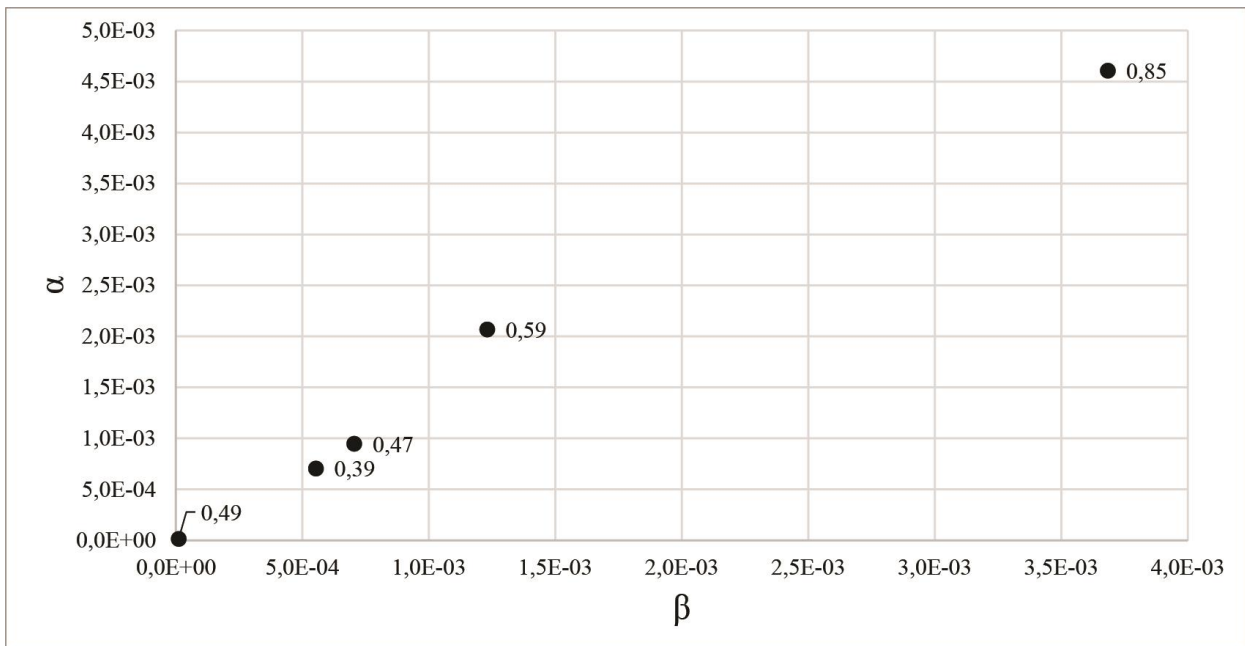
Figure 71 - C4 case

Figure 72 - C6 case

Figure 73 - C8 case

Figure 74 - C10 case

5. DEVELOPMENT OF FRAGILITY CURVES

The aim of this Thesis is to propose a new approach and methodology to predict the effect of slow-moving landslide on churches. In Chapter 4 for this reason, starting from different set of slopes, FEM analyses has been performed and both horizontal and vertical displacements have been defined for each set. Then, LEM analyses has been carried out with the aim of defining the safety factor of the slope and consequently the hazard factor FH, as the geotechnical strength properties of soil decrease, which have been associated with every couple of horizontal and vertical displacements.

This chapter focuses on the development of the fragility curves with the assumption that the hazard factor FH of the slope acts as the intensity parameter, in order to give a simple tool for use, as it can be obtained by a limit equilibrium analysis. At this stage of analyses, the criterion proposed for the evaluation of the damage level, for a given value of FH, is the one implemented by Son and Cording (2005) which complemented the criterion proposed by Boscardin and Cording (1989) and Burland and Wroth (1974) by including the effects of horizontal strains. The procedure will be applied on a case study.

Some of the contents of this Chapter are published in:

Cambiaggi L., Ferrero C., Berardi R, Calderini C. Effect of landslides on churches in Liguria region: a geotechnical approach. *12th International Conference on Structural Analysis of Historical Constructions (SAHC) 2020*

Berardi R., Cambiaggi L. (2020). *Prediction of slope movement effects on churches for the development of a fragility curve approach.* In: Calvetti F., Cotecchia F., Galli A., Jommi C. (eds) Geotechnical Research for Land Protection and Development. CNRIG 2019. Lecture Notes in Civil Engineering, vol 40. Springer, Cham, First Online 23 June 2019, Print ISBN978-3-030-21358-9, Online ISBN978-3-030-21359-6, DOI: https://doi.org/10.1007/978-3-030-21359-6_9, pp. 82-91.

Cambiaggi L., Berardi R. Investigation on the damages induced by slope movements on historic buildings: the case of San Nicolò di Capodimonte church in Liguria. *XVII European Conference on Soil Mechanics and Geotechnical Engineering ECSMGE, Reykjavik Iceland 2019 ISBN 978-9935-9436-1-3.*

5.1 PROCEDURE FOR THE DEVELOPMENT OF FRAGILITY CURVES

A challenge in vulnerability assessment is to build some fragility curves, which express the probability of reaching a given damage state of the structure for a given intensity of hazard (e.g. horizontal and vertical differential displacements in our case). Fragility curves are an important tool for assessing natural hazard risks. Every building or structure has its own fragility curve. The fragility curves can be used as follows:

(i)   for assessing potential effects and risks, including functional, economic and loss in lives,

(ii)   for emergency or disaster response planning,

(iii)   for risk mitigation efforts (retrofitting).

Figure 75 shows an example of fragility curves developed for seismic risk. On x-axis is represented the intensity measure IM, for seismic engineering it is usually the peak ground acceleration PGA, in this Thesis will be the hazard factor FH. On y-axis is reported the probability of reaching a damage state, hereafter called DS. The length of the section between two curves ($P[DS_i]$) is the DS probability distribution, for a given value of the IM. It can be obtained from fragility functions; as in the case proposed in Figure 75, for k=1, 2 and 3, the discrete probabilities are given by:

$$p_{DSk}(im) = p_{LSk}(im) - p_{LSk+1}(im) \qquad (5.1)$$

With respect to DS4, it is worth noting that analytical methods usually are not able to define the higher level of damage; this DS occurs after significant local collapse mechanisms after which the mechanical model become meaningless.
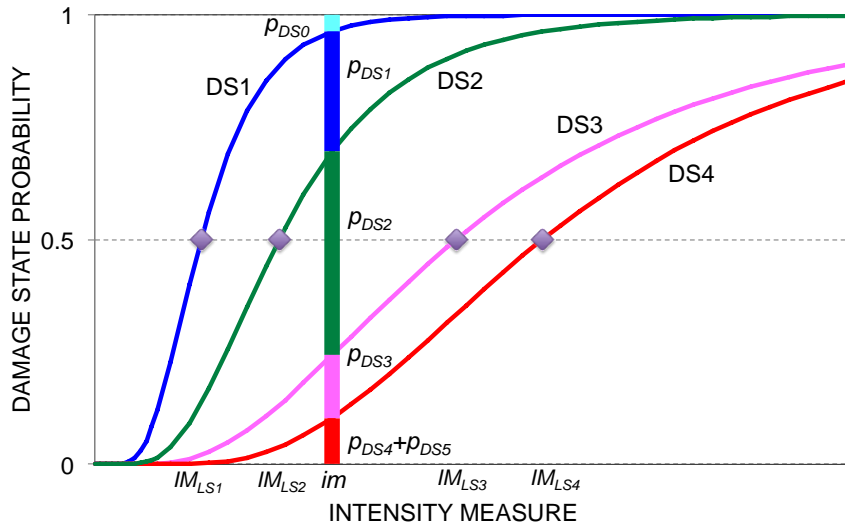
Figure 75- Example of fragility curves to quantify the conditional probability of being or exceeding a certain level of seismic damage (Di) given a seismic intensity measure (IM).

In order to complete the DS distribution, it is necessary to evaluate the probability that the building has "no damage" (DS0):

$$p_{DS0}(IM) = 1 - p_{LS1}(IM) \qquad (5.2)$$

Figure 76 shows a typical discrete damage distribution of damage states, directly obtained from fragility functions of Figure 75 for a given value IM=*im*.
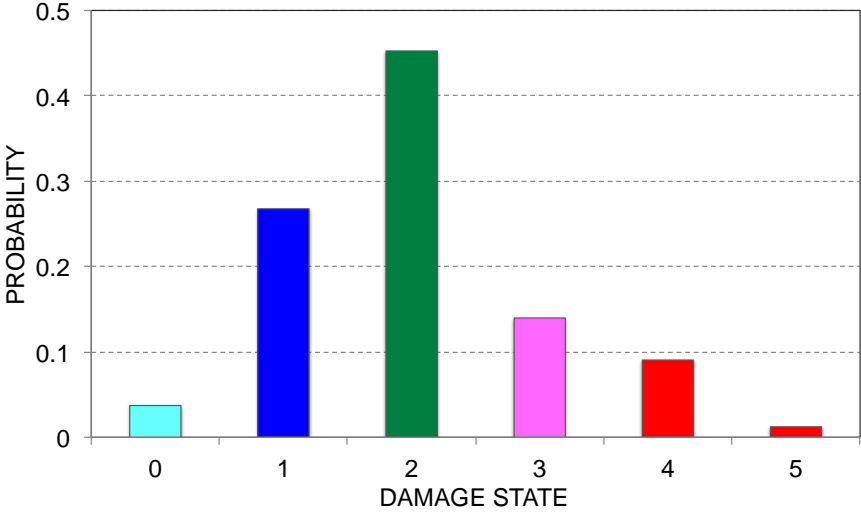
Figure 76 - Damage States probability distribution

In this thesis, the Author has chosen the local damage indicators based on theory proposed by Son and Cording (2005), which complemented the criterion proposed by Burland and Wroth (1974) by including the effects of horizontal strains. Starting from the results of the FEM analysis, horizontal and vertical displacements have been obtained and, subsequently, angular distortion and lateral strain. LEM analyses have been carried out and have allowed the definition of the safety factor. The hazard factor FH has been introduced for each pair of slope angle, to be linked with the pattern of displacement (Figures 65 to 74). Each point has been reported to the figure proposed by Son and Cording in order to define the damage state. It is important to highlight that the analyses have been carried out in free-field conditions with the aim of generating fragility curves for masonry structures, using the criterion proposed by Son and Cording, verifying their adaptability to churches with some case studies. Figure 77 shows five damage levels (DL) (equivalent to the damage states DS in Figure 75 and Figure 76) proposed by the authors. The definition of the critical tensile strain is given in Chapter 1.

Damage level	Critical tensile strain, $\varepsilon_c\,(\times10^{-3})$
Negligible	0−0.5
Very slight	0.5−0.75
Slight	0.75−1.67
Moderate to severe	1.67−3.33
Severe to very severe	>3.33

Figure 77 - Damage level proposed by Son and Cording (2005)

Under the assumption that the hazard factor FH is the representative intensity parameter (IM) of the slow moving landslide that induced different levels of damage to the church, fragility curves were derived. For

this purpose, the frequency of occurrence of each level of damage has been calculated for different classes of FH. Three classes of FH have been considered: 0-0.4, 0.4-0.8, and 0.8-1. Then, the cases have been grouped according with the geometry of the slope: this choice has been made because the inclination of the slope is the parameter that mostly influences the pattern of displacement of the area of interest. Table 14 shows the cases that have been grouped together. Therefore, five classes of fragility curves have been developed.

Table 14 - Set of cases analysed for fragility curves

	Case for fragility curves development				
Slope angle	**F1**	**F2**	**F3**	**F4**	**F5**
$i_1=$	15	15	15	20	25
$i_2=$	15	20	25	15	15

Figure 78 to 82 show the frequency of occurrence for the five groups of analysis referring to different geometries of the slope.
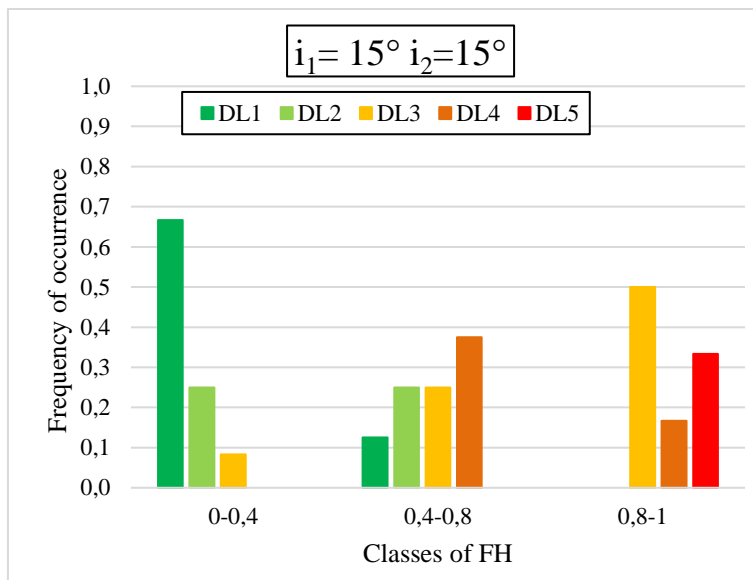
Figure 78 - Frequency of occurrence con case $i_1=15°$, $i_2=15°$
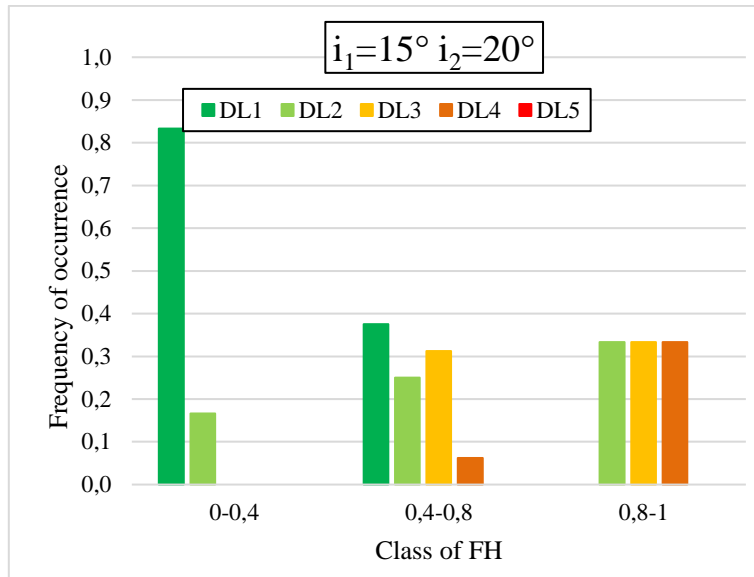
Figure 79 - Frequency of occurrence con case $i_1=15°$, $i_2=20°$
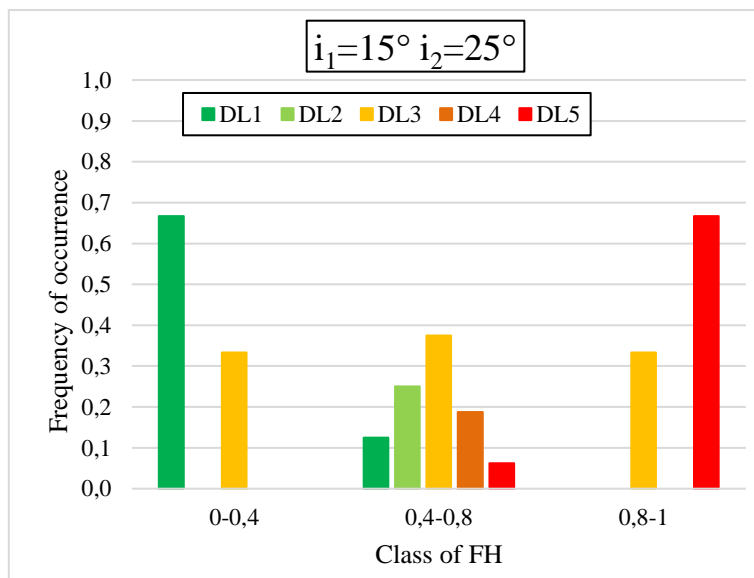
Figure 80 - Frequency of occurrence con case $i_1=15°$, $i_2=25°$
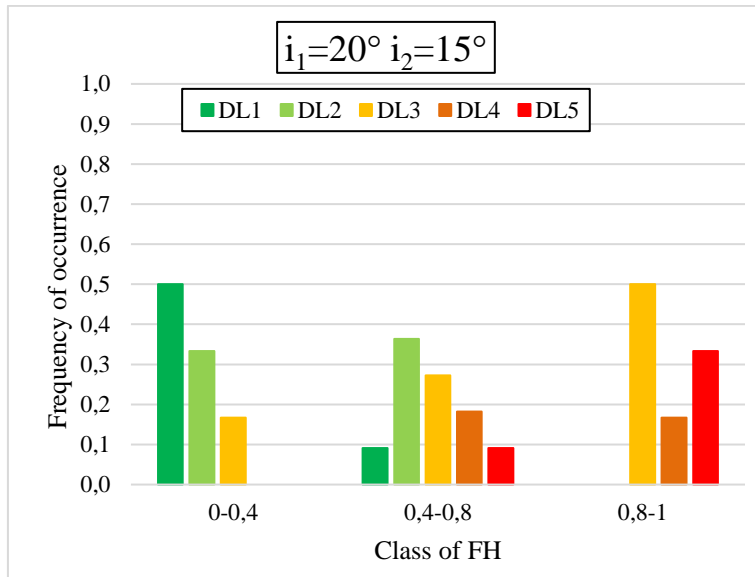
Figure 81 - Frequency of occurrence con case $i_1=20°$, $i_2=15°$
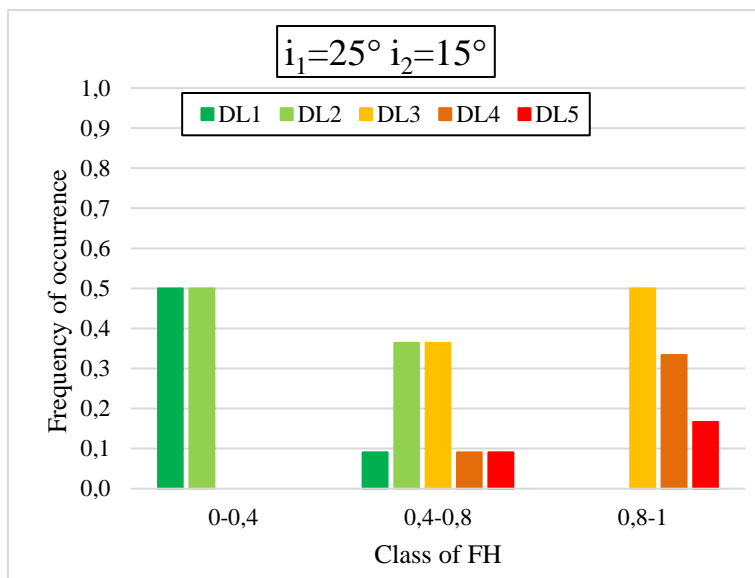
Figure 82 - Frequency of occurrence con case $i_1=25°$, $i_2=15°$

It is worth noting that for small levels of FH, the damage level is low as well, only few cases reach a damage level of 3. When FH is between 0.4-0.8 and therefore the slope is in less stable conditions, more severe levels of damage may occur. In cases where the slope is close to failure (FH closed to 1) a collapse condition can be reached.

For each case the mean value of damage μ_D has been calculated as:

$$\mu_D = \sum_{i=1}^{5} DL_i \cdot P[DL]_i \tag{5.3}$$

μ_D represents, with a given value of IM (in this case FH), the medium level of damage that may occur when IM=FH is fixed.

Table 15 – Mean value of damage for each case

i_1=15° i_2=15°			
	FH		
	0-0,4	0,4-0,8	0,8-1
μD	1,4	2,9	3,8

i_1=15° i_2=20°					i_1=20° i_2=15°			
	FH					FH		
	0-0,4	0,4-0,8	0,8-1			0-0,4	0,4-0,8	0,8-1
μD	1,2	2,1	3	μD		1,7	2,8	3,8

i_1=15° i_2=25°					i_1=25° i_2=15°			
	FH					FH		
	0-0,4	0,4-0,8	0,8-1			0-0,4	0,4-0,8	0,8-1
μD	1,7	2,8	4,3	μD		1,5	2,7	3,7

As shown in Table 15, all the analysed cases are characterized by an increasing value of μ_D, this denotes a good trend of the numerical results.

Then, using methods common in different engineering fields (Fotopoulou et al., 2013a,b; Mavrouli et al., 2014; Negulescu and Foerster, 2010; Negulescu et al., 2014), the probabilities were calculated using a two-parameter lognormal distribution function, adopted due to its simple parametric form to represent a fragility curve for a predefined damage/limit state:

$$P(Damage \geq D_i / IM) = \Phi\left[\frac{1}{\beta}\ln\left(\frac{IM}{\overline{IM}_i}\right)\right] \tag{5.4}$$

where $P(\cdot)$ is the probability of reaching or exceeding a particular damage level D_i for a fixed intensity parameter IM ; $\Phi[\_]$ is the standard normal cumulative distribution function; $\overline{IM}$ is the median value of IM where the building reaches each D_i; and β is the standard deviation of the natural logarithm of IM for each Di. The median values of FH, corresponding to each D_i, are those that give 50% probability of exceeding each damage level; whereas the standard deviation β describes the variability associated with each fragility curve. This choice has been made because the log-normal distribution function well approximates the data obtained by the numerical analysis. Different procedures can be applied to estimate the log- normally distributed fragility parameters (median and log- standard deviation) given the simulated

damage data. The Maximum Likelihood Method is implemented in this study as it was found to be more efficient (predicting lower log-standard deviation values) for the simulated dataset.

The likelihood function is introduced as:

$$L(IM_1, IM_2, IM_3, IM_4, IM_5, \beta) = \prod_{i=1}^{N} \prod_{j=0}^{5} P_j \left[IM_i; E_j \right]^{y_{ij}} \tag{5.5}$$

Where:

- E_j is the specified damage state for no damage (j=0), at least negligible damage (j=1), at least very slight damage (j=2), at least very slight damage (j=3), at least moderate to severe damage (j=4), and severe damage (j=4).

- y_{ij}=1 if the damage state E_j occurs for the i simulation of the structure subject to the landslide intensity IM_i or 0 otherwise.

Then the maximum likelihood estimates for $\overline{IM}$ and β are obtained by solving the following equations to maximize lnL and hence L:

$$\frac{d \ln L}{d\overline{IM}} = \frac{d \ln L}{d\beta} = 0 \tag{5.6}$$

The computation is performed numerically using a standard optimization algorithm in MATLAB. Table 16 presents the derived median and log-standard deviation for all the analysed models when using FH as parameter of intensity for the landslide.

Table 16 – Median and standard deviation for fragility curves

Median and standard deviation parameters										
Case F1	**Damage level**				**Case F2**		**Damage level**			
	2	**3**	**4**	**5**			**2**	**3**	**4**	**5**
Median	0,30	0,47	0,70	1,10		Median	0,40	0,80	1,20	
Standard deviation	0,50	0,50	0,60	0,70		Standard deviation	0,50	0,50	0,45	
Case F3	**Damage level**				**Case F4**		**Damage level**			
	2	**3**	**4**	**5**			**2**	**3**	**4**	**5**
Median	0,28	0,37	0,75	0,85		Median	0,20	0,48	0,80	1,10
Standard deviation	0,50	0,50	0,45	0,40		Standard deviation	0,50	0,60	0,60	0,50
Case F5	**Damage level**									
	2	**3**	**4**	**5**						
Median	0,20	0,55	0,90	1,50						
Standard deviation	0,60	0,45	0,60	0,60						

Figure 83 to Figure 87 shows the fragility curves obtained for the five different schemes of slope. It is important to underline that, as already explained, failure condition is difficult to reach because the mechanical model become meaningless. For this reason, in Figure 84 there is no evidence of DL5.
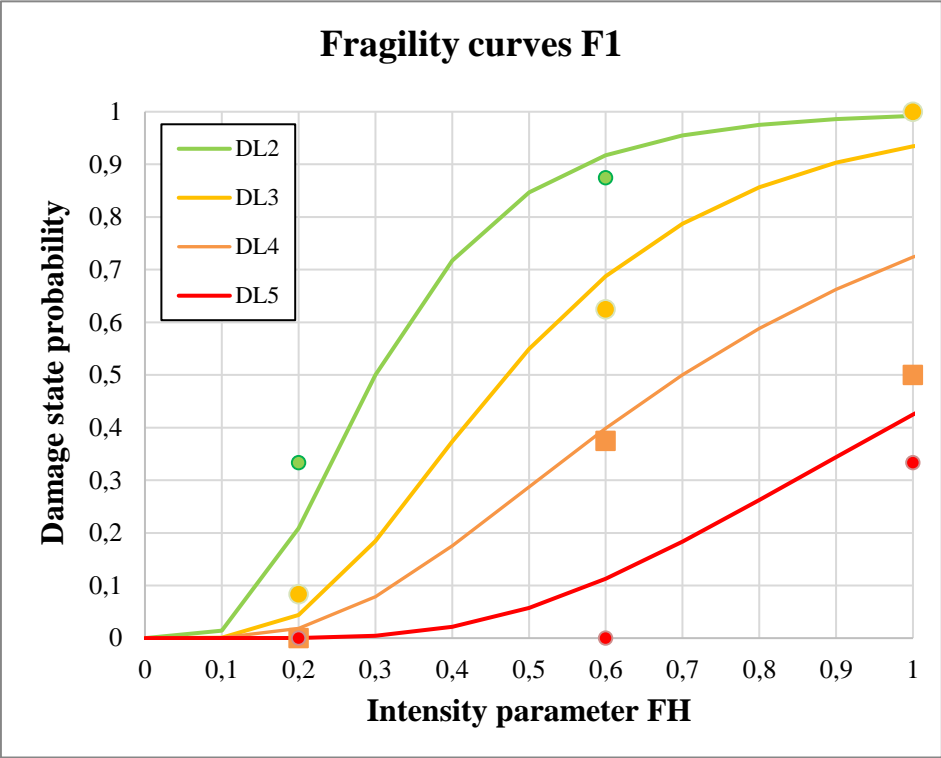
Figure 83 - Fragility curves F1
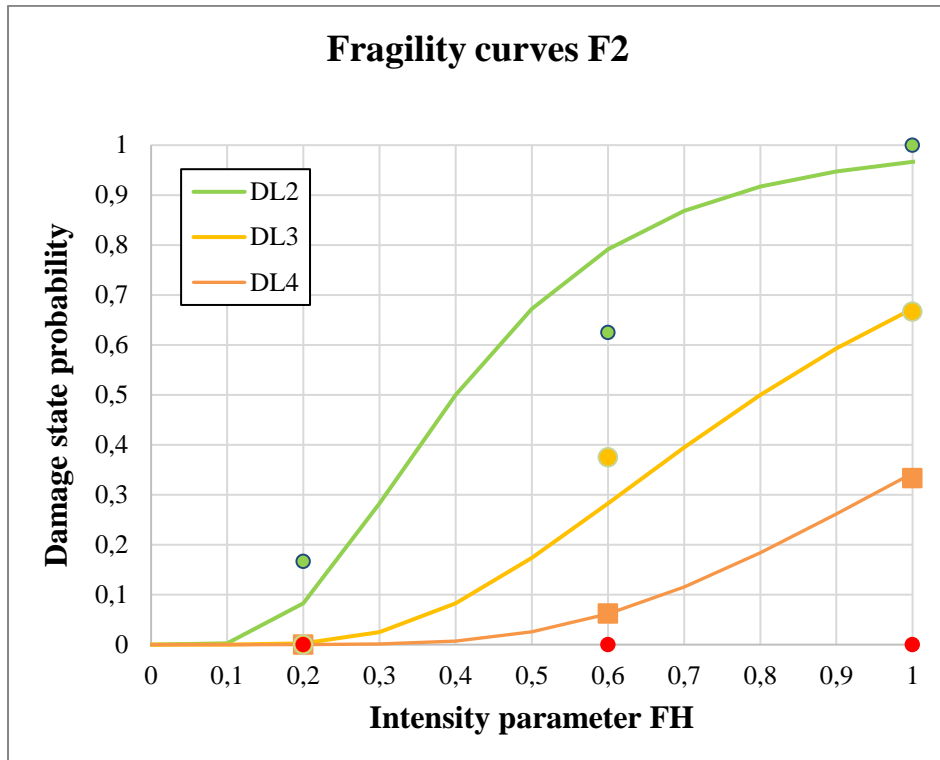
Figure 84 - Fragility curves F2
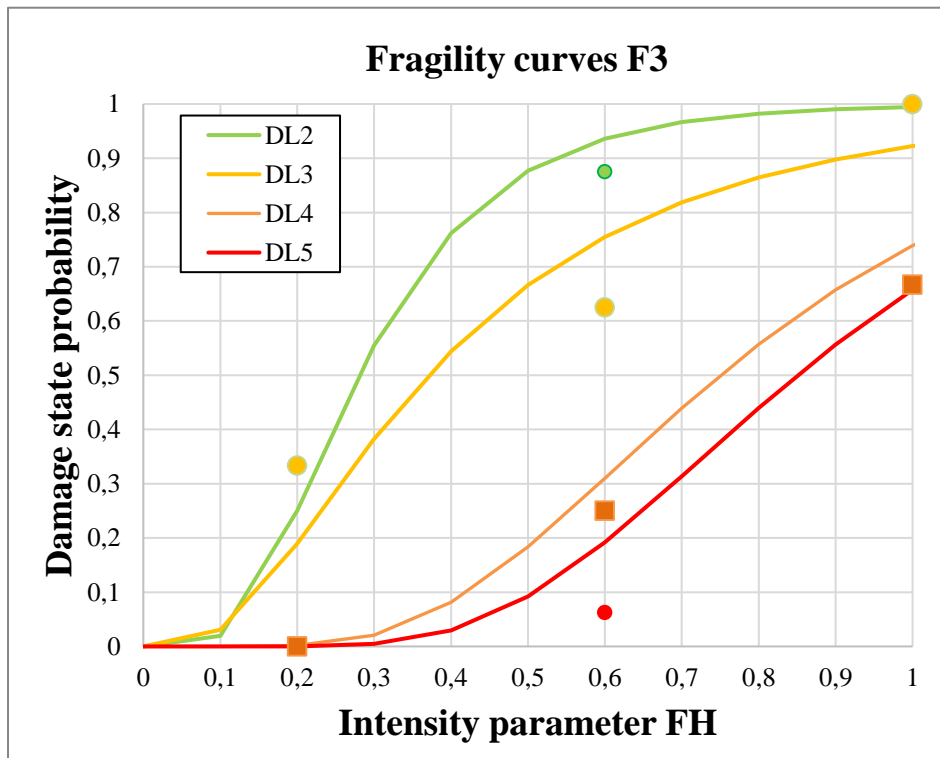
Figure 85 - Fragility curves F3
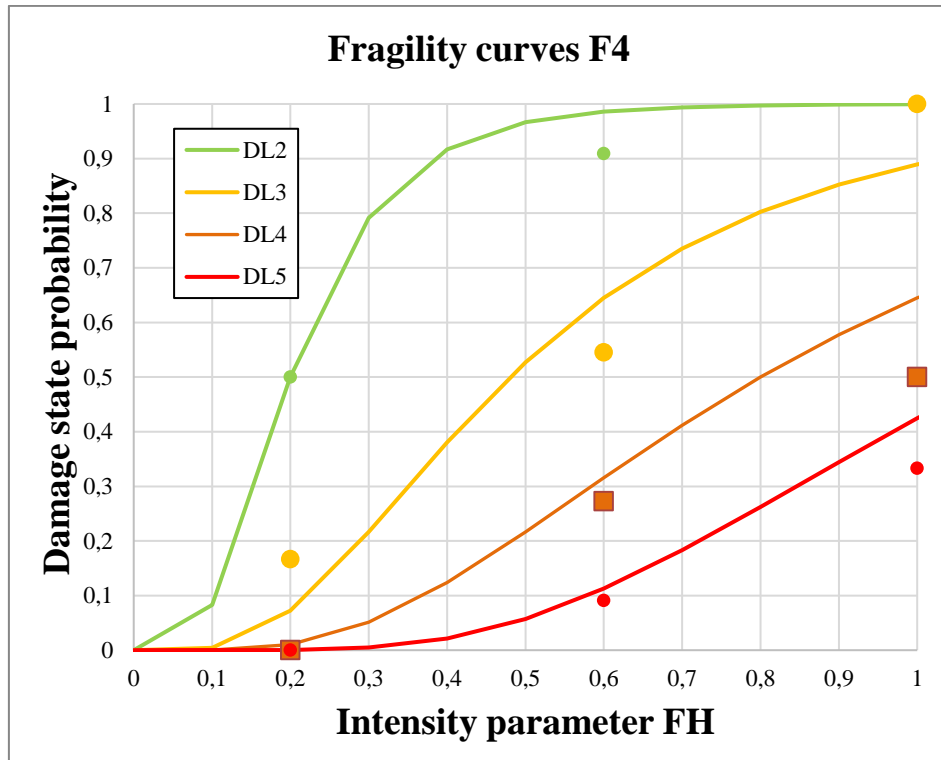
Figure 86 - Fragility curves F4
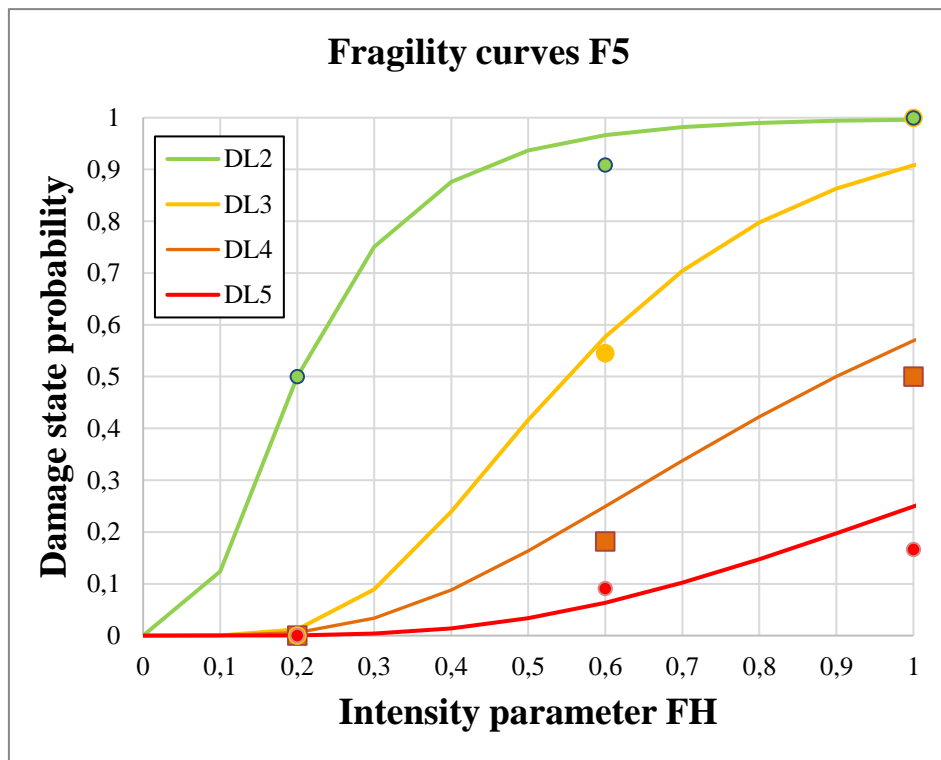
Figure 87 - Fragility curves F5

Since the aim of this research was the development of a new methodology to study the effects of slow moving landslide on churches, the analysis have been carried out under some assumption that have led to sufficiently accurate results. It is important to point out that other analyses should be carried out in order to investigate the role of the soil properties and the water table as well for the response of the slope.

5.2 APPLICATION OF THE PROPOSED METHOD TO ONE OF THE CASE STUDIES: SAN CARLO DI CASSINGHENO CHURCH

The case study analysed is the Church of San Carlo in Cassingheno, municipality of Fascia, in the district of Genoa. It is a single nave church, about 20m. long, built in 1595, located in an active landslide area classified as complex (Varnes, 1978). Referring to Chapter 2, hereafter it will be called CH_28.

Using a GIS software and the acquisition of DTM data of the area, it was possible to obtain a sufficiently precise topographic survey, in order to trace longitudinal sections along the slope, particularly along the direction on the landslide (Figure 88).
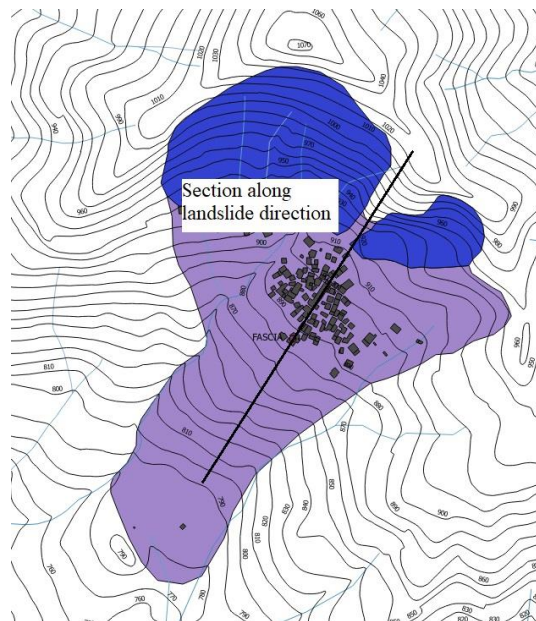
Figure 88 – Landslide of Cassingheno and section analysed

Table 17 - Geotechnical characterization

Soil	γ (kN/m3)	c (kPa)	ϕ (°)	ψ (°)	E (MPa)	ν
Blanket A	19	5	24	0	25	0.4
Blanket B	21	2	27	0	30	0.3
Transition C	24	45	25	5	70	0.25
Bedrock D	26	70	40	5	150	0.4

The church and the village of Cassingheno are located on a medium-low inclined slope (about 20°), probably being the accumulation zone of a relict deep slide.

Some boreholes referred in previous investigations (Figure 89) have allowed to define the stratigraphical sequence, which indicates a thick layer (10-15 m) of very heterogeneous blanket (sand with clasts, clayey silts) separated from the bedrock (shales) by a transition zone (1-3 m) of weathered rock. The ground water table, whose oscillations follow mainly the seasonality, is located within the blanket.

The investigation supplied information about the soil identification properties and values of N_{SPT} and RQD that partially allowed the assessment of the geotechnical mechanical properties. They have been defined, as shown in Table 17, also by a parametric analysis, based on parameters taken from the characterization of similar soils in an analogous context.

Finally, it is worth mentioning that some inclinometers were installed during the REMOVER monitoring project of the Liguria Region, now completed. They show small movements of the blanket at variable depths along the slope; all the instruments indicate a possible failure surface located at depth 9-12 m from ground surface. Figure 89 shows a sketch of the position of the boreholes and inclinometers, as well as of the adopted stratigraphical sequence, along the section chosen for the analyses, corresponding to the landslide direction.
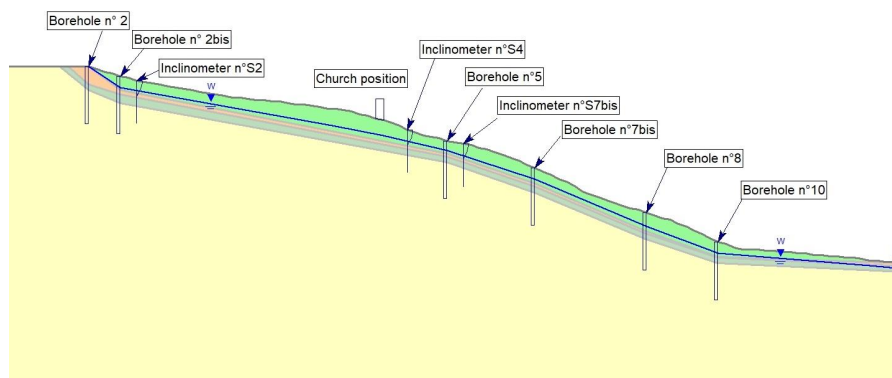
Figure 89 - Localization of boreholes, inclinometers and the church of San Carlo

5.2.1   GEOTECHNICAL NUMERICAL ANALYSIS AND RESULTS

Both limit equilibrium (LEM) analyses and FEM analyses were performed in order to associate slope displacements with slope safety factors and, consequently, with the proposed hazard factor FH.

In FEM analyses, carried out by Plaxis 2D, a simple linear elastic perfectly-plastic model with Mohr-Coulomb failure criterion has been adopted for all the soil layers. The geotechnical properties are synthesized in Table 17. It is important to underline that in order to reduce the safety factor and trigger slope movements, different levels of water table were considered. Twelve phreatic levels surfaces have been modelled, simulating different hydrologic conditions that actually could occur.

Each numerical analysis refers to a different phreatic level to which the relevant vertical and horizontal displacements, in sections of interest, can be associated with. In Figure 90 an example of the horizontal displacements (u_x profile) is shown.

It is worth noting that two different zones of instability are generated (the highest displacements are shown in red): one zone under the church and the other at a lower level, where the safety factors FS are always the lowest.

Once all analyses have been performed, the values of the displacements in the section under the church have been collected in order to be linked to the results of the limit equilibrium analyses.

By the limit equilibrium analyses (carried out by Slide 2D - Rocscience Inc.), potential failure surfaces have been obtained, referring to the slope sections where displacements were evaluated using FEM (particularly in the church area).

With the same parameters, slope geometry and phreatic levels assumed, the LEM analyses have led to results that are completely comparable with those of FEM analyses, as exemplified in Figure 91, which shows the safety factors associated with the two areas of maximum displacement already highlighted in Figure 90. The minimum FS value from the LEM analyses is 1.105, while in the FEM analyses FS min = 1.09 was estimated.
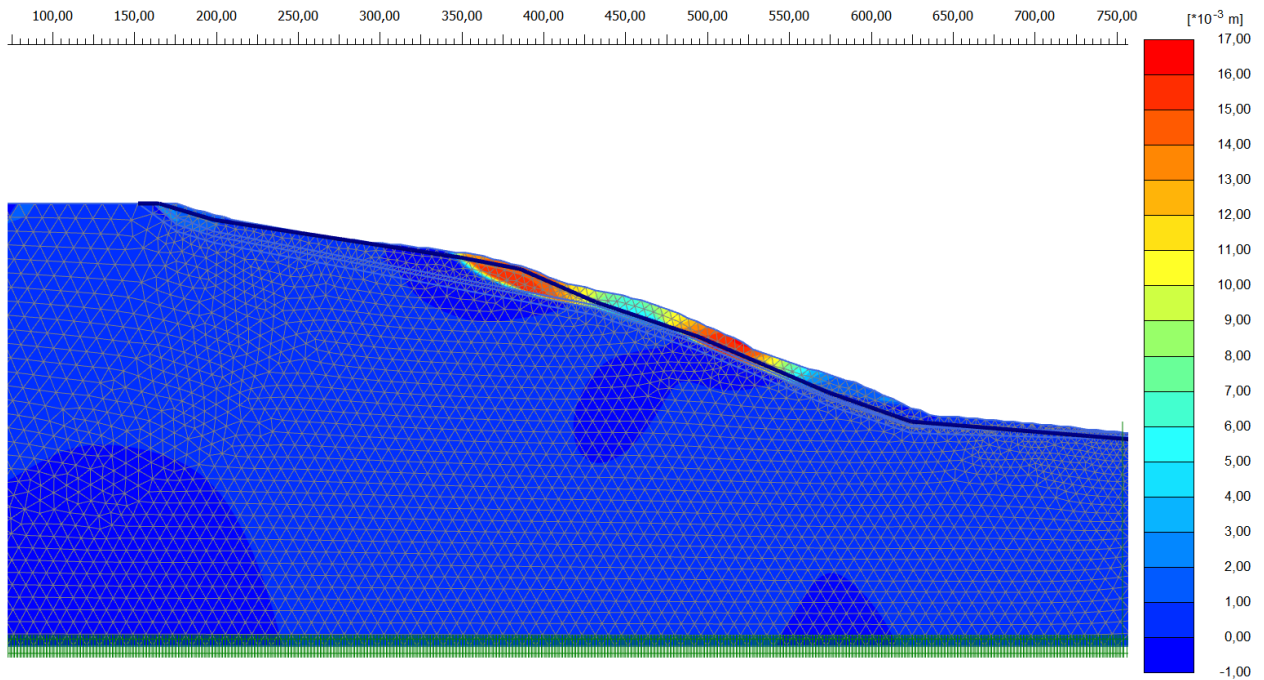
Figure 90 - Horizontal displacements (ux profile, in mm) obtained in FEM analyses
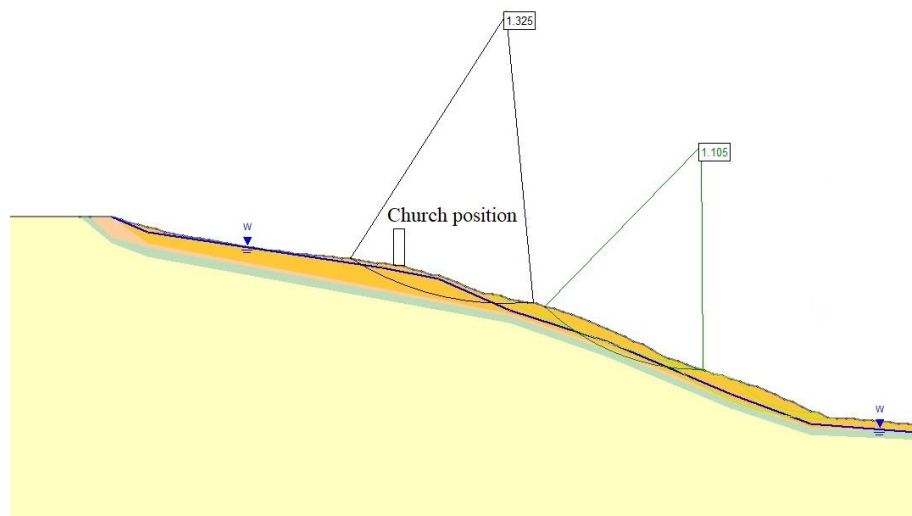
Figure 91 - Potential failure surfaces and factors of safety obtained in LEM analyses

Furthermore, both approaches agree with the inclinometer measurements, as they indicate critical conditions on surfaces affecting the blanket at depths varying between 10 and 12 m. For each hypothesized phreatic level and for curves affecting the church area the calculated safety factors (Bishop method) are: $FS_0 = 1.88$; $FS = 1.85$-1.77-1.62-1.50-1.33-1.29.
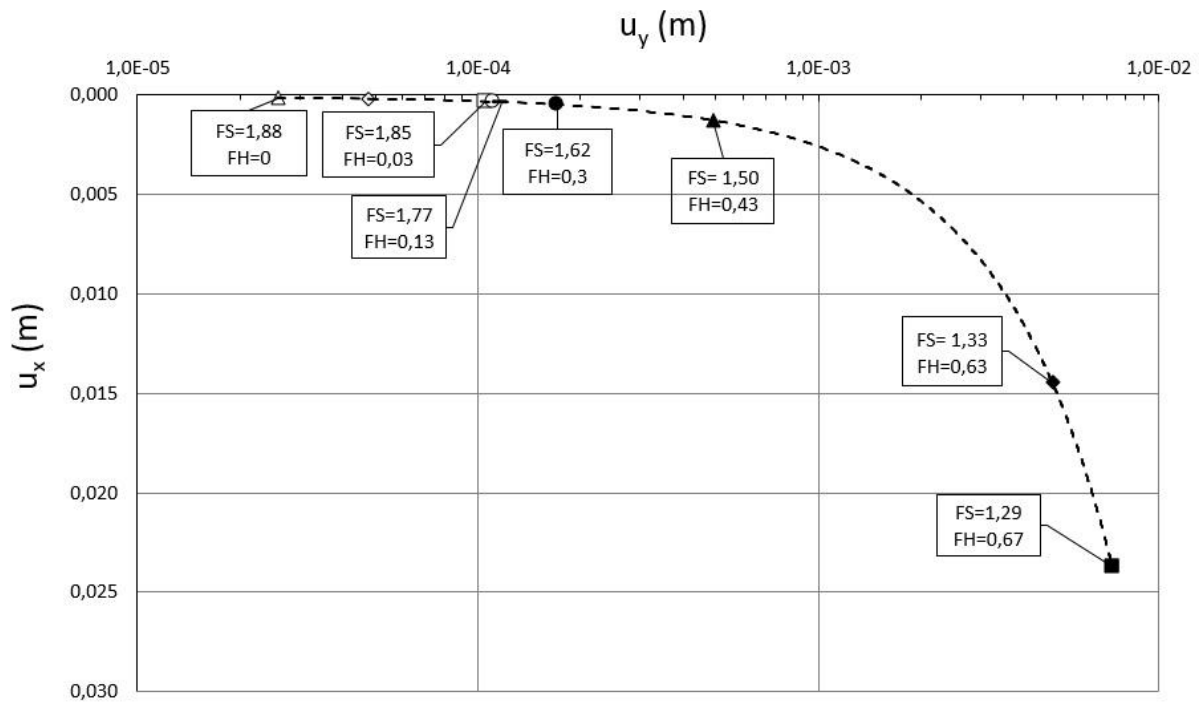
Figure 92 - Horizontal and vertical displacements in the church area associated to the hazard factor FH

Once the horizontal (u_x) and vertical (u_y) displacements have been estimated in the area of interest, to which a different value of the safety factor FS and hazard factor FH are associated for each single simulation, they have been plotted as shown in Figure 92. The trend of the horizontal and vertical displacements is in good agreement with the results of the numerical analysis of Chapter 4.

Finally, it is worth noting that the displacements referable to a hazard index FH ≈ 0.7 (FS ≈1.2) are of the same order of magnitude of those measured by inclinometers and can be compared to the width of the detected cracks.

5.2.2   PROCEDURE FOR THE EVALUATION OF THE DAMAGE LEVEL

The first step for the application of the methodology proposed in this study is the evaluation of the geometry of the slope. The church and the village of Cassingheno are located on a medium-low inclined slope, the slope inclination downhill i_1 is equal to 15° as the uphill angle i_2 =15°. Therefore, the fragility curves for this case study is F1 (Figure 83). Through this fragility curves, it is possible to define the medium damage associated with the intensity parameter FH for the slope of interest.

The intensity parameter, for practical engineering use, can be estimate by LEM analysis as explained in the previous paragraph. Starting from an initial condition of the slope, characterized by a fixed value of FS, different set of analysis can be performed in order to simulate the evolution of FS and, consequently, FH.

The fragility curves can be an important tool to better understand the probability of reaching or exceeding a certain damage level, thus being able to plan interventions to prevent more severe damage levels that could led to collapse of the structure. In this paragraph is proposed an example of damage evaluation as FH increases.

For hypothesis, it can be assumed that three level of FH are fixed as the stability condition of the slope decreases.

- FH_1=0.4;
- FH_2=0.6;
- FH_3=0.8.

Figure 93 shows for fragility curves F1 the values of FH considered in this paragraph.

Fragility curves F1
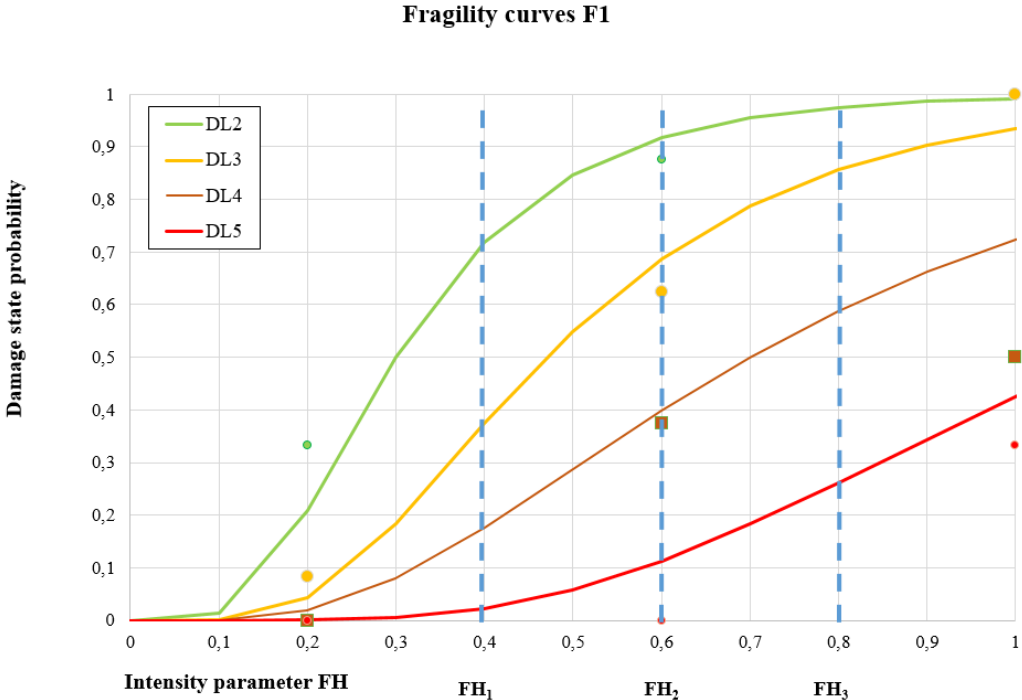
Figure 93 – Fragility curves F1 with fixed FH value

Having defined the three intensity parameters, for each of them it is possible to evaluate the mean damage as expressed in Eq. 5.3. Figure 94 shows for each intensity parameter the probability of occurrence for each damage level.

Fragility curves F1
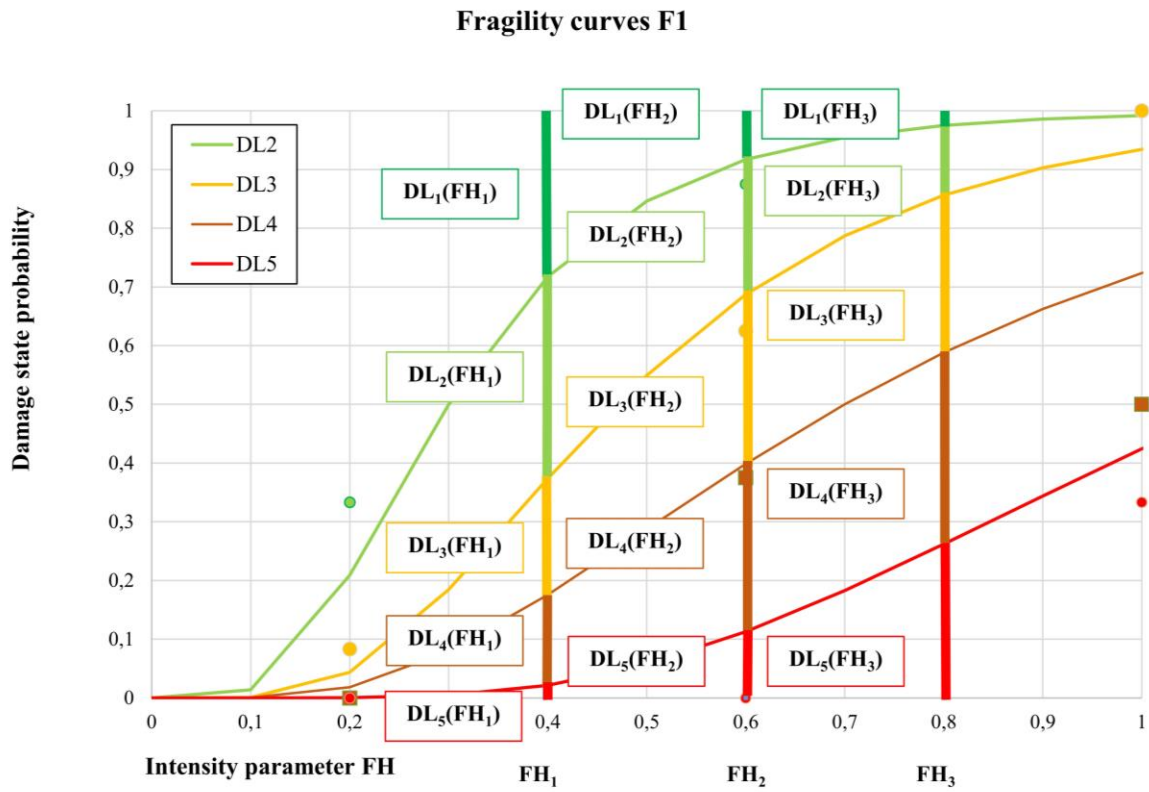
Figure 94 - Fragility curves F1 and damage state probability

The mean damage value for each FH has been calculated starting from the value given by the log-normal distribution as shown in Table 18:

Table 18 - Value of the lognormal distribution for F1

FH	P[DL2]	P[DL3]	P[DL4]	P[DL5]
0,100	0,014	0,001	0,015	0,000
0,200	0,209	0,044	0,059	0,000
0,300	0,500	0,185	0,145	0,005
0,400	0,717	0,374	0,242	0,022
0,500	0,847	0,549	0,337	0,057
0,600	0,917	0,687	0,424	0,113
0,700	0,955	0,787	0,500	0,183
0,800	0,975	0,856	0,566	0,262
0,900	0,986	0,903	0,623	0,344
1,000	0,992	0,934	0,672	0,424
1,200	0,997	0,970	0,750	0,569

Table 19 – Evaluation of mean level of damage

FH 1			FH2			FH3	
P[DLiDL1|FH=0,4]	0,283		P[DLiDL1|FH=0,6]	0,083		P[DLiDL1|FH=0,8]	0,025
P[DLiDL2|FH=0,4]	0,344		P[DLiDL2|FH=0,6]	0,230		P[DLiDL2|FH=0,8]	0,119
P[DLiDL3|FH=0,4]	0,131		P[DLiDL3|FH=0,6]	0,264		P[DLiDL3|FH=0,8]	0,290
P[DLiDL4|FH=0,4]	0,221		P[DLiDL4|FH=0,6]	0,311		P[DLiDL4|FH=0,8]	0,304
P[DLiDL5|FH=0,4]	0,022		P[DLiDL5|FH=0,6]	0,113		P[DLiDL5|FH=0,8]	0,262

μ_D	μ_D	μ_D
2,4	3,1	3,7
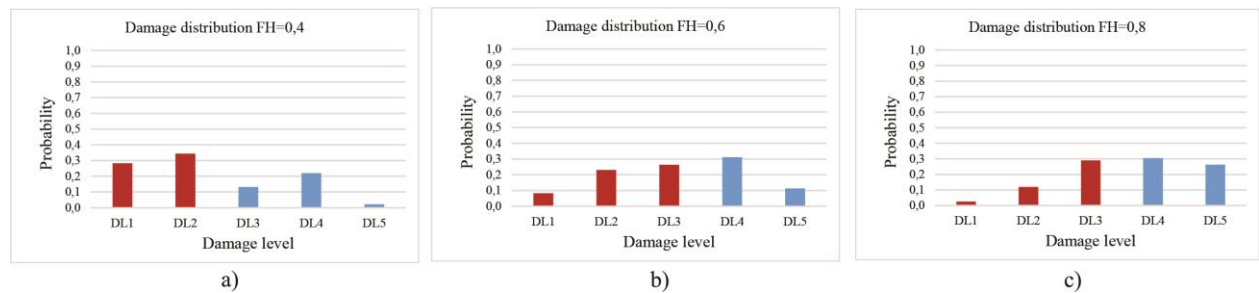
Figure 95 – Damage distribution as FH increase

Table 19 and Figure 95 show the value of μ_D as the intensity factor increases. It can be seen that when FH is equal to 0.8, the damage level is close to 4, which means moderate to severe damage.

If a certain level of damage (thus associated with the safety factor of the slope through FH) could result in a seriousness of damage to the cultural heritage that would compromise the historical-artistic value and structural safety, the procedure helps in the decision process of planning interventions to increase the stability of the slope or reduce the vulnerability of the structure.

5.2.3   VERIFICATION OF FRAGILITY CURVES FOR CH_28

In this section, the objective is the validation of the fragility curves generated from the numerical analysis with the real damage level of the church. The Author, in collaboration with Prof. Chiara Calderini and Ph.D. candidate Chiara Ferrero from University of Genoa, Department of Civil, Chemical and Environmental Engineering, performed the crack survey of the church of the sample selected (Chapter 2). The damage pattern is described below for the different structural elements composing the church: floors, walls and pillars, and arches and vaults.

- The church is characterized by cracks that originate from the floor and propagate upwards into the walls, as shown in Figure 96. The presence of two large parallel cracks (18 mm the largest one, in good agreement with the inclinometric measure) highlight the significant horizontal component of the soil movement.
- The apse wall, Figure 97a, exhibits vertical cracks while the longitudinal walls show several diagonal cracks indicating the presence of a settlement in the centre of the church.
- Extensive damage in vaults in the form of longitudinal shear cracks were also found (Figure 97c).

The crack pattern (Figure 98) denotes the presence of both horizontal and vertical components of the movements and the church exhibits a global response leading to the cooperation of the different elements composing the structure. This type of behaviour is probably due to slow-moving landslides because it evolves slowly over time, result in soil displacements of small instantaneous magnitude, which can be more easily accommodated by historic masonry structures, thanks to their high ductility.

In this church, referring to Chapter 2, it is possible to individuate two mechanisms: extension mechanism and shear deformation mechanism:

- extension mechanism: two large parallel gaps are observed in the floor and the tiles moved apart in the horizontal direction without experiencing any local vertical displacement. In addition, vertical cracks occur in the apse that propagate from the level of the ground This mechanism indicate the presence of the horizontal component of displacement.

- shear deformation: severe diagonal cracks propagating from the level of the ground are observed in the longitudinal walls at both sides of the church and are localized in a single portion of the wall. A crack/gap in the floor propagates between the cracks affecting the opposite walls. This damage mechanism may be attributed to a differential settlement, in the direction of the longitudinal axis of the church. The laser scanner analysis performed after the survey shows a vertical displacement along the nave wall of over 16 cm (Figure 99). This denotes the high ductility of the structure and a significant vertical component of the soil movements.

Considering the width of the cracks (from 5 to 15 mm) observed in the survey, applying the damage classification proposed by Burland et al. (1977), the damage level can be set equal to 3. Also based on the expert judgment, considering the diffusion of the cracks, their width and the clear manifestation of two of the four identified mechanisms proposed in Chapter 2, the damage level of the church was defined equal to 3.

a)

b)
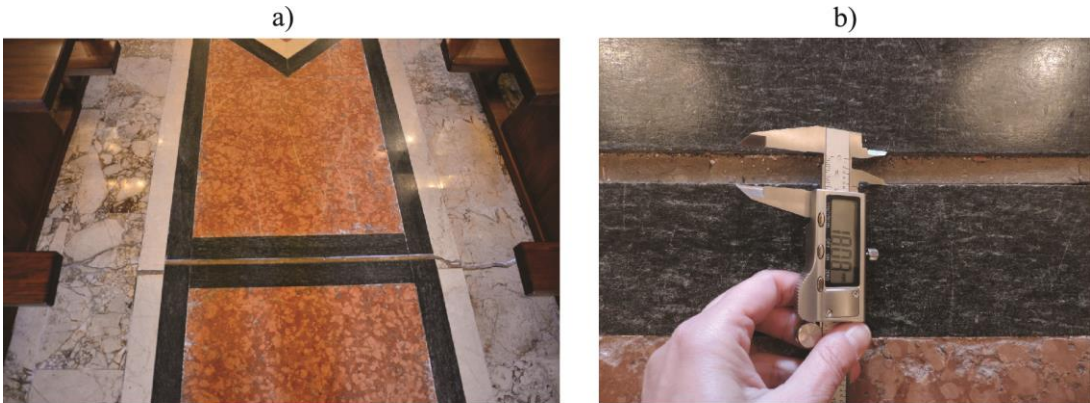
Figure 96 – Cracks of the floor (a) and its measured (b)

a)

b)

c)
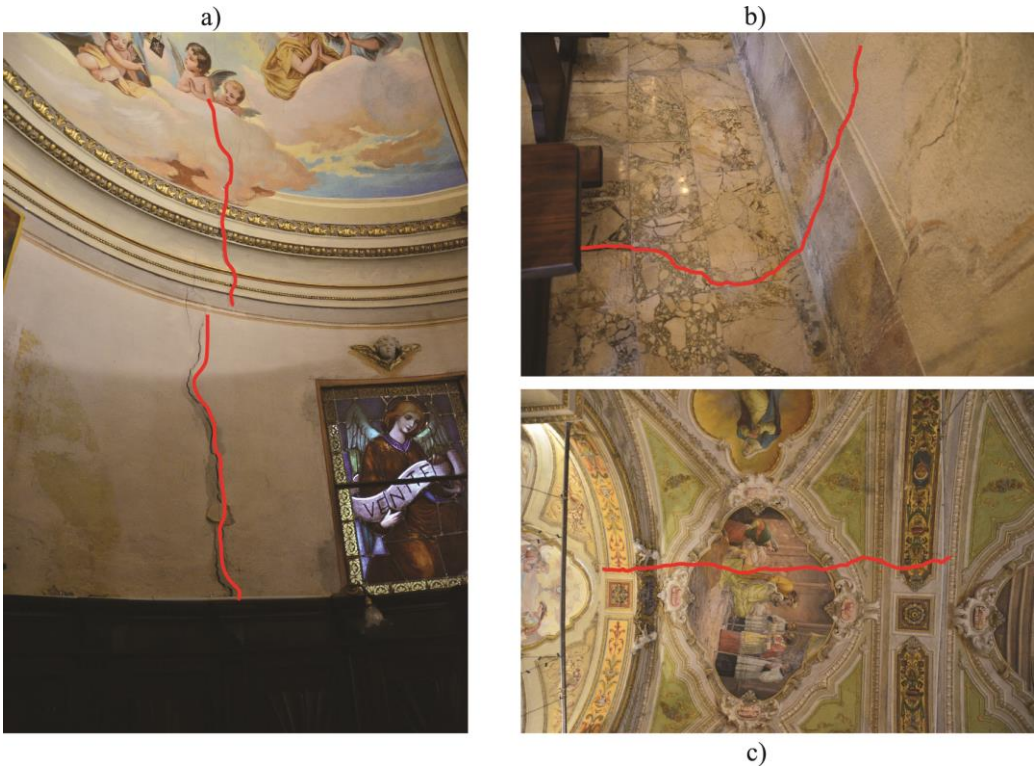
Figure 97 – Cracks on the apse wall (a), cracks propagating from the floor to the walls (b), cracks of the vault
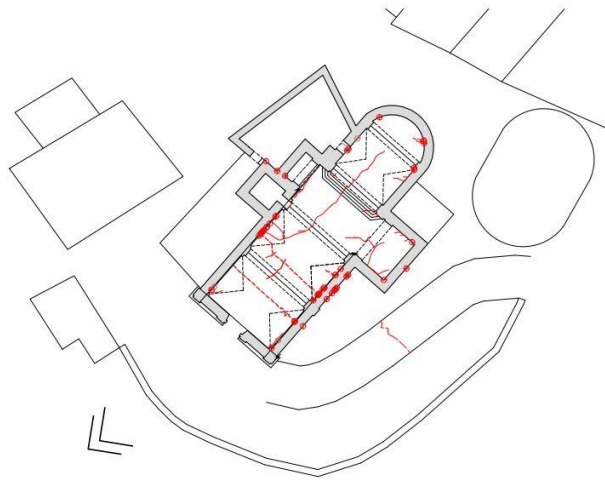
CH_28 - SAN CARLO CHURCH, Fascia (Loc. Cassingheno) (GE)

Figure 98 - Crack pattern of the church
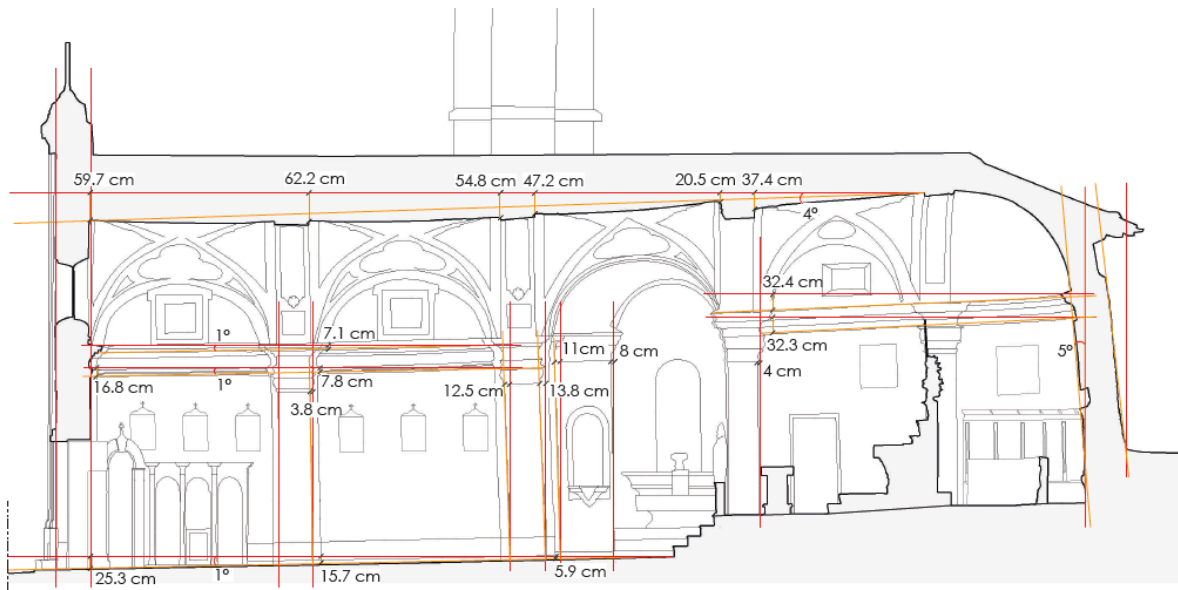
Figure 99 - Laser scanner survey

Combining the results of the numerical analysis that led to an evaluation of FH equal to 0.7, referred to displacements in agreement with the inclinometric measure, with the definition of the damage level of the church, it is possible to verify the reliability of the fragility curves developed.

The church and the village of Cassingheno are located on a medium-low inclined slope, the slope inclination downhill i_1 is equal to 15° while the uphill angle i_2 is between 15-20°. Through the fragility

curves, it is possible to define the medium damage associated with the intensity parameter FH. Table 20 shows the probability of exceedance when FH is equal to 0.7 for all the damage level.

Table 20 – Probability of exceedance

FH	P[DL2]	P[DL3]	P[DL4]	P[DL5]
0,100	0,014	0,001	0,015	0,000
0,200	0,209	0,044	0,059	0,000
0,300	0,500	0,185	0,145	0,005
0,400	0,717	0,374	0,242	0,022
0,500	0,847	0,549	0,337	0,057
0,600	0,917	0,687	0,424	0,113
0,700	0,955	0,787	0,500	0,183
0,800	0,975	0,856	0,566	0,262
0,900	0,986	0,903	0,623	0,344
1,000	0,992	0,934	0,672	0,424
1,200	0,997	0,970	0,750	0,569

P[DL$_i$≥DL2|FH=0,7]	0,168
P[DL$_i$≥DL1|FH=0,7]	0,045
P[DL$_i$≥DL3|FH=0,7]	0,287
P[DL$_i$≥DL4|FH=0,7]	0,317
P[DL$_i$≥DL5|FH=0,7]	0,183
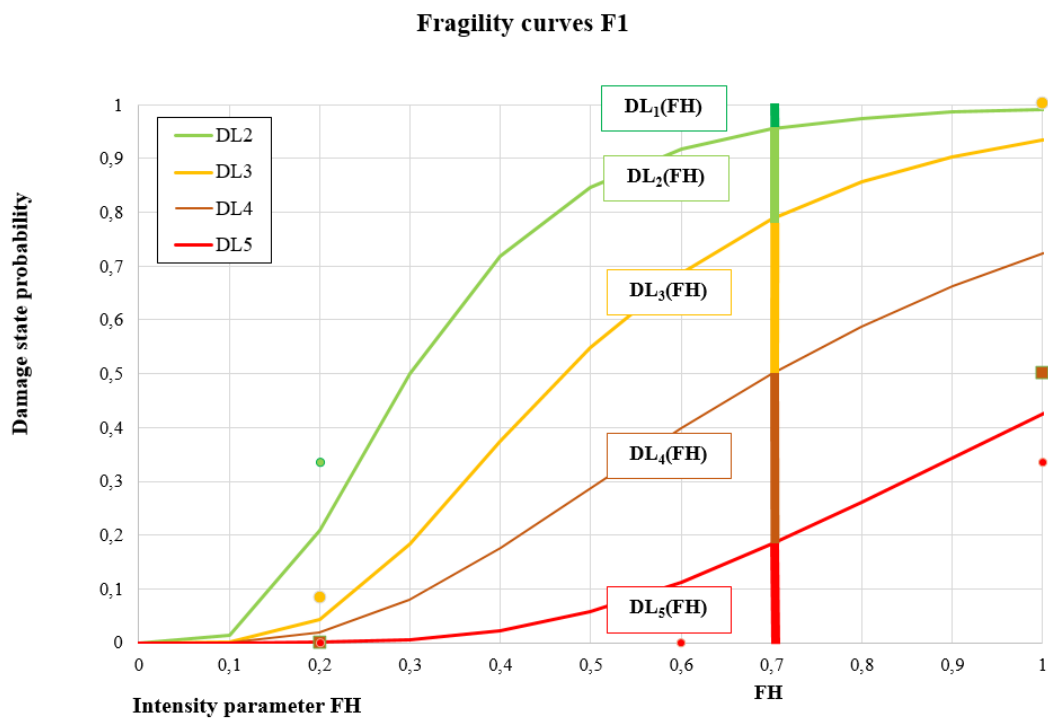
Figure 100 – Fragility curves when FH=0.7
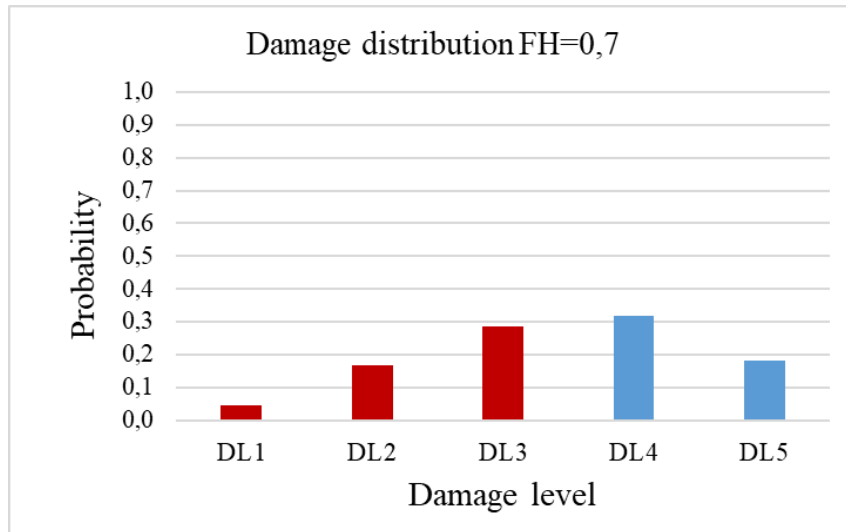
Figure 101 – Damage distribution when FH=0.7

From Figure 100 and Figure 101, the medium level of damage can be calculated by:

$$\mu_D = \sum_{i=1}^{5} DL_i \cdot P[DL]_i$$

The average level of damage from fragility curves is 3.5, in agreement with the damage level defined by Burland et al. and the expert judgment.

6. CONCLUSIONS

Protecting cultural heritage from natural hazards (i.e. earthquakes, floods, landslides, etc.) has always been a topic of great interest in many fields, from the engineering to the social- cultural case. Italy, in relation to this, is one of the most vulnerable countries in the world, both from a geomorphologic point of view and for the large number of monuments and historical sites present throughout the national territory.

In the current research, the attention is payed to the development of a new methodology to predict the effects induced by slow-moving landslides on cultural heritage elements, in order to give a contribution for establishing a reliable forecasting method applicable to intervention management. In particular, in the framework of this interdisciplinary research programme, churches have been chosen as exposed structures, for their historical importance and for their structural and geometric characteristics and complexities.

The main aim of this PhD Thesis was the generation of fragility curves, which correlate the probability of overcoming a certain damage index with reference to the intensity of the event triggering the damage itself. In the scientific literature, fragility curves have been thoroughly developed for earthquakes (e.g. Lagomarsino et al., 2006), less contributions are related to subsidence (e.g. Saeidi et al., 2009) and slow-moving landslide (e.g. Negulescu and Foerster, 2010) phenomena. Most of these approaches are related to RC frame buildings and to masonry and reinforced masonry buildings as well; indeed scientific literature is lacking about fragility curves specifically devoted to churches (more complex in geometry and response than buildings) subjected to landslide movements.

The work addressed included:

i) a literature review on the main features of the analysed phenomena (slow-moving landslide) and their consequences on structures, the relevance of the consequence analysis for the quantification of the risk to the exposed buildings with the main damageability criteria adopted in engineering practice along with the newly proposed probabilistic approaches for the analysis and prediction of the damage to buildings (Chapter 1);

ii) the proposal of a methodology adopted for the choice of a set of churches in Liguria region affected by slow-moving landslides. The inspection method is described in detail as well as the damage analysis carried out on the churches. The proposal of four general damage mechanisms is finally presented. (Chapter 2);

iii) the procedure for the analysis and prediction of the effects of slow-moving landslides via numerical approach: preliminary Finite Element Method analyses have been performed to assess soil displacements referring to the infinite slope model and preliminary Limit Equilibrium analyses have supplied the values of the relevant slope safety factors to be combined with these displacements. A new hazard factor, assumed as intensity parameter,

iv)   is then introduced in order to link slope displacements with slope stability conditions. (Chapter 3);

iv)   the procedure proposed in Chapter 3 has been applied to different set of slopes, with particular features and layout obtained from the analysis of real slopes of the date base described in Chapter 2. Several numerical analyses have been performed in order to correlate soil displacements, both vertical and horizontal to the new hazard factor. For each case, deformation values have been calculated as well. Each couple of values led to the definition of a damage level, by the application of the approach proposed by Son and Cording (2005) for deep excavations. Chapter 4 has allowed the definition of a numerical data base where deformation referred to particular slope geometry and footprint of the church has been correlated with the damage level;

v)   fragility and vulnerability curves have been proposed (Chapter 5). This chapter focused on the development of the fragility curves with the assumption of the hazard factor FH of the slope as the intensity parameter, in order to give a simple tool for practical use, as it can be obtained by a limit equilibrium analysis. The procedure has been applied on a case study.

6.1 SUMMARY OF RESULTS

The first part of this work consisted of a systematic damage survey investigation of historic masonry churches subjected to slow-moving landslides in order to understand the effect of this phenomenon on churches. Despite landslide displacements inducing differential vertical and horizontal displacements which are small in their instantaneous value, can lead to severe damage and even collapse over time; in fact many cases showed serious damage or were closed to the public for structural restructuring. Surveys were fundamental for collecting sets of parameters relating to the slopes and soils. It is important to underline that very few geotechnical data were available for the samples analysed. Given the lack of soil test available, it was considered essential to develop a tool that would allow to provide information on the damage status of the structure starting from simplified analysis of the slope. In this respect, fragility curves were developed. Surveys were also important in order to better understand the collapse mechanism of churches subjected to slow-moving landslide. The mechanisms proposed in Chapter 2 show the presence of both horizontal and vertical components of the displacement that may induced shear cracks or extension cracks. This is in good agreement with the simple scheme proposed by Son and Cording (2005), aimed to assess possible damage levels on blocks or masonry walls.

To generate fragility curves, damage severity levels have to be identified, through the definition of an intensity parameter of the landslide effects. The proposed intensity parameter, defined as "hazard factor" is directly linked to the global safety factor of the slope, in order to provide a simple but representative index

to use in engineering practice. In addition, vertical and horizontal slope movements have to be related to the relevant hazard factors as well as to possible permitted damage levels of the church.

The numerical analysis performed, summarized below, have led to different results. LEM analysis allow the definition of the evolution of FS by the introduction of the hazard factor FH and represent a simple tool for engineering analysis of real cases. FEM analysis allows the evaluation of the pattern of settlement, fundamental for define the damage level that will be correlate with the hazard factor FH.

The first analyses have been carried out modelling the slope as the infinite slope model, in order to define the methodology in a simple case. FEM analyses have been performed and the behaviour of the slope as the geotechnical strength parameter of the soil decreases has been studied. The analysis led to the identification and quantification of soil displacements, both vertical and horizontal, in sections of interest along the slope. Each pair of values was associated with the safety factor of the slope. The evolution of FS is described by the introduction of a "hazard factor" FH. The following methodology has been proposed:

- choice of sections of interest, definition of stratigraphical sequence and geotechnical parameters;

- assessment of the initial safety factor;

- reduction of the initial safety factor up to failure conditions;

- evaluation of the displacement values for each decrease in FS;

- definition of the reference deformations associated with the computed displacements;

- comparison of the computed displacement and strain patterns and levels with the detected ones;

- representation of displacement and deformation evolution by introducing the hazard factor FH.

The next step of the research concerned the modelling of the slope in a more realistic way. For this purpose, over thirty real slopes, characterized by the presence of both active or dormant slow-moving landslides and historic masonry churches in Liguria territory, have been analysed.

Following the methodology proposed, magnitudes of soil displacement, lateral strain and angular distortion were evaluated along the possible footprint of the church. LEM analysis were also performed in order to define the safety factor of the area of interest of the cultural heritage. Hazard factor was evaluated as well.

After having evaluated the pattern of displacement and deformation, with the associated FH value, the next step concerned the attribution to the pairs of points obtained to a damage level. The Author has chosen the local damage indicators based on the approach proposed by Son and Cording (2005), which complemented the criterion proposed by Burland and Wroth (1974) by including the effects of horizontal strains. Each point obtained from numerical analysis was reported to the graph proposed by Son and Cording in order to define the damage state. It is worth noting that the results obtained from the numerical analysis are in good agreement with the results proposed by the authors. This suggests that, despite the

simplifications adopted in the numerical analyses, the results are reliable when compared with well-known methods found in the literature.

Then, the fragility curves were evaluated using a two-parameter log-normal distribution function, adopted due to its simple parametric form. The log-normal distribution well represents the results obtained from the numerical analysis. Five sets of fragility curves were developed in order to simulate a particular geometry of the slope. This choice has been made in order to provide a tool for engineering use: once the geometry of the slope has been defined, it is possible to evaluate which fragility curves well describe the case study.

It is worth noting that the introduction of FH as the intensity parameter instead of FS allows monitoring of the evolution of slope stability. It is also important to underline that FS is representative of an instantaneous stability condition of the slope and, even if is higher and failure condition are not close to the case analysed, the evolution of the instability, that can be monitored by FH, can lead to a damage condition, verifiable by fragility curves, that is not admissible.

A case study was modelled which highlighted the use of fragility curves both as a predictive tool of the state of damage fixed FH value and to evaluate the evolution of the damage level as FH increases. In relation to this the fragility curves can help with the planning of interventions or monitoring both of the slope and the structure. The results obtained in the case study are good, it was possible to verify the damage level of the structure with that obtained from the fragility curves and thus verify the applicability of the approach proposed in this Thesis..

6.2 FURTHER DEVELOPMENTS

It is important to underline that several hypotheses have been made for the modelling of the slope, for example the analyses were carried out in free field conditions and with a very schematic stratigraphical sequences. The justification for these choices lies in the objective of defining a simple methodology for the study of such a complex and multidisciplinary problem, it is worth noting that in the literature there is lack of contributions aimed at studying the effects of landslide on churches. The aim is therefore to verify the applicability of well-known damage assessment methods for this particular problem.

The proposed methodology for simulating slow moving landslide effects has only been studied for some particular cases of slope geometry and geotechnical conditions. The influence of soil characterization, water-table condition and the model of the structure should be investigated for further validation. Future research should be devoted to analysing other geometries of slope and sets of geotechnical parameters to increase the set of the numerical analysis. A very simple soil constitutive model has been used, with operational soil stiffness based on results of preliminary 2D analyses, and no check has been made on stress paths and pore pressures. Water-table condition should be analysed as well: it is well known that water

plays an important role in slope stability. Regarding the church model, it is very difficult to define general criteria for modelling such a site-specific type of structure: churches are quite different from masonry buildings that have been previously studied in literature: irregular geometry (like arches, vaults and wide openings), material heterogeneity and its strongly non-linear behaviour make this structural typology different from the others especially if studied to evaluate the effects of the slope movements.

The case records analysed in this Thesis, even if numerous, show how often the geotechnical data are missing and necessitate more integration. This project underlines the importance of having more complete data with the aim of performing more accurate analyses.

REFERENCES

Abramson L.W., Lee T.S., Sharma S., Boyce G.M., (2002). Slope Stability and Stabilization Methods, John Wiley & Sons, New York.

Alexander D., (1986). Landslide damage to buildings. Environmental Geology and Water Science, 8: 147-151.

Audell H.S., (1996). Geotechnical nomenclature and classification system for crack patterns in buildings. Environmental and Engineering Geoscience, 2:225-248.

Beeby A.W. and Miles J. R. (1969). Proposals for the control of deflection in the new unified Code. Concrete, 3(3):101–110.

Berardi R., Cambiaggi L. (2019). Prediction of slope movement effects on churches for the development of a fragility curve approach. In: Calvetti F., Cotecchia F., Galli A., Jommi C. (eds) Geotechnical Research for Land Protection and Development. CNRIG 2019. Lecture Notes in Civil Engineering, vol 40. Springer, Cham, First Online23 June 2019, Print ISBN978-3-030-21358-9, Online ISBN978-3-030-21359-6, DOI: https://doi.org/10.1007/978-3-030-21359-6_9, pp. 82-91.

Bhattacharya S. and Singh M.M.., (1985). Development of subsidence damage criteria, final report. Engineers International Inc. Westmont for U.S. Department of the Interior, Office of Surface Mining Reclamation and Enforcement, pp. 229.

Bilgin H. and Korini O., (2012). Seismic capacity evaluation of unreinforced masonry residential buildings in Albania. Natural Hazards Earth Systems Sciences, 12:3753-3764.

Bird J. F., Bommer J. J., Crowley H., Pinho R., (2005b). Modelling liquefaction-induced building damage in earthquake loss estimation. Soil Dynamic Earthquake Engineering, 26:15–30.

Bird J. F., Crowley H., Pinho R., Bommer, J. J., (2005a). Assessment of building response to liquefaction-induced differential ground deformations. Bulletin of New Zealand Society for Earthquake Engineering, 38(4), 20 pp.

Bishop, A.W., 1955. The use of the slip circle in the stability analysis of slopes, Geotechnique, 5(1), pp.7-17.

Bjerrum L., (1963). Allowable Settlement of Structures. Proceedings of the 3rd European Conference on Soil Mechanics and Foundation Engineering, Wiesbaden, 2, Brighton, England, 135–137.

Boone S. J., (1996). Ground-Movement-Related Building Damage, Journal of Geotechnical Engineering-ASCE, 122(11): 886–896.

Boscardin M. D. and Cording E. G., (1989). Building Response to Excavation Induced Settlement. Journal of Geotechnical Engineering- ASCE, 115:1–21

Bui H.H., Fukagawa R, Sako K, Ohno S (2008) Lagrangian meshfree particles method (SPH) for large deformation and failure flows of geomaterial using elastic–plastic soil constitutive model. Int J Numer Anal Methods Geomech 32(12):1527–1570

Building Research Establishment, (1981). Assessment of damage in lowrise buildings with particular reference of progressive foundation movement. UK Building Research Establishment Digest, 251, pp 8.

Burd H. J., Houlsby G. T., Augarde C. E., Liu G., (2000). Modelling tunnelling-induced settlement of masonry buildings. Proc. Institution of Civil Engineers, Geotechnical Engineering, 11831, 143:17–29.

Burland J. B., (1995). Assessment of risk of damage to buildings due to tunnelling and excavation. Invited Special Lecture, 1st International Conference on Earthquake Geotechnical Engineering, IS.Tokyo '95.

Burland J.B., Broms B.B., De Mello V.F.B. (1977). Behaviour of foundations and structures. Proceedings of 9th International Conference SMFE – Vol 2. Tokyo. pp. 495-546.

Burland, J.B. and C.P. Wroth 1974. Settlements on buildings and associated damage. In: Proceedings of Conference on Settlement of structures, Cambridge 611-54. London, UK: Pentech Press.

Cambiaggi L., Berardi R. (2019). Identification and modelling of displacement fields due to slope movements for the vulnerability analysis of historic buildings. Proceedings of the XVII ECSMGE-2019 Geotechnical Engineering foundation of the future, ISBN 978-9935-9436-1-3, doi: 10.32075/17ECSMGE-2019-0357.

Cascini L., Fornaro G., Peduto D. (2010). Advanced low-and full-resolution DInSAR map generation for slow-moving landslide analysis at different scales. Engineering Geology, 112 (2010), pp. 29-42.

Cascini L., Peduto D., Pisciotta G., Arena L., Ferlisi S., Fornaro G., (2013a). The combination of DInSAR and facility damage data for the updating of slow-moving landslide inventory maps at medium scale. Natural Hazards Earth Systems Sciences, 13:1527–1549

Cascini, L., Bonnard, Ch., Corominas, J., Jibson, R., and Montero-Olarte, J. (2005) Landslide hazard and risk zoning for urban planning and development. State of the Art report, in: Landslide Risk Management, Proceedings of the International Conference on Landslide Risk Management, edited by: Hungr, O., Fell, R., Couture, R., and Eberhardt, E., 31 May–3 June 2005, Vancouver, Canada, A.A. Balkema Publishers, 199–235.

Cattari S., Curti E., Giovinazzi S., Lagomarsino S., Parodi S., Penna A. (2004). A mechanical model for the vulnerability assessment and damage scenario of masonry buildings at urban scale. In: Proc. 11th Italian conference on earthquake engineering, Genoa, Italy.

Chiocchio C., Iovine G., Parise M., (1997). A proposal for surveying and classifying landslide damage to buildings. In: Marinos, P.G., Koukis, G.C., Tsiambaos, G.C. & Stournaras G.C. (eds) Engineering Geology and the Environment, Proceedings of the IAEG International symposium on engineering geology and the environment, Athens, June, 1997. Balkema - Rotterdam, pp. 553-558.

Cleary P.W., C.S. Campbell (1993). Self-lubrication for long-runout landslides: examination by computer simulations J. Geophys. Res., 98 pp. 21911-21924

Cleary PW, Prakash M (2004) Discrete-element modelling and smoothed particle hydrodynamics: potential in the environmental sciences. Philos Trans R Soc A 362(1822):2003–2030

Cooper A.H., (2008). The classification, recording, databasing and use of information about building damage caused by subsidence and landslides. Quarterly Journal of Engineering Geology and Hydrogeology, 41(3):409-424.

Cording, E. J., Long, J. H., Son, M., and Laefer, D. F. (2001). Modelling and analysis of excavation-induced building distortion and damage using a strain-based damage criterion. Proc., London Conf. for Responses of Buildings to Excavation-Induced Ground Movements in London, London.

Corominas J., van Westen C., Frattini P., Cascini L., Malet J. P., Fotopoulou S., Catani F., Van Den Eeckhaut M., Mavrouli O., Agliardi F., Pitilakis K., Winter G.M., Pastor M., Ferlisi S., Tofani

Crosta G.B., J.J. Clague. (2009). Dating, triggering, modelling, and hazard assessment of large landslides Geomorphology, 103, pp. 1-4

Crosta GB, Frattini P, Fugazza F, Caluzzi L (2005) Cost-benefit analysis for debris avalanche risk management. In: Hungr O, Fell R, Couture R, Eberhardt E (eds) Landslide risk management. Proceedings Vancouver Conference. Taylor and Francis Group, London, pp 517–524

Cruden D.M. (1991). A simple definition of a landslide. Bulletin of IAEG, 43: 27-29.

Cruden D.M., R. Fell. Landslide Risk Assessment, Proceedings International Workshop on Landslide Risk Assessment, Honolulu, 19–21 February 1997, Balkema, Rotterdam (1997) 371 pp.

Cruden D.M., Varnes D.J. (1996). Landslide types and processes. Landslides: investigation and mitigation. Transportation Research Board, Special Report, No. 247, National Research Council, National Academy Press, Washington DC, USA 36-75.

Cundall P.A., Strack, O.D.L. (1979). A discrete numerical model for granular assemblies. Géotechnique, 29(1) (1979), pp. 47-65

Dai FC, Lee CF, Ngai YY (2002) Landslide risk assessment and management: an overview. Eng Geol 64(1):65–87

DeJong, M. J. 2016. Settlement effects on masonry structures. In: Proceedings of 10th International Conference on Structural Analysis of Historical Constructions, Leuven, Belgium.

Di Maio C., Fornaro G., Gioia D., Reale D., Schiattarella M., Vassallo R. (2018) In situ and satellite long-term monitoring of the Latronico landslide Italy: displacement evolution damage to buildings and effectiveness of remedial works, vol. 245, pp. 218-235.

Dyka CT, Ingel RP (1995) An approach for tension instability in smoothed particle hydrodynamics (SPH). Comput Struct 57(4):573–580

EEA (2012). Annual report 2012 and Environmental statement (2013). European Environment Agency, pp. 95, ISSN 1561-2120 - ISBN: 978-92-9213-393, doi:10.2800/91164

Eurocode 7 - Geotechnical design, European Committee for Standardization (CEN), Brussels (2007)

Federici, P.R. and A. Chelli. 2007. Atlante dei Centri Abitati Instabili della Liguria. IV. Provincia di Imperia (Atlas of the Unstable Inhabited Centres of Liguria. IV. Imperia province). Regione Liguria.

Federici, P.R., F. Baldacci, A. Petresi, and A. Serani. 2001. Atlante dei Centri Abitati Instabili della Liguria. I. Provincia della Spezia (Atlas of the Unstable Inhabited Centres of Liguria. I. La Spezia province. Regione Liguria.

Federici, P.R., M. Capitani, A. Chelli, N. Del Seppia, and A. Serani. 2004. Atlante dei Centri Abitati Instabili della Liguria. II. Provincia di Genova (Atlas of the Unstable Inhabited Centres of Liguria. II. Genova province). Regione Liguria.

Federici, P.R., M. Capitani, A. Serani, and S. Stano. 2006. Atlante dei Centri Abitati Instabili della Liguria. III. Provincia di Savona (Atlas of the Unstable Inhabited Centres of Liguria. III. Savona province). Regione Liguria.

Fell R., Corominas J., Bonnard C.h., Cascini L., Leroi E., Savage W.Z. (2008). On behalf of the JTC-1 Joint Technical Committee on Landslides and Engineered Slopes. Guidelines for landslide susceptibility, hazard and risk zoning for land-use planning, Commentary. Engineering Geology, 102:99–111.

Fell R., Corominas J., Bonnard C.h., Cascini L., Leroi E., Savage W.Z. (2008). On behalf of the JTC-1 Joint Technical Committee on Landslides and Engineered Slopes. Guidelines for landslide susceptibility, hazard and risk zoning for land-use planning, Commentary. Engineering Geology, 102:85–98.

Fell, R., Ho, K.K.S., Lacasse, S., Leroi, E., 2005a. A framework for landslide risk assessment and management. In: Hungr, O., Fell, R., Couture, R., Eberhardt, E. (Eds.), Landslide Risk Management. Taylor and Francis, London, pp. 3–26.

Fell, R., MacGregor, P., Stapledon, D., Bell, G., 2005b. Geotechnical Engineering of Dams. Balkema, Leiden.

Ferlisi S., and Pisciotta G. (2007). A preliminary study of landslide induced property damages to wards consequence analysis. In: First North American Landslide Conference Vail (Colorado, USA), pp. 180-190.

Ferrero C., Cambiaggi L., Vecchiattini R. & Calderini C. (2020) Damage Assessment of Historic Masonry Churches Exposed to Slow-moving Landslides, *International Journal of Architectural Heritage, DOI: 10.1080/15583058.2020.1799259*

Finno R. J., Voss F. T., Rossow E., Blackburn J. T., (2005). Evaluating Damage Potential in Buildings Affected by Excavations. Journal of Geotechnical and Geoenvironmental Engineering, 131(10):1199–1210.

Fotopoulou S. D. and Pitilakis K. D. (2013a). Vulnerability assessment of reinforced concrete buildings subjected to seismically triggered slowmoving earth slides. Landslides, 10:563-582.

Fotopoulou S. D. and Pitilakis K. D., (2013b). Fragility curves for reinforced concrete buildings to seismically triggered slow-moving slides. Soil Dynamics and Earthquake Engineering, 48:143-161.

Freeman T.J., Littlejohn G.S., Driscoll R.M.C., (1994). Has your house got cracks: a guide to subsidence and heave of buildings on clay. Institution of Civil Engineers and Building Research Establishment, pp. 114

G.U. no. 120, 25/05/1989 (suppl. ord. no. 38). Law no. 183 of 18/05/1989, Norme per il riassetto organizzativo e funzionale della difesa del suolo.

G.U. no. 45, 24/02/2004 (suppl. ord. no. 28). Legislative Decree no. 42 of 22/01/2004, Codice dei beni culturali e del paesaggio, ai sensi dell'articolo 10 della legge 6 luglio 2002, n. 137.

Geomorphological Services Ltd., (1991). Coastal Landslip Potential Assessment: Isle of Wight Undercliffe, Ventnor. Technical Report for the department of the Environment. Research Contract RECD 7/1/272.

Glade T (2003) Vulnerability assessment in landslide risk analysis. Die Erde 134(2):121–138

Griffiths D.V., J.S. Huang, G.A. Fenton. 2011. Probabilistic infinite slope analysis Comput. Geotech., 38 (4) (2011), pp. 577-584

Griffiths, D. V., and Lane, P. A. (1999). Slope stability analysis by finite elements. Geotechnique, 49(3), 387–403

Grünthal G., (1998). European Macroseismic Scale 1998, Cahiers du Centre Europèen de Gèodynamique et de Seismologie. Conseil de l'Europe, Luxembourg.

Gutfraind R, Savage SB (1998) Flow of fractured ice through wedge-shaped channels: smoothed particle hydrodynamics and discrete-element simulations. Mech Mater 29(1):1–17

Guzzetti F. (2000). Landslide fatalities and the evaluation of landslide risk in Italy. Engineering Geology 58 (2000) 89–107

Guzzetti, F., M. Cardinali, P. Reichenbach, F. Cipolla, C. Sebastiani, M. Galli and P. Salvati. 2004. Landslides triggered by the 23 November 2000 rainfall event in the Imperia Province, Western Liguria, Italy. Engineering Geology 73 (2004) 229–245

Hoek, E. and Bray, J.W. 1981. Rock slope engineering. 3rd edn. London: Instn Min.Metall.

Humphreys H. and Partners, (1993). Subsidence in Norwich. London, HMSO, pp. 99

Hungr O. (1995). A model for the runout analysis of rapid flow slides, debris flows, and avalanches. Canadian Geotechnical Journal, 32 (1995), pp. 610-623

Hungr O., Evans S.G., Bovis M.J., Hutchinson J.N. (2001). A review of the classification of landslides of the flow type. Environmental & Engineering Geoscience, VII (3), pp.221 – 238.

Hungr O., Leroueil S., Picarelli L. (2014). The Varnes classification of landslide types, an update. Landslides, 11:167:194.

Hungr, O., Corominas, J., Eberhardt, E., 2005. Estimating landslide motion mechanisms, travel distance and velocity. In: Hungr, O., Fell, R., Couture, R., Eberhardt, E. (Eds.), Landslide Risk Management. Taylor and Francis, London, pp. 99–128.

Hutchinson J.N. (1968) Mass movement. In: Fairbridge RW (ed) Encyclopedia of geomorphology. Reinhold Publishers, New York, pp 688–695

Hutchinson J.N. (1988). Morphological and Geotechnical parameters of Landslides in relation to Geology and Hydrogeology. State of the art Report. Proc. V Intl. Symposium on Landslides, Lausanne, Vol. 1, pp. 3– 35.

Huvaj N., Maghsoudloo A. (2013). Finite Element Modeling of Displacement Behavior of a Slow-Moving Landslide. Geo-Congress 2013. March 3-7, 2013 | San Diego, California, United States pp. 670 – 679

ISPRA: Italian Landslide Inventory Project (IFFI) 2007. [online]. Web: http://www.progettoiffi.isprambiente.it (last access: April 10, 2019).

IUGS/WGL—International Union of Geological Sciences Working Group on Landslides (1995). A suggested method for describing the rate of movement of a landslide. IAEG Bull 52:75–78.

Janbu N., (1954) Application of composite slip surface for stability analysis. Proceedings of the European Conference on Stability of Earth Slopes, Stockholm, pp 43–49

Janbu, N., 1973. Slope stability computations, Embankment & Dam Engineering, Casagrande Memorial Volume, J.Wiley, New York, pp.47 86.

Johnson G.R., Beissel S.R. (1996) Normalized smoothing functions for SPH impact computations. Int J Numer Methods Eng 39(16):2725–2741

Johnson R., (2005). Significance of cracks in low-rise buildings – what you need to know. Civil Engineering, Paper 13014, 158:30-35

Karapetrou S.T., Fotopoulou S.D., Pitilakis K.D., (2016). Seismic vulnerability assessment of high-rise non-ductile RC buildings considering soil–structure interaction effects. Soil Dynamics and Earthquake Engineering, 73:42-57.

Keefer D.K., Johnson A.M. (1983). Earthflows: morphology, mobilization and movement. USGS Professional Paper 1264

Kjekstad O. and L. Highland (2009). Economic and Social Impacts of Landslides. Sassa, K., Canuti, P. (Eds.), Disaster Risk Reduction. Springer-Verlag, Berlin Heidelberg, pp. 573–588.

Lacaze, L., J. C. Phillips, and R. R. Kerswell (2008), Planar collapse of a granular column: Experiments and discrete element simulations, Phys. Fluids, 20, 063302

Lagomarsino S. and Giovinazzi S. (2006). Macroseismic and mechanical models for the vulnerability and damage assessment of current buildings. Journal of Earthquake Engineering, 4:415_43.

Lagomarsino S., Penna A., Galasco A., Cattari S. (2013). TREMURI program: an equivalent frame model for the nonlinear seismic analysis of masonry buildings. Engineering Structures, 56:1787–1799.

Leroi, E., Bonnard, C., Fell, R., McInnes, R., 2005. Risk assessment and management. In: Hungr, O., Fell, R., Couture, R., Eberhardt, E. (Eds.), Landslide Risk Management. Taylor and Francis, London, pp. 159–198.

Leroueil S, Locat A, Eberhardt E, Kovacevic N (2012) Progressive failure in natural and engineered slopes. In: Eberhardt E, Froese C, Turner AK, Leroueil S (eds) Landslides and Engineered Slopes. Proceedings, 11th International Symposium on Landslides, Banff, 1:31, CRC Press, Boca Raton

Leroueil S., Locat J., Vaunat J., Picarelli L., Lee H., Faure R.(1996). Geotechnical characterization of slope movements. Proceedings 7th International Symposium Land-slides, Trondheim, Norway 1:53-74.

Lewis, J. (1999). Development in disaster-prone places. Studies of vulnerability. London, Intermediate Technology Publications Ltd.

Liu G., G.T. Houlsby, C.E. Augarde2-dimensional analysis of settlement damage to masonry buildings caused by tunnelling. Struct. Eng., 79 (1) (2000), pp. 19-25

Losacco N., (2011). Development and testing of a simplified building model for the study of soil-structure interaction due to tunnelling in soft ground. Phd Thesis, pp.231.

Losacco N., A. Burghignoli, L. Callisto. (2014). Uncoupled evaluation of the structural damage induced by tunnelling Géotechnique, 64 (2014), pp. 646-656

Lowe J., Zaccheo P.F., (1991). Subsurface explorations and sampling. in Foundation Engineering Handbook, (H-Y Fang Ed.), Van Nostrand Reinhold, New York, pp. 1-71.

Mangeney-Castelnau, A., F. Bouchut, J. P. Vilotte, E. Lajeunesse, A. Aubertin, and M. Pirulli (2005), On the use of Saint-Venant equations to simulate the spreading of a granular mass, J. Geophys. Res., 110, B09103, doi:10.1029/2004JB003161.

Maquaire O, Thiery Y, Malet J-P, Weber C, Puissant A, Wania A (2004). Current practices and assessment tools of landslide vulnerability in mountainous basins – identification of exposed elements with a semi-automatic procedure. In: Lacerda W, Ehrlich M, Fontoura SAB, Sayão ASF (Eds.). Landslides: evaluation and stabilization. Proc of the 9th Int Symp on Landslides. A.A. Balkema Publishers – Vol. 1, pp. 171- 176

Mavrouli O., Fotopoulou S., Pitilakis K., Zuccaro G., Corominas J., Santo A., Cacace F., De Gregorio D., Di Crescenzo G., Foerster E., Ulrich T. (2014). Vulnerability assessment for reinforced concrete buildings exposed to landslides. Bulletin of Engineering Geology and the Environment, 73:265-289.

Maxwell, H. and Ravenberg, N.M. (1974). Geophysical exploration. In G.A. Fletcher & V.A. Smoots (eds.), Construction guide for soils and foundations. Ch. 6. New York. Wiley.

Medvedev S., Sponheuer W., Karnick V., (1965). The MSK Intensity Scale, Veroff Institute für Geodynamic, Jena, 48:1-10

Morgenstern NR (1992) The evaluation of slope stability: a 25 year perspective. In: Seed RB, Boulanger RW (eds) Stability and performance of slopes and embankments, ASCE Geotechnical Special Publication 31, 1:1–26

Morgenstern, N.R., Price, V.E., 1965. The analysis of the stability of general slip surfaces, Geotechnique, 15, pp.79-93.

Nadim, F., Einstein, H., Roberds, W., 2005. Probabilistic stability analysis for individual slopes in soil and rock. In: Hungr, O., Fell, R., Couture, R., Eberhardt, E. (Eds.), Landslide Risk Management. Taylor and Francis, London, pp. 63–98.

National Coal Board, (1975). Subsidence Engineers Handbook. National Coal Board Production Dept., U.K.

Negulescu C. and Foerster E. (2010). Parametric studies and quantitative assessment of the vulnerability of a RC frame building exposed to differential settlements. Natural Hazards and Earth System Science, 10(9):1781-1792.

Nicodemo G, Peduto D, Ferlisi S, Gullà G, Borrelli L, Fornaro G, Reale D (2017) Analysis of building vulnerability to slow-moving landslides via A-DInSAR and damage survey data. In: Mikoš M, Tiwari B, Yin Y, Sassa K (Eds). Advancing Culture of Living with Landslides – Proc of the 4th World Landslide Forum, Ljubljana, Slovenia, May 29 – June 02, 2017, © 2017 Springer International Publishing Switzerland, Vol. 2, pp. 889–907

Palmisano F., Vitone C., Cotecchia F., (2016). Landslide damage assessment at the intermediate to small scale. Aversa et al. (eds.), Landslides and Engineered Slopes Experience, Theory and Practice, Vol. 1, pp. 1549-1557.

Peduto D, Pisciotta G, Nicodemo G, Arena L, Ferlisi S, Gullà G, Borrelli L, Fornaro G, Reale D, (2016b) A procedure for the analysis of building vulnerability to slow-moving landslides. Proceedings of 1st IMEKO TC4 International Workshop on Metrology for Geotechnics, 17-18 March 2016. Benevento, Italy. pp. 248-254. ISBN 978-92-990075-0- 1.

Peduto D., Nicodemo G., Maccabiani J., Ferlisi S. (2017). Multi-scale analysis of settlement-induced building damage using damage surveys and DInSAR data: A case study in The Netherlands. Engineering Geology, 218:117–133.

Peduto, D., M. Korff, G. Nicodemo, A. Marchese, and S. Ferlisi. 2019. "Empirical Fragility Curves for Settlement-Affected Buildings: Analysis of Different Intensity Parameters for Seven Hundred Masonry Buildings in The Netherlands." Soils and Foundations 59: 380–397.

Penna A., Lagomarsino S., Galasco A. (2013). A nonlinear macroelement model for the seismic analysis of masonry buildings. Earthquake Engineering & Structural Dynamics, http://dx.doi.org/10.1002/eqe.2335.

Piano di Bacino Stralcio per l'Assetto Idrogeologico, Regione Liguria, 2017. [online]. Carte della Suscettività al Dissesto (Landslide Susceptibility Maps). Web: http://www.pianidibacino.ambienteinliguria.it (last access: April 10, 2019).

Piano Stralcio per l'Assetto Idrogeologico, Autorità di bacino distrettuale del fiume Po, 2017. [online]. Atlante dei Rischi Idraulici e Idrogeologici (Atlas of Hydraulic and Hydrogeological Risks). Web: http://www.pai.adbpo.it/ (last access: April 10, 2019).

Picarelli, L., Oboni, F., Evans, S.G., Mostyn, G., Fell, R., 2005. Hazard characterization and quantification. In: Hungr, O., Fell, R., Couture, R., Eberhardt, E. (Eds.), Landslide Risk Management. Taylor and Francis, London, pp. 27–62.

Pitilakis K. D. and Fotopoulou S. D. (2015). Vulnerability assessment of buildings exposed to co-seismic permanent slope displacements. Proceedings of the XVI ECSMGE – Geotechnical Engineering for Infrastructure and Development, 151-173.

Polshin D. E. and Tokar R. A., (1957). Maximum Allowable Nonuniform Settlement of Structures. Proc. 4th Int. Conference Soil Mechanics and Foundation Engineering, London, Butterworths Scientific Publications, 402–405.

Potts D. M. and Addenbrooke, (1997). A structure's influence on tunneling-induced ground movements. Proc. Instn. Civ. Engrs. Geotech. Engng., Vol 125, 109-125.

Gutfraind R., Savage S.B. (1998). Flow of fractured ice through wedge-shaped channels, smoothed particle hydrodynamics and discrete-element simulations. Mechanics of Materials, 29 , pp. 1-17

Rahman MS (1997) Instability and movement of oceanfloor sediments: a review. Int J Offshore Polar Eng 7(3):220–225

Roberds, W., 2005. Estimating temporal and spatial variability and vulnerability. In: Hungr, O., Fell, R., Couture, R., Eberhardt, E. (Eds.), Landslide Risk Management. Taylor and Francis, London, pp. 129–158.

Roca P., Cervera M., Gariup G., Pelà L. (2010) Structural analysis of masonry historical constructions. Classical and advanced approaches. Arch Comput Methods Eng, 17 (2010), pp. 299-325

Rossetto T., Elnashai A., (2003). Derivation of vulnerability functions for European-type RC structures based on observational data. Engineering Structures, 25:1241–1263.

Rota M., Penna A., Strobbia C., (2006). Typological fragility curves from Italian earthquake damage data. Proceedings 1st European conference on earthquake engineering and seismology, Geneva, paper (No. 386).

Rüsch H. and Mayer H., (1964). Bauschaden als Folge der Duchbiegung von Stahlbeton-Bauteilen, Deutscher Ausschuss fur Stahlbeton, Berlin, No. 10. (in German).

Sabetta F., Goretti A. and A. Lucantoni, (1998). Empirical fragility curves from damage surveys and estimated strong ground motion. 11th European Conference on Earthquake Engineering, Paris, CD-ROM, ISBN 90 5410 982 3, Balkema

Saeidi A., Deck O. and Verdel, T. (2009). Development of building vulnerability functions in subsidence regions from empirical methods. Engineering Structures, 31, 10:2275–2286.

Saeidi A., Deck O., Verdel T. (2012). Development of building vulnerability functions in subsidence regions from analytical methods. Geotéchnique, 62 (2):107–120.

Safeland Deliverable 2.5, (2011). Physical vulnerability of elements at risk to landslides: Methodology for evaluation, fragility curves and damage states for buildings and lifelines. Edited for the SafeLand European project by: Stumpf, A., Malet, J.-P., and Kerle, N., available at: http://www.safeland-fp7.eu.

Savage, S. B., K. Hutter, 1991. The dynamics of avalanches of granular materials from initiation to runout, I, Analysis, Acta Mech., 86, 201–223.

Skempton A. W. and MacDonald D. H., (1956). Allowable Settlement of Buildings. P. I. Civil Eng., 5, Part III, 727–768.

Skempton A.W. (1953). The colloidal activity of clays. Proc. 3rd International Conference on Soil Mechanics and Foundation Engineering, Zurich, pp. 7-61.

Son M. and Cording J., (2007). Evaluation of Building Stiffness for Buuilding Response Analysis to Exavation-Induced Ground Movements. Journal of Geotechnical and Geoenvironmental Engineering:-ASCE, 995–1002.

Son, M. (2003). The response of buildings to excavation-induced ground movements. PhD thesis, Univ. of Illinois at Urbana-Champaign, Urbana, Ill.

Sowers G. F., (1962). Shallow Foundations. Foundation Engineering, G. A. Leonards (eds.), McGraw-Hill Book Co., New York, NY, USA, 525–632, 1962.

Spencer E (1973) Thrust line criterion in embankment stability analysis. Geotechnique 23(1):85–100

Staron, L. & Hinch, E. J. 2007 The spreading of a granular mass: role of grain properties and initial conditions. Granular Matter 9, 205–217

Swegle JW, Hicks DL, Attaway SW (1995) Smoothed particle hydrodynamics stability analysis. J Comput Phys 116(1):123–134

Tang G., F. Li, X. Liu, Y. Long, X. Yang (2009). Research on the slope spectrum of the loess plateau. Sci. China Ser. E: Technol. Sci., 51 (2008), pp. 175-185

Terzaghi K. (1950). Mechanism of landslides. Paige, S., Editor, 1950. Application of Geology to Engineering Practice Geol. Soc. Am., Berkey Vol., pp. 83–123.

Timoshenko S. P., (1955). Vibration Problems in Engineering, 3rd edn. Toronto, New York, London: D. van Nostrand Co.

Trigila A., Iadanza C., 2008. Landslides in Italy—Special Report 2008. ISPRA, Roma, Report 83/2008, 32 pp.

Trigila, A., C. Iadanza, M. Bussettini and B. Lastoria. 2018. Dissesto idrogeologico in Italia: pericolosità e indicatori di rischio. Edizione 2018. ISPRA, Rapporti 287/2018.

V., Hervàs J., Smith J. T. (2014). Recommendations for the quantitative analysis of landslide risk (2014). Bulletin of Engineering Geology and the Environment, 13:209-263.

van Rooy J.L., (1989). A proposed classification system for dolomitic areas south of Pretoria. Contributions to Engineering Geology, 1:57-65.

Varnes D. J. (1978). Slope Movement Types and Processes. Special Report 176: Landslides: Analysis and Control, edited by: Schuster, R. L. and Krizek, R. J., TRB, National Research Council, Washington, DC, 11–33, 1978.

Varnes D.J. (1958). Landslide Types and Processes. *In Special Report 29: Landslide and Engineering Practice (E.B. Eckel, ed.)*, HRB, National Researh Council, Washington, D.C., pp. 20-47.

Varnes D.J., (1984). Landslide hazard zonation: a review of principles and practice. *Natural Hazards 3*, UNESCO, Paris, pp. 63.

Vincoli architettonici puntuali   http://www.liguriavincoli.it/

Wong, H.N., 2005. Landslide risk assessment for individual facilities. In: Hungr, O., Fell, R., Couture, R., Eberhardt, E. (Eds.), Landslide Risk Management. Taylor and Francis, London, pp. 237–298.

Wood H.O., F. Neumann. 1931. Modified Mercalli intensity scale of 1931 Seismolog. Soc. am. Bull., 21 (1931), pp. 277-283

WP/WLI (International Geotechnical Societies=UNESCO Working Party on World Landslide Inventory), 1993. Multilingual Landslide Glossary. BiTech Publishers Ltd.

Wu T.H., (2012) Root reinforcement of soil: review of analytical models, test results, and application ti design. Canadian Geotechnical Journal, 50: pp.259-274.

Wu TH, Tang WH, Einstein HE (1996) Landslide hazard and risk assessment. In: Turner and AK, Schuster RL (eds) Landslides. Investigation and mitigation. Transportation Research Board Special Report. National Academy Press, Washington, pp 106–118

Zenit, R. 2005 Computer simulations of the collapse of a granular column. Phys. Fluids 17, 031703

Zhang L.M., Ng A.M.Y. (2005). Probabilistic limiting tolerable displacements for serviceability limit state design of foundations. Geotéchnique, 55 (2):151–161.

Zuccaro G., Cacace F., (2015). Seismic vulnerability assessment based on typological characteristics. The first level procedure "SAVE". Soil Dynamics and Earthquake Engineering, 69:262-269.